

Louisiana Transportation Research

Construction and Comparison of Louisiana's Conventional and Alternative Base Courses Under Accelerated Loading

by

J. B. Metcalf
S. Romanoschi
Yongqi Li
LSU

M. Rasoulian
LTRC

Freddy L. Roberts
Ludfi Djakfar
LTU

LTRC

Louisiana Transportation Research Center

Sponsored Jointly by the Louisiana Department of Transportation and Development and Louisiana State University

1. Report No. FHWA/LA-00/347		2. Gov. Accession No.		3. Recipient's Catalog No.	
4. Title and Subtitle Construction and Comparison of Louisiana's Conventional and Alternative Base Courses Under Accelerated Loading		5. Report Date November 2001		6. Performing Organization Code	
		8. Performing Organization Report No. 347			
7. Author(s) JB Metcalf, Freddy L. Roberts, M Rasouljian, S Romanoschi, Yongqi Li, Ludfi Djakfar		10. Work Unit No. 98-3 ALF, 94-2 ALF		11. Contract or Grant No. State Project Numbers: 736-99-0516, 736-99-0170	
9. Performing Organization Name and Address Dept of Civil and Environmental Engineering; Louisiana State University, Baton Rouge LA 70803 Civil Engineering Department, LA Tech University. Ruston, LA 71272		13. Type of Report and Period Covered Final Report, 1994 - 1999			
12. Sponsoring Agency Name and Address Louisiana Department of Transportation and Development, Louisiana Transportation Research Center 4101 Gourrier Avenue Baton Rouge La, 70808		14. Sponsoring Agency LTRC		15. Supplementary Notes Conducted in Cooperation with the U. S. Department of Transportation, FHWA	
		16. Abstract: This report describes the test results of the first project at the Louisiana Transportation Research Center's Accelerated Loading Facility. In 1995, nine test lanes were constructed at the Louisiana Pavement Research Facility (PRF) in Port Allen, Louisiana. These test lanes consisted of 3.5 in of type 8 wearing and binder course and crushed limestone or soil cement bases made with either four percent or ten percent cement and either plant-mixed or mixed in-place courses. These mixed courses had the same structural capacity but with variable shrinkage cracking potentials. The lanes were loaded to failure using the Accelerated Loading Facility (ALF) and the results were used to compare the performance of the various base materials. The experiment was organized into three phases, which allowed for the establishment of performance characterization (standard or conventional sections) that could be used for this and future tests. Phase I of the program evaluated a flexible pavement with a typical crushed stone base and compared it to two innovative flexible pavement designs. Phase II compared plant mix stabilized soil bases. Phase III compared other stabilized pavement layer configurations, including the conventional (benchmark) pavement. Pavement condition was monitored by measuring surface deformation (profile), cracking, and FWD surface deflection. A number of lined bores allowed monitoring of moisture content by down-the-hole meters. Ambient climate was recorded and "in pavement" temperatures were measured. Since traffic loading on each section stopped at different distress levels, all test sections were compared at a standard failure level for rutting. Regression models were developed for each test lane in order to be able to predict the number of ESALs carried to a standard rutting failure level of 0.75 in (19 mm). A post-mortem was conducted after loading to investigate the pavement failure modes and base conditions. A pavement performance comparison among various lanes and survival analysis on pavement life was conducted. The relative performance comparisons showed that the stone base performed as well as the soil cement base and that the stone over a cement stabilized base performed best of all. Using an A-4 soil, the four percent cement treated bases performed as well as the ten percent cement stabilized bases and the mixed-in-place bases performed similarly to the plant-mixed bases. The Phase I test results suggested a layer coefficient for the stone stabilized soil of 0.10. Estimating the Present Serviceability Index (PSI) from the roughness, fatigue cracking, and rutting results provides a reasonable relationship for lanes with crushed stone or cement-stabilized soil bases that could be applied in pavement management systems models. Phase II and III test results suggested a layer coefficient for the cement stabilized subbase of 0.16. Performance of the stone over cement stabilized base ("inverted" design) pavement structure was significantly different from that of the other lanes in both failure mode and fatigue life. Cracking was found to initiate at the bottom of the asphalt layer or to reflect into the asphalt layer from the soil cement bases in all pavements except for the "inverted" base pavement where cracking initiated at the surface. A literature survey was conducted to identify analytical pavement models that could be used to predict the performance of the test lanes using pavement material properties, layer thicknesses, and wheel loads applied by the ALF. The VESYS 3A-M and FLEXPASS models were used to predict rutting, cracking, and roughness development with traffic loads and to predict the performance of the test lanes with granular bases. Both reasonably predicted rutting and roughness, but the fatigue cracking results were highly variable. Both models predicted adequately the performance of the control section, which consisted of an 8.5 in (216 mm) limestone base over geofabric, while FLEXPASS predictions matched the performance of a test section consisting of 4 in (102 mm) of limestone over (152 mm) stone-stabilized soil. In addition, Jameson and Asphalt Institute models were used to adequately predict the pavement fatigue life for three of the four cement stabilized base layers but not for the "inverted" base. The fatigue prediction model for cement-stabilized base asphalt pavement with a stone interlayer should be further investigated.			
17. Key Words: Pavement performance, cement stabilized base, crushed stone base, rutting, profile, FWD, Accelerated Loading Facility, ALF, Full-Scale Loading, VESYS, FLEXPASS, Performance Comparisons, Rutting, Cracking, PSI		18. Distribution Statement Unrestricted. This document is available through the National Technical Information Service, Springfield, VA, 21161.			
Security Classif. (Of this report) N/A		20. Security Classif. (Of this page) N/A		21. No. of Pages 84	
				22. Price N/A	

FINAL REPORT

Construction and Comparison of Louisiana's Conventional and Alternative Base Courses Under Accelerated Loading

By

J.B. Metcalf, Freeport McMoran Professor, LSU, Freddy L. Roberts, T.L. James Professor, LTU

M. Rasoulian, Project Manager, LTRC

S. Romanoschi and Yongqi Li, Graduate Research Assistants, LSU

Ludfi Djakfar, Graduate Research Assistant, LTU

LTRC Report No. 347

Research Project No. 98-3ALF

&

Research Project No. 94-2ALF

Conducted for

Louisiana Department of Transportation and Development

Louisiana Transportation Research Center

in cooperation with

U.S. Department of Transportation

FEDERAL HIGHWAY ADMINISTRATION

The contents of this report reflect the views of the authors, who are responsible for the facts and the accuracy of the data presented herein. The contents do not necessarily reflect the official views or policies of the Louisiana Department of Transportation and Development or the Federal Highway Administration. This report does not constitute a standard, specification or regulation.

November 2001

ACKNOWLEDGMENTS

The direction and support of the Technical Advisory Committee for this project is acknowledged. The support of the original project managers, Steve Cumbaa and William Temple, gratefully made this project possible. They were responsible for the experimental design, site selection construction, and ALF installation. They were always prepared to help generate the needed information, equipment, materials, and other help required to get the work done. Their assistance was invaluable.

The help of the ALF site team led by the Pavement Research Facility site manager, Bill King, is gratefully acknowledged. The efforts by Keith Gillespie and George Crosby in keeping ALF running and collecting the on-site data is appreciated and has made our work possible. The help of many members of the Louisiana Transportation Research Center and Louisiana Department of Transportation and Development staff was also essential and is gratefully acknowledged. The contribution of Mark Martinez who prepared detailed minutes of all ALF activities and edited the final report is also acknowledged.

The pavement material testing and evaluation work supervised by Dr. Louay Mohammad was invaluable in describing the material properties used in the pavement performance models.

ABSTRACT

This report describes the test results of the first project at the Louisiana Transportation Research Center's Accelerated Loading Facility. In 1995, nine test lanes were constructed at the Louisiana Pavement Research Facility (PRF) in Port Allen, Louisiana. [These test lanes consisted of 3.5 in of type 8 wearing and binder course and crushed limestone or soil cement bases made with either four percent or ten percent cement and either plant-mixed or mixed in-place courses. These mixed courses had the same structural capacity but with variable shrinkage cracking potentials.] The lanes were loaded to failure using the Accelerated Loading Facility (ALF) and the results were used to compare the performance of the various base materials.

The objective of this first experiment was to evaluate the various base courses, analyze the performance data obtained from full scale field test lanes at the PRF site, and compare the actual field performance with predictions from analytical models. The scope of the project was to compare the performance of the nine base courses under accelerated loading to the point of failure. The experiment was organized into three phases, which allowed for the establishment of performance characterization (standard or conventional sections) that could be used for this and future tests. Phase I of the program evaluated a flexible pavement with a typical crushed stone base and compared it to two innovative flexible pavement designs. Phase II compared plant mix stabilized soil bases. Phase III compared other stabilized pavement layer configurations, including the conventional (benchmark) pavement.

Pavement condition was monitored by measuring surface deformation (profile), cracking, and FWD surface deflection. A number of lined bores allowed monitoring of moisture content by down-the-hole meters. Ambient climate was recorded and "in pavement" temperatures were measured. Since traffic loading on each section stopped at different distress levels, all test sections were compared at a standard failure level for rutting. Regression models were developed for each test lane in order to be able to predict the number of ESALs carried to a standard rutting failure level of 0.75 in (19 mm). A post-mortem was conducted after loading to investigate the pavement failure modes and base conditions. A pavement performance comparison among various lanes and survival analysis was conducted on pavement life. The relative performance comparisons showed that the stone base performed as well as the soil cement base and that the stone over a cement stabilized base performed best of all. Using an A-4 soil, the four percent cement treated bases performed as well as the ten percent cement stabilized bases and the mixed-in-place bases performed similarly to the plant-mixed bases.

The Phase I test results suggested a layer coefficient for the stone stabilized soil of 0.10. Estimating the Present Serviceability Index (PSI) from the roughness, fatigue cracking, and rutting results provides a reasonable relationship for lanes with crushed stone or cement-stabilized soil bases that could be applied in pavement management systems models. Phase II and III test results suggested a layer coefficient for the cement stabilized subbase of 0.16. Performance of the stone over cement stabilized base ("inverted" design) pavement structure was significantly different from that of the other lanes in both failure mode and fatigue life. Cracking was found to initiate at the bottom of the asphalt layer or to reflect into the asphalt layer from the soil cement bases in all pavements except for the "inverted" base pavement where cracking

IMPLEMENTATION STATEMENT

The performance of base materials in the Pavement Research Facility (PRF) test lanes indicate that the Louisiana Department of Transportation and Development (DOTD) should utilize granular base materials instead of cement stabilized bases (CTB) throughout Louisiana where economically feasible. In addition, the test results demonstrate that when an A-4 soil was used in the mix, the cement treated bases with four percent cement performed as well as those stabilized with ten percent cement. Test results show no substantive difference in the performance of the central plant mix and mixed in-place CTBs. Therefore, DOTD should construct roadways using these alternative base course combinations in order to verify the performance in the field and to determine how reflection cracking is affected by the reduction in cement.

The two computer programs VESYS 3A-M and FLEXPASS both can be used to predict future performance of pavements in rutting and serviceability. The prediction of fatigue cracking did not fit the actual field cracking as accurately as did rutting and serviceability. However, either program can be used to compare the performance of candidate pavements.

The conclusions and recommendations of this report have been accepted by the Louisiana Department of Transportation and Development to change practice:

1. In relation to stone stabilized base course, adopting a layer equivalency factor of 0.10 and planning full scale long term road trials,
2. In relation to cement treated base course by adopting thicker layers at lower cement contents and planning full scale long term road trials,
3. By initiating the use of "inverted" pavements for which an experimental pavement has been built using recycled asphalt pavement in place of the crushed rock base, and
4. The current practice of in-place mixing should be continued.

TABLE OF CONTENTS

Acknowledgments	iii
Abstract	v
Implementation Statement	vii
Table Of Contents	ix
List Of Tables	xi
List Of Figures	xiii
Introduction	1
Objective	3
Scope	5
Methodology	7
Historical Review of AIF Use	7
Location of the Test Facility	8
Pavement Test Section Structures	8
The Test Pavements	8
Materials	9
Hot Mix Asphalt Materials	11
Crushed Stone Materials	12
Soil Cement Materials	13
Loading	13
Evaluation Criteria and Pavement Failure Definition	14
Permanent Surface Deformation	14
Pavement Surface Cracking	14
Pavement Surface Deflections	15
In Pavement Instrumentation	30
Ambient Climate	30
Post-Mortem	30
Selection of Analytical Models	35
Overview of Vesys 3a-M	36
Overview of Flexpass	39
Development of Data for Distress Prediction Modeling	41
Vesys Data	41
Flexpass Data	42
Discussion of Results	47
Summary of Phase I	47
Summary of Phases II and III	50
Comparison of Performance of Base and Subbase Materials	52
Rutting Performance Comparison	52
Roughness Evaluation	54
Cracking Development	56
Performance Analysis	57
Pavement Performance Models	66
Vesys Output	66
Flexpass Output	68
Lane 002	68
Lane 003	71
Lane 004	74
Conclusions	77
Recommendations	79
References	81

LIST OF TABLES

Table 1	Asphalt layer thickness (mm).....	9
Table 2	Properties of the embankment and select subgrade soil.....	10
Table 3	Laboratory compressive strength and resilient modulus for stabilized soil	10
Table 4	Properties of materials used in the ALF test sections	13
Table 5	ALF Loading Log.....	16
Table 6	FWD backcalculated moduli for the subgrade soil and the asphalt concrete (Mpa).....	25
Table 7	Strain measured and predicted from the backcalculated moduli - lane 009 (microstrain).....	31
Table 8	VESYS Attributes [35]	38
Table 9	Estimated layer moduli, in ksi (MPa), and fatigue coefficients, k_1 and k_2	41
Table 10	Permanent deformation coefficients α and μ and Poisson's ratio	42
Table 11	Type 8 Wearing Course moduli for lanes 002, 003, and 004 as determined by interpolating between laboratory test values	42
Table 12	Limestone base resilient moduli K- θ model parameters	43
Table 13	Material characteristics for various materials used in ALF test sections	43
Table 14	Select subbase and subgrade resilient modulus model parameters determined from laboratory testing	44
Table 15	Slope of creep compliance plot selected for FLEXPASS analysis	44
Table 16	Fatigue constants used in FLEXPASS analysis from LTRC laboratory testing and method suggested by reference 32.....	45
Table 17	Estimation of layer equivalency for lanes 002 and 004.....	49
Table 18	Pavement Life (x 1000 ESALs)	51
Table 19	Regression model for rut depth versus ESALs	53
Table 20	Approximate relation between IRI, SN, and RN for each lane	56

LIST OF FIGURES

Figure 1	Material configurations of the ALF test lanes.....	11
Figure 2	Loading history 1996-1999	15
Figure 3	ALF loading profile.....	15
Figure 4	Rutting development - Phase I	16
Figure 5	Rut depth development - Phase II	17
Figure 6	Rut depth development - Phase III	17
Figure 7	Roughness development - Phase I.....	18
Figure 8	Roughness development - Phase II.....	18
Figure 9	Roughness development - Phase III	19
Figure 10	Cracking development - Phase I.....	19
Figure 11	Cracking development - Phase II	20
Figure 12	Cracking development - Phase III	20
Figure 13	Crack pattern at the end of loading - Phase I.....	21
Figure 14	Crack pattern at the end of loading - Phase II	22
Figure 15	Crack pattern at the end of loading - Phase III	23
Figure 16	Backcalculated moduli - lane 005	26
Figure 17	Backcalculated moduli - lane 006	27
Figure 18	Backcalculated moduli - lane 007	27
Figure 19	Backcalculated moduli - lane 009	28
Figure 20	Backcalculated moduli - lane 010	28
Figure 21	Backcalculated moduli - lane 008A	29
Figure 22	Backcalculated moduli - lane 003A	29
Figure 23	Post-mortem of lane 006	32

Figure 24	Base course deformation - lane 006	32
Figure 25	Asphalt core showing the separation of the two lifts of asphalt layer - lane 003	33
Figure 26	Crack in asphalt layer reflected from cement stabilized base - lane 008	33
Figure 27	Modular structure of VESYS [35]	37
Figure 28	Simplified Framework of FLEXPASS	40
Figure 29	Pavement slippage failure - lane 003	47
Figure 30	Discrepancy between predicted and measured strains	48
Figure 31	Average rutting development for lanes 002 through 010	53
Figure 32	Performance comparison at a rut depth of 0.75 in (19 mm)	54
Figure 33	Summary of IRI roughness development for lanes 002 through 010	55
Figure 34	Crack development for lanes 002 through 010	56
Figure 35	Performance comparison lane 002 vs. 004	58
Figure 36	Performance comparison lane 005 vs. 006	59
Figure 37	Crack development comparison - lane 006, 007, 010 vs. 005, 008, & 008A	60
Figure 38	Rutting development comparison - lane 006, 007, 010 vs. 005, 008, & 008A	61
Figure 39	Performance comparison lane 006 vs. 007	61
Figure 40	Performance comparison lane 005 vs. 010	63
Figure 41	Cracking development - all lanes	63
Figure 42	Rutting development - all lanes	64
Figure 43	PSI evolution - all lanes	64
Figure 44	Predicted fatigue cracking and field data	66
Figure 45	Predicted rutting development from VESYS (upper and lower bound) and field data at transverse stations 1 through 8 along test lane 002	67
Figure 46	Fatigue crack development for lane 002	69
Figure 47	Rut depth development for lane 002	70
Figure 48	Present serviceability index development for lane 002	70

Figure 49	Fatigue crack development for the portion of lane 003 with no slip.....	71
Figure 50	Rut depth development for the portion of lane 003 with no slip	72
Figure 51	PSI development for the portion of lane 003 with no slip	72
Figure 52	Fatigue crack development for the portion of lane 003 with slip.....	73
Figure 53	Rut depth development for the portion of lane 003 with slip.....	73
Figure 54	PSI development for the portion of lane 003 with slip.....	74
Figure 55	Fatigue crack development for lane 004	75
Figure 56	Rut depth development for lane 004	75
Figure 57	PSI development for lane 004	76

INTRODUCTION

Since trucks tend to operate close to the maximum legal gross vehicle load or the maximum legal axle loads, there has been a gradual increase in the average gross weight of trucks over time [1]. As axle loads have increased, higher tire pressures have occurred, which decrease the tire contact area and reduce tire rolling friction forces. Heavier axle loads and increased tire pressures have accelerated pavement damage, shortening pavement life. The damage caused by these heavier loads shows up primarily as premature fatigue cracking, increased rutting, or both.

Cement-stabilized subgrade soils have been extensively used as a primary load carrying material for the vast majority of non-interstate flexible pavements on the very weak soils prevalent in middle and south Louisiana. These materials are economical, easily constructed, and provide a stiff foundation for flexible pavements [2]. However, this type of material cracks, due to shrinkage caused by hardening of the Portland cement and soil mixture. This produces cracking in the hot mix asphalt (HMA) layer as the cracks reflect from the base to the surface. These cracks allow moisture to enter the pavement, softening pavement materials. This contributes to rideability and other performance problems. Other types of materials and new blending methods are being considered as a replacement for the standard mixed in-place soil cement base material used in Louisiana.

The Louisiana Pavement Research Facility (PRF) is an experimental site housing a full scale pavement testing area on which an Australian designed Accelerated Loading Facility (ALF) is operated. The Louisiana ALF is the second of three to be installed and operated in North America [3]. ALF is an automated moving wheel pavement surface loading device to test full scale pavements to failure. The first experiment was conducted in three phases on nine test lanes. Construction details are given in King [4] and an interim report on development of the experiment and on Phase I testing is given in Metcalf, et al [5].

The three phases of the project were designed to establish "benchmarks" for the performance characterization of this and future test series by determining the performance of two pavements typical of current DOTD design and construction practice. The two "benchmark" designs consisted of a fully flexible, crushed stone base pavement and an in-place cement stabilized, silty soil, semi-rigid pavement. The nine lanes were:

- Lane 002: The control section - A 215 mm (8.5 in) limestone base placed upon a geofabric, which acts as a separator to reduce infiltration of fines into the base layer.
- Lane 003: A 140 mm (5.5 in) crushed limestone base with a high strength geo-grid at the bottom of the stone layer.
- Lane 004: A 100 mm (4 in) limestone base over a 150 mm (6 in) limestone stabilized select soil, acting as a subbase. In this lane, there is no separator geo-fabric.
- Lane 005: A 215 mm plant mixed soil cement (10 percent cement) base.
- Lane 006: A 215 mm plant mixed soil cement (4 percent cement) base.
- Lane 007: A 215 mm plant mixed soil cement (4 percent cement plus fibers) base.
- Lane 008: A 215 mm in-place mixed soil cement (10 percent cement) base.
- Lane 009: A 100 mm limestone base over 150 mm in-place mixed soil cement (10 percent cement) subbase.
- Lane 010: A 300 mm plant mixed soil cement (4 percent cement base).

Phase I of the program compared the three flexible crushed stone pavements (lanes 002, 003 and 004). Lane 002 established the "control" pavement performance standard for the lanes of the typical, Louisiana Department of Transportation and Development (DOTD) design. The relative performance of a stone stabilized soil base was established. The results from the geo-textile reinforced limestone base pavement were verified in at a repeat test due to premature failure on first run. The results indicated that geo-textile can be used to strengthen the pavement layer.

The pavements in Phase II compared the relative performance (strength and cracking characteristics) of lanes 005, 006 and 007. Lane 008 was compared to a plant-mixed soil cement base having the same soil cement content. Lane 008 was also compared to a plant-mixed soil cement base having a reduced soil cement content, both with and without fibers. All lanes were the same thickness.

Phase III compared three cement stabilized bases 1) the typical DOTD cement-stabilized mixed in-place soil base pavement, lane 008, as the "benchmark"; 2) an "inverted" pavement, lane 009, with a cement stabilized soil subbase under a limestone base; and 3) a thicker cement stabilized soil base, lane 010, with a lower cement content.

New DOTD specifications require pug-mill blending of the soil cement bases in lieu of the traditional in-place stabilization process for Class 1 base course. The new requirements will increase the costs associated with the construction of soil-cement base courses yet will provide for a more uniformly blended and consistent construction (base) material. It is not known at this time what effect the pug-mill mixing will have on the hydration process and the resulting shrinkage cracking associated with soil-cement base courses. It is believed that shrinkage cracking and reflective block cracking will continue to occur but at a somewhat reduced rate or intensity.

The effectiveness of incorporating a rigid base material under a flexible pavement surfacing has been questioned for many years. It has been suggested that bases that are less stiff (aggregate or relatively weaker soil cement) may offer improved performance characteristics due to reduced shrinkage. However, additional base thickness may be required.

Current laboratory tests to compare materials are improving, but there still remains a need to evaluate base designs and materials that are placed on a soil foundation using full-scale paving technologies and are then subjected to repeated heavy loads. The ALF device at Louisiana's Pavement Research Facility provides this opportunity.

The experimental work was conducted by the LTRC pavement research group who operated the ALF and collected pavement performance data. The LSU research team led by Dr. Metcalf collected profile data and conducted analyses of loading, pavement distress, and performance evaluations. Dr. Roberts investigated the pavement performance prediction models using the data from LTRC and LSU, and Dr. Mohammad of LTRC characterized the materials. This final report presents a compilation of the work reported by each research team.

OBJECTIVE

The objective of this experiment was to evaluate alternative base courses with similar structural capacity but with variable shrinkage cracking potentials, to analyze the performance data obtained from full scale field test lanes at the Pavement Research Facility site, and to compare the actual field performance with predictions from analytical models such as VESYS 3A-M and FLEXPASS.

SCOPE

A specific comparison of performance was obtained from nine test lanes constructed of alternative base materials under accelerated loading conditions. Test strip materials selection, construction specifications and procedures, and acceptance testing were accomplished through prior experience, engineering judgment, and laboratory testing. The methodology used for performance evaluation incorporated loading and environmental records, pavement instrumentation, destructive and nondestructive testing, and visual observation. The pavement observations were supported by laboratory testing of the materials.

A second part of the scope of this study involved comparing the ability of two computer programs, VESYS 3A-M and FLEXPASS, to predict the actual performance of the test sections involving hot mix asphalt and crushed stone bases. This comparison was conducted to determine which of these programs can be used to adequately predict performance of pavements in Louisiana.

METHODOLOGY

Historical Review of ALF Use

ALF is a full scale transportable pavement test device that simulates the effect of traffic loading on full scale pavements by applying controlled wheel loading in a repetitive manner [6]. The machine was first designed and manufactured for AUSTRROADS by the Road Transport Authority (RTA) in New South Wales, Australia. In 1984, the FHWA purchased the U.S. manufacturing rights from the RTA, and the first ALF machine in the U.S. was assembled and located at the Turner-Fairbanks Highway Research Center (TFHRC). The second one was purchased by the LTRC and delivered to the Pavement Research Facility outside Port Allen, Louisiana, in April 1994.

The ALF machine is a 94.8 ft (28.9 m) long structural steel frame with a moving wheel assembly at the front and the rear. This load wheel travels on rails at speeds up to 11 mph (18 km/h) on a 38 ft (12 m) long test section. The movement is generated by an electric geared motor attached to the wheel which maneuvers uni-directionally. At the ends of the frame, the rails curve upward to permit gravity to accelerate, decelerate, and change the direction of the wheel assembly [7].

Loads are applied to the pavement in one direction, representing the real traffic load, and can be distributed laterally to simulate traffic wander, producing the wheel path observed on highways.

The ALF can apply approximately 380 load cycles per hour using either a single or dual tire wheel assembly that models one-half of a single axle. The loads applied to the pavement can be varied from 9,750 lb (43.39 kN) to 25,000 lb (111.25 kN) by adding or subtracting ballast weights. By 1993, the Australian ALF had applied over 15 million cycles of loads (equivalent to 158 million 18 kip (80 kN) ESAL repetitions) to over 40 pavement types [8].

The ALF can provide many benefits to highway agencies. Primary among these benefits is the ability to observe the behavior and the damage patterns that develop under traffic loads in a short period of time, thereby avoiding the need for full scale pavement tests like the AASHTO Road Test. Bonaquist et al [7] used the ALF to evaluate the effects of tire pressure on flexible pavement response and performance. Sebaaly et al [9] used data from previous ALF research to evaluate relationships between surface cracking and the structural capacity of both thin and thick pavements.

The overall utilization rate of the ALF machine in Australia increased with familiarity and use. At the first trial, the efficiency of the ALF was only about 30 percent. After the second trial, the efficiency increased to nearly 80 percent. This utilization increase is attributed to the continuous improvement in the mechanical performance and the quality of maintenance and repair following early experience by the agencies [10]. The latest reported weekly utilization rate from Australia was between 85-90 percent.

The cost of ALF experiments in Australia has begun to decrease, particularly after the third trial. Increased efficiency of the ALF utilization is the primary reason. In addition, "The overall benefit/cost ratio was found to range between 4.0, at an eight percent discount rate, and 5.0, at four percent discount rate, indicating a healthy rate of return is being obtained on the investment in this machine" [11].

Location of The Test Facility

The pavement research facility is on a six-acre tract that is accessible by road, rail, and water just south of Port Allen, Louisiana, across the Mississippi River from Baton Rouge. The facility is located about 1 mile (1.61 km) south of I-10 on LA 1 South two miles (3.22 km) west of the Intercoastal Waterway overpass on North Line Road.

Pavement Test Section Structures

LTRC constructed nine sets of pavement sections divided into three phases numbered 1, 2, and 3. Phase 1 consisted of lanes 002, 003 and 004; phase 2 consisted of lanes 005, 006, and 007; and phase 3 consisted of lanes 008, 009 and 010. The materials in each lane are shown in figure 1. All lanes received the same 3.5 in (89 mm) LA DOTD type 8 wearing course mix, which was placed in two lifts.

The select A-4 soil has a variable thickness required to make the total thickness of the base and select soil 12 in (305 mm). Such an arrangement allowed the surface of the test bed to be at the same grade when the wearing course was placed.

The foundation consisted of 3 ft (914 mm) of a uniform embankment A-4 soil with a PI between 0 to 10 placed over the natural soils existing at the Port Allen facility. The natural soil was highly variable, highly organic, fat clay with high water content. This clay material was a dredge soil spread over the site from canal construction across the road from the site. The water table is highly variable, and at times there was positive water pressure, indicating an artesian condition when the Mississippi River is at high water levels.

The Test Pavements

Nine pavements were built for the first experiment and tested in three phases. The construction is described by King et al [4] and testing of the first phase by Metcalf et al [5]. The thickness of the layers was carefully monitored by leveling during construction, later by ground radar, and, again, when post-mortem examinations of the pavements were conducted. The asphalt layer thicknesses for the test sections are reported in table 1.

The layer thickness was checked during construction by measuring the level at the top of each pavement layer using the rod-and-level method. In addition, cores taken outside the loaded areas were used to measure the thickness of each asphalt concrete lift. The coefficient of variation (ratio between the standard deviation and the average value) of the thickness of the asphalt layer along a lane was between two percent and ten percent; thus it was within the range indicated by Freeman [12]. The average asphalt layer thickness for a lane varied between 78 and 112 mm. Good agreement was found between core length and rod and level thickness except in lanes two and four. Ground radar data indicated the same order of variability but greater mean thicknesses, presumably attributable to the dielectric constant used.

Table 1
Asphalt layer thickness (mm)

Method	Lane Number								
	002	003	004	005	006	007	008	009	010
Rod and Level Average (n = 11)	78.4	90.2	111.8	76.2	84.1	76.4	79.8	91.9	82.0
Standard Deviation	1.9	2.5	11.7	3.9	2.7	3.1	2.0	4.5	2.6
Ground Radar Average	165.9	146.1	113.3	61.5	103.1	102.9	105.7	103.4	101.9
Standard Deviation	4.3	4.6	3.3	3.5	3.0	1.8	4.6	3.3	3.3
Cores Average(n=5)	95.6	95.5	90.1	83.6	82.6	79.1	81.0	90.6	84.4
Standard Deviation	2.6	2.6	5.7	6.5	4.4	4.6	2.5	4.6	5.4

Materials

The embankment and select soil materials properties are summarized in table 2 as extracted from King et al [4] and Metcalf et al [5]. In situ compaction levels for the embankment were satisfactory. The select soil layers, used to make up differences in total pavement thickness to give a common overall surface level, were, in general, too thin to test.

The cement stabilized A-4 soil base had properties shown in table 3. All layers had comparable field densities between 1698 kg/m³ (106 lb/ft³) and 1752 kg/m³ (109 lb/ft³). The unconfined compressive strengths were adequate.

Table 2
Properties of the embankment and select subgrade soils

		Embankment (A-4)			Select subgrade soil (A2)		
		Density (kg/m ³)	m/c %	Modulus MPa	Density (kg/m ³)	m/c %	Modulus MPa
Laboratory Proctor	Standard	1683.5	18.3	8 - 15	1749.2	15.5	
	Modified	1818.1	15.2	10 - 28			
Compaction In situ	(0.3m)	1773.2	12.2				
	(0.6m)	1371.2	35.6				
Composition	%sand	4			57		
	%silt	69			33		
	%clay	23			10		
	%organic	4					
LL		27			NP		
PI		6			-		
UCS(psi)		33			-		
CBR		10			-		

Table 3
Laboratory compressive strength and resilient modulus for stabilized soil*

Lane Number			007				010	
Cement content (%)			10	4	4	10	10	4
Mix process ()			(plant)	(plant)	(plant)	(in-place)	(in-place)	(plant)
Resilient modulus (GPa)	100% compact.	28 days	1.95	1.13	1.64	2.36	2.40	1.49
		56 days	3.49	1.18	1.27	-	-	1.24
Unconfined compressive strength (MPa)	100% compact.	7 days	1.92	0.76	0.96	1.67	2.35	0.98
		28 days	2.50	1.12	1.23	2.32	3.00	1.35
		56 days	3.25	1.01	1.52	-	-	1.52
	95% compact.	7 days	-	-	-	0.98	1.47	-
		28 days	1.92	0.59	0.88	1.43	2.05	0.78
		56 days	2.08	0.92	1.08	-	-	0.96

*Each result mean of 3 samples.

Lane	Structure*
002	8.5 in (216 mm) Stone over fabric over 3.5 in (89 mm) select soil
003	5.5 in (140 mm) Stone over grid & fabric over 6.5 in (165 mm) select soil
004	4 in (102 mm) Stone over 6 in (152 mm) Stone stabilized soil over 2 in (51 mm) select soil
005	8.5 in (216 mm) 10% cement, plant mixed over 3.5 in (89 mm) select soil
006	8.5 in (216 mm) 4% cement, plant mixed over 3.5 in (89 mm) select soil
007	8.5 in (216 mm) 4% cement, plant mixed w/ fibers over 3.5 in (89 mm) select soil
008	8.5 in (216 mm) 10% cement, mixed in-place over 3.5 in (89 mm) select soil
009	4 in (102 mm) Stone over 6 in (152 mm) 10% cement, mixed in-place over 2 in (51 mm) select soil
010	12 in (305 mm) 4% cement, plant mixed

*All lanes received 89 mm (3.5 in) HMAC type 8

Figure 1
Material configurations of the ALF test lanes

Hot Mix Asphalt Materials

A typical Louisiana DOTD high stability type 8 dense-graded hot mix asphalt (HMA) was used as a wearing course. The original mix design incorporated 70.8 percent 0.5 in (12.5 mm) crushed gravel, 14.2 percent coarse sand, and 9.5 percent fine sand. The optimum binder content was determined from the standard Marshall mix design. The binder is a polymer modified asphalt cement meeting the Louisiana DOTD specification PAC-40HG. This mixture design was tested for stability, as defined by the Gyratory Shear Index (GSI) using the U.S. Army Corps of Engineers Gyratory Testing Machine (GTM). The GSI values for this mixture were in excess of 1.20. Mixes with GSI values of greater than 1.00 to 1.10 are considered unstable. Consequently, the contractor submitted a modified mixture design that consisted of 54.9 percent 0.5 in (12.5 mm) crushed gravel, 16.1 percent 0.19 in (No.4) crushed gravel, 13.3 percent coarse sand, and 10.4 percent granite fines. The maximum GSI value observed for this mixture was 0.98 indicating a stable mix. The modified mixture design was used in pavement construction for both the 2.0 inch binder course lift as well as the 1.5 inch wearing course lift.

Trial mix data from July, August, September, and October 1995 provided ample quality control data that pointed to some problems with the mix, which required changes in the plant prior to the actual construction of the test lanes. Some of the trial mix produced was placed on the parking areas of the ALF facility. The most significant problem was traced to the screens in the old Barber Green Batch plant. The aggregates were overriding several screens causing inconsistent gradations. The contractor made the decision to remove the screens and run a screenless batch plant. Also, the stockpile of granite fines was covered to reduce moisture variation.

Finally, the binder course construction began on November 10, 1995. Samples were taken from every truck and tested for gradation, which was determined to be well within the specifications. The plant had some dusting problems when the Arkansas Granite Fines dropped into the weigh bin from the recycle feed. Approximately 100 tons (90 tonnes) of binder course were produced on November 9th and stored overnight in a silo. When this material was placed in the field, the compaction temperatures were as low as 240°F (120°C). Seven passes with the steel roller and two passes with the rubber tire roller were used for compaction of both the binder and wearing course. The wearing course was placed on November 22, 1995. Overnight storage was not allowed and the plant temperatures were maintained at a 320°F (160°C) minimum.

The final in-place density of wearing course asphaltic concrete was 94.7 percent and the wearing course asphaltic concrete was 95.2 percent of plant briquettes.

Crushed Stone Materials

The crushed stone used in the base course in lanes 002, 003, 004, and 009 was specified to meet the gradation below:

Sieve Size	Specified % Passing	Actual % Passing
1 1/2"	100	100
1"	90 - 100	94.9
3/4"	70 - 100	79.7
No.4	35 - 65	23.3
No.40	12 - 32	4.6
No.200	5 - 12	1.5

As can be noted above, the actual field gradation was coarser than the specified value. The percent passing the No. 40 sieve was less than the minimum percent specified for passing the No. 200 sieve. Several things have resulted from this coarser gradation:

- 1) The field density was lower than could be expected from a denser gradation,
- 2) The permeability of the base course should be considerably greater than for the denser specification gradation, and
- 3) The resilient modulus should not be significantly affected by the coarser gradation.

Nuclear density results in lanes 002, 003, and 004 averaged 138.2, 137.4, and 137.2 pcf, respectively. The average water content for lanes 002, 003, and 004 were 4.2, 4.3, and 5.0 percent, respectively.

Soil Cement Materials

In Louisiana, soil cement bases are commonly used under most moderate to high volume roads. Typically 10 percent cement is included in the silty subgrade to produce a strong base course. The Louisiana standard specifications allow mixing operations to be accomplished in-place or in a central plant. As would be anticipated, reflection cracking occurs in the HMA surface as a result of the extensive shrinkage cracking in the soil cement base.

The use of soil cement bases is predicated on the presence of weak and often wet soils prevalent in middle and south Louisiana. In an attempt to minimize the problem of reflection cracking and to reduce the cost of producing the soil cement, the DOTD elected to investigate the performance of bases constructed by reducing the cement content of typical soil cement bases from 10 percent to four percent. These alternate soil cement combinations were used in four lanes: 005, 006, 008 and 010. Additionally, lane 006 was repeated with fibers added to the soil cement. These fibers were made available by a manufacturer at no cost, and were incorporated in lane 007. Lane 009 included a crushed stone base over a reduced thickness soil cement subbase. A description of the constituents in each lane was presented in figure 1. Properties of the soil cement materials are included in table 4.

Table 4
Properties of materials used in the ALF test sections

Material	Density (kg/m ³)	Moisture Content (%)	CBR	UCS (MPa)	Moduli* (MPa)
Type 8 WC	2212	-	-	-	2,000 - 3,900
Crushed stone	2203	-	-	-	135 - 150
Stabilized stone	1933	-	-	-	135 - 150
Select soil	1715	12	-	-	35 - 75
Embankment	1700	16	10	-	25 - 35
Soil Cement:				-	1,020 - 1,070
10% In-place	1720	14.4	-	2.01 (7 days) 2.66 (28 days)	
4% Plant-mixed	1720	14.1	-	0.98 (7 days) 1.35 (28 days)	

*Predicted from backcalculation

Loading

The accelerated loading was applied on a single set of dual wheels (i.e. half an axle). The tire pressure was 105 psi (724 kPa). The load was applied in the same direction (east to west), with a normal transverse distribution of over 1.23 ft (0.375 m) about the center line, meaning that the outer edges of the tires reached 1.80 ft (0.55 m) from that center line. The loading started at a deadweight of 10 kips (43 kN).

Loading was applied in sets of 25,000 passes (taking about 3 days) on each lane. Then, the performance measurements were made. The loading sequence is shown in table 5. The pattern

selected applied the "standard" 87 kN axle load (a wheel load of 43.5 kN) initially, then increased to 107 kN at 100,000 cycles until failure occurred. A typical loading curve is presented in figure 2.

Phase I (lanes 002-004) was tested between February 1996 and September 1996 [5]. Loading continued on phase III (lanes 008-010) in November 1996 and was completed by May 1997. Phase II loading began in July 1997 and was completed in February 1998. Lane 008 showed a localized failure and was therefore retested (as lane 008A) between February 1998 and August 1998. Lane 003 also showed a localized failure, which led to its retesting (as lane 003A) between October 1998 and January 1999.

The vertical load applied by the ALF machine is monitored by a group of four load cells. Figure 3 shows the total vertical ALF load, as measured by the load cells, during one pass of the wheel (three seconds) over lane 002. Even though the highest load peak at the start of the three second load pass is measured when the wheel lands on a metal plate outside the loaded area, the vertical load is not completely uniform. Similar variations in the vertical load were recorded on the other lanes. However, the load is sensibly constant at about 50kN over 85 percent of the test section.

Evaluation Criteria and Pavement Failure Definition

Each lane had the same, extremely strong asphalt surface. The intent was to ensure that failure would primarily be due to permanent deformation of the base, subbase, and/or subgrade. Performance was monitored and determined by measuring the development of rutting and cracking in the trafficked area and deflection under the Falling Weight Deflectometer (FWD) and Dynaflect equipment.

A rut of greater than 19 mm at the surface and/or cracking of more than 50 percent of the loaded area having a crack density of 5 m/m^2 were selected as initial failure criteria. A secondary criterion was any significant change in estimated pavement layer moduli. Loading ceased when these criteria were exceeded or if, in the judgement of the project manager, the lane had reached a condition where it would be rehabilitated under normal DOTD practice.

Permanent Surface Deformation

The surface deformation was determined using the ALF profilograph to collect data on eight transverse and three longitudinal profiles. Transverse rut depth is defined as the maximum depth under a 1.2 meter straight edge. The data measured on the central longitudinal profile was only used for the determination of the surface roughness, the slope variance (SV), and the international roughness index (IRI). Since larger depressions develop in the area where the ALF machine tire first contacts the pavement and this area is subjected to higher loading than the rest of the test areas, the elevation readings on the first 1.5 m were not used for the IRI and SV computations [5].

The development of rut depth is shown in figures 4, 5, and 6 and the roughness, estimated as IRI (250 mm), is given in figures 7, 8, and 9. The regressions shown are the best fit, (i.e. the highest R^2).

Pavement Surface Cracking

Surface cracking was recorded by sketching in relation to a coordinate grid 1.8 by 2.4 meters with

cross wires at 300 mm centers. The cracks were then sketched to scale on graph papers and a distance measuring device was used to determine the length of the crack as drawn. Only cracks wider than 0.1 mm were recorded [5].

The development of cracking is shown in figures 10, 11 and 12. The pattern of cracking in lane 008 took an exceptional form when premature failure occurred with local heaving of the surface. The patterns of cracking in the lanes differed as shown in figures 13, 14 and 15. Pumping was evident in lanes 008 and 010. The behavior of lane 009, the inverted pavement, was similar to that of the flexible, crushed stone base pavement, lanes 002-004.

Pavement Surface Deflections

Pavement surface deflections were measured by the Dynaflect and the KUAB Falling Weight Deflectometer (FWD) methods in phase I. For phases II and III, the KUAB equipment was replaced by a Dynatest unit. The measurements were performed on the centerline of the loading path of each pavement test section at intervals of 1.5 meters along the centerline. Dynaflect deflection measurements were performed at the same locations as the FWD measurements after a short time interval in order to avoid important changes in asphalt temperatures.

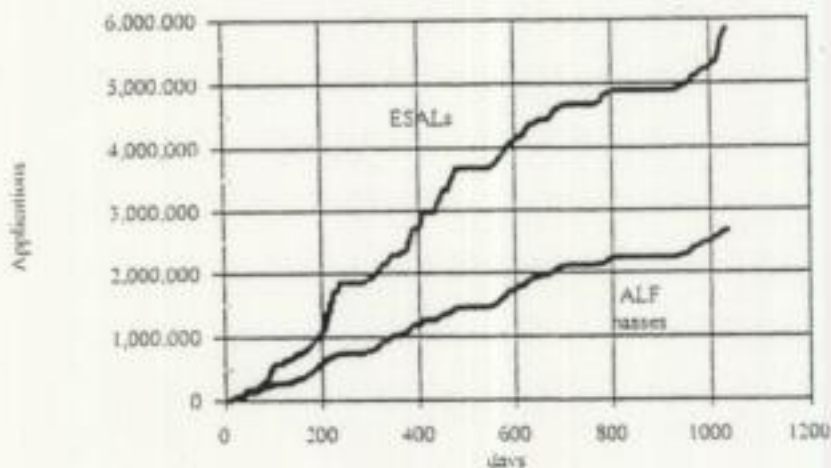


Figure 2
Loading history 1996 - 1999

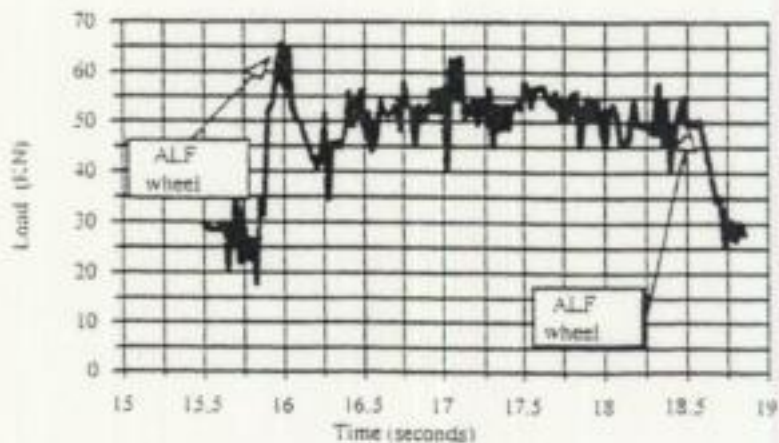


Figure 3
ALF loading profile

TABLE 5
ALF Loading Log

Lane	Date	ALF(KN) ⁽¹⁾ load(kip)	Passes	ESALS ⁽²⁾	River stage (m) ⁽³⁾	Rainfall (mm) ⁽⁴⁾	Air temperature (°C) ⁽⁵⁾
S002	2/06-6/05, 96	43.4	224172	308765	9.5	472	17.3
		63.8	50194	324404			
S003	6/11-7/01, 96	43.4	74991	103290	10.4	49	25.5
S004	7/09-9/04, 96	43.4	283230	396109	4.4	218	26.1
		63.8	41369	261368			
S002	9/05-9/16, 96	63.8	47419	306411	2.5	27	26.0
S003	9/20-9/27, 1996	43.4	20566	28710	3.1	57	22.7
S005	10/7/97-2/25/98	43.4	200000	275700	4.9	178	12.9
S006	9/30/97-2/18/98	43.4	200000	275700	4.7	290	16.7
S007	7/17/97-2/12/98	43.4	200000	275700	4.1	504	22.4
S008	11/4/96-2/17/97	43.4	100000	137736	5.4	53	9.9
S008	2/17/97-3/14/97	53.6	55000	176764	9.8	22	18.5
S009	11/22/96-3/4/97	43.4	100000	137736	6.5	136	13.8
S009	3/4/97-5/29/97	53.6	360000	1157064	10.8	115	16.7
S010	11/19/96-2/14/97	43.4	100000	137736	5.7	86	10.7
S010	2/14/97-5/5/97	53.6	100000	354564	11.0	46	18.2
S008A	4/25/98-5/25/98	43.4	157317	216246	10.4	103	23.9
S003A	9/25/98-1/25/99	43.4	374186	468560	4.5	101	20.7
S003A	1/25/99-2/4/99	63.8	84011	480860	7.2	-	-

1 Axle load KN

2 ESALS converted with a power exponent of 4

3 Height in m at Baton Rouge

4 Total between dates shown

5 Mean daily air temperature

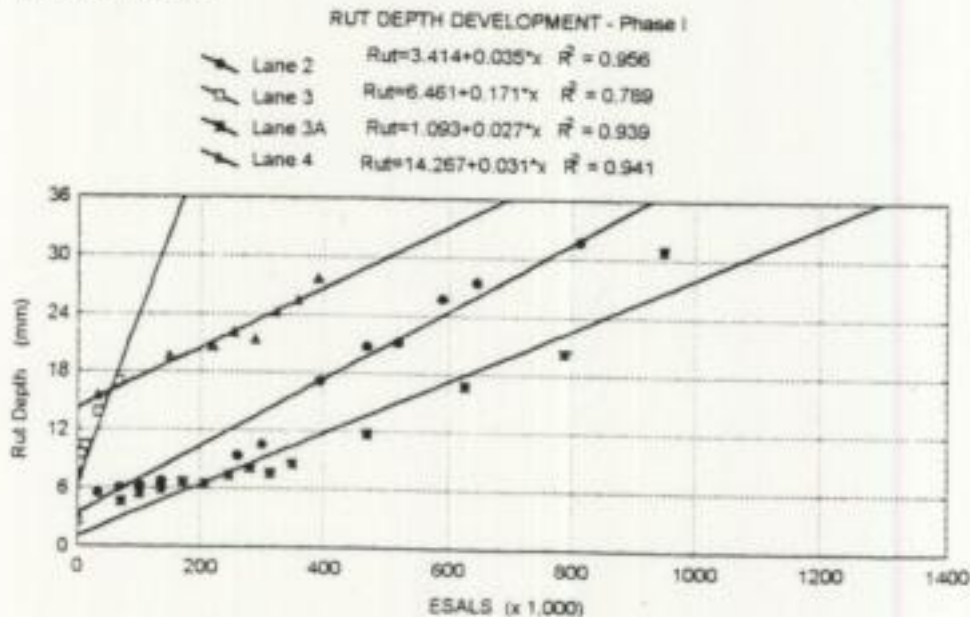





Figure 4
Rutting development – Phase I

RUT DEPTH DEVELOPMENT - Phase II

-  Lane 5 $Rut = -0.25 + 0.073 \cdot x$ $R^2 = 0.895$
-  Lane 6 $Rut = 2.078 + 0.052 \cdot x$ $R^2 = 0.611$
-  Lane 7 $Rut = 4.378 + 0.029 \cdot x$ $R^2 = 0.708$

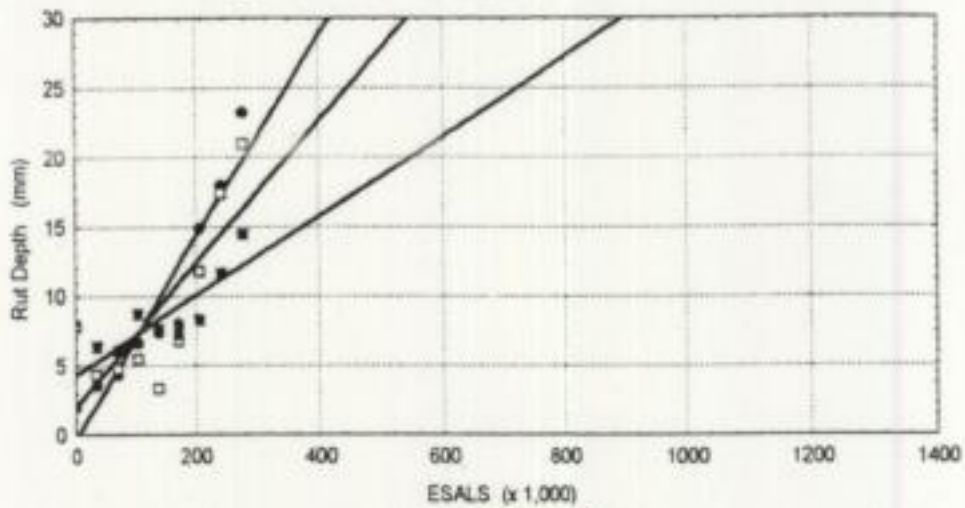






Figure 5
Rut depth development - Phase II

RUT DEPTH DEVELOPMENT - Phase III

-  Lane 8 $Rut = -1.511 + 0.063 \cdot x$ $R^2 = 0.992$
-  Lane 9 $Rut = -1.163 + 0.022 \cdot x$ $R^2 = 0.992$
-  Lane 10 $Rut = -1.509 + 0.041 \cdot x$ $R^2 = 0.992$
-  Lane 8A $Rut = 1.679 + 0.062 \cdot x$ $R^2 = 0.992$

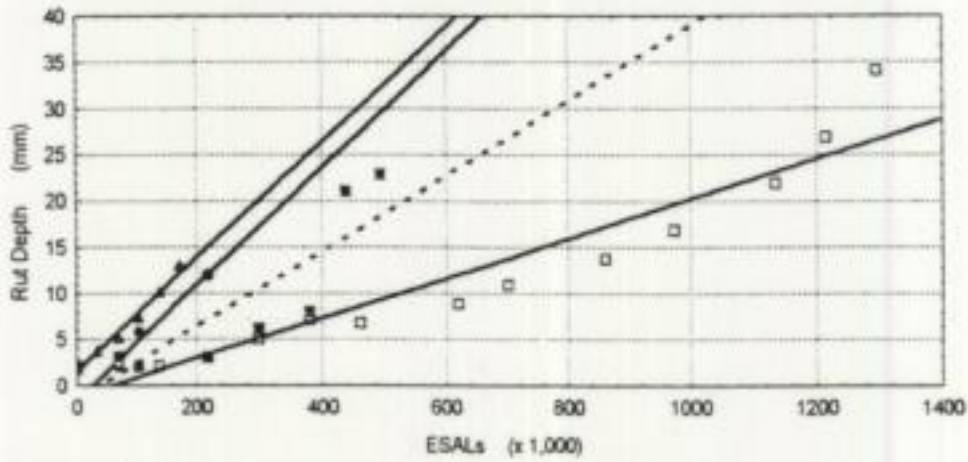


Figure 6
Rut depth development - Phase III

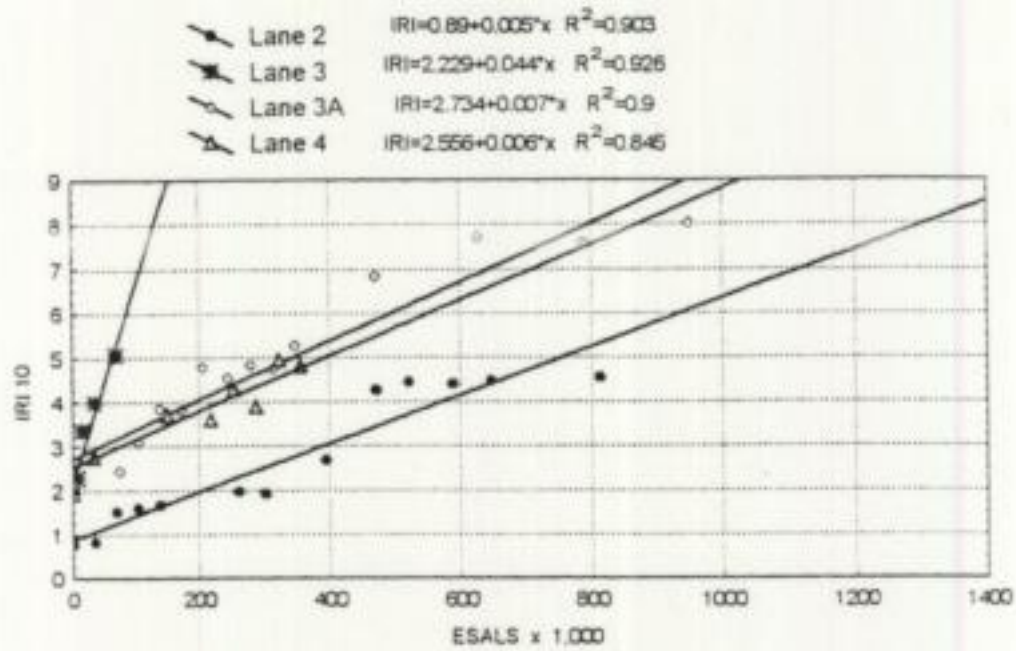


Figure 7
Roughness development - Phase I

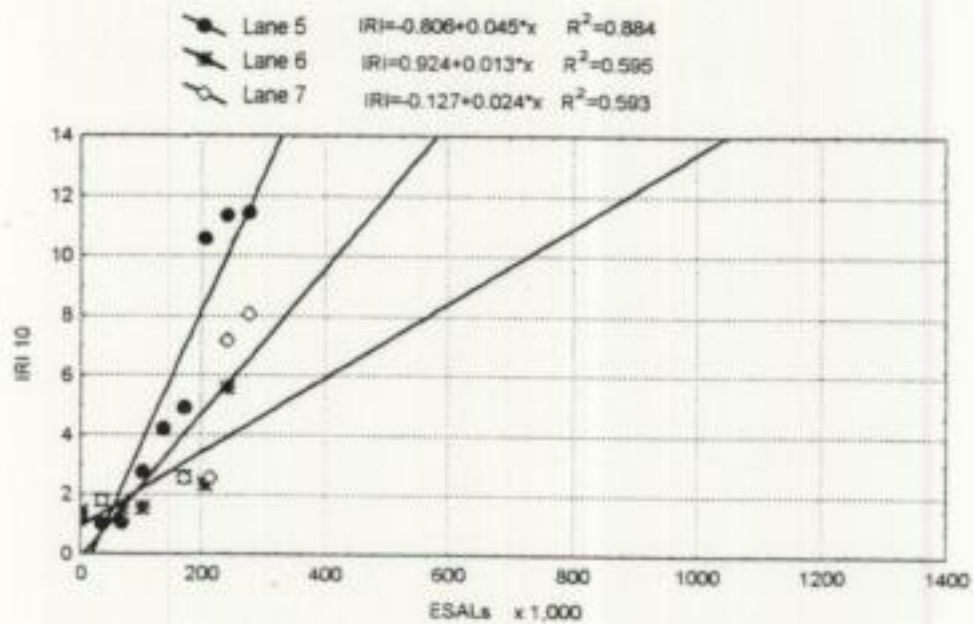


Figure 8
Roughness development - Phase II

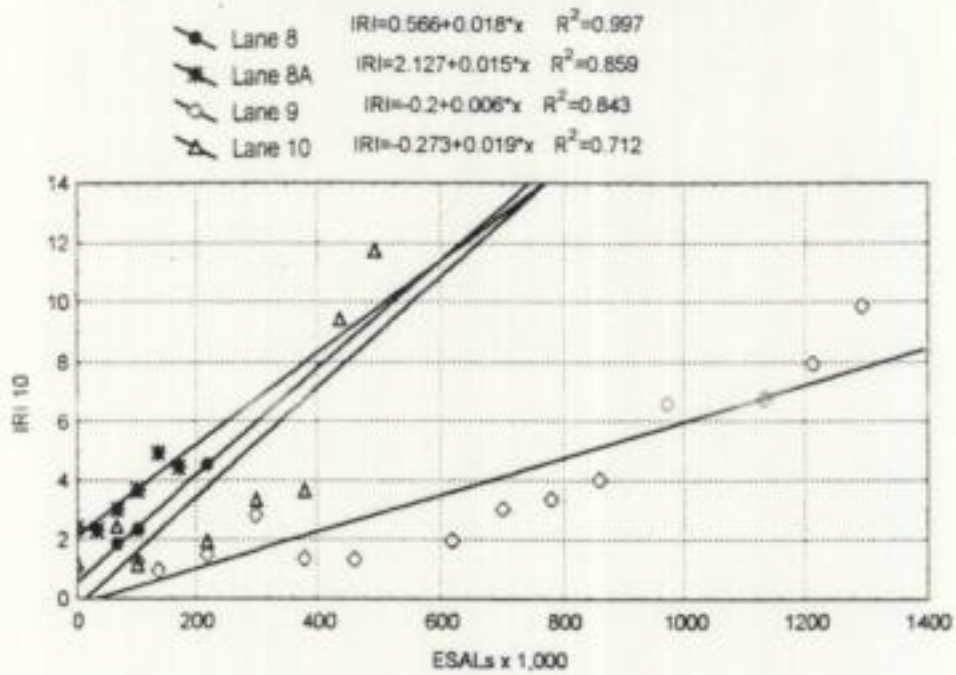


Figure 9
Roughness development - Phase III

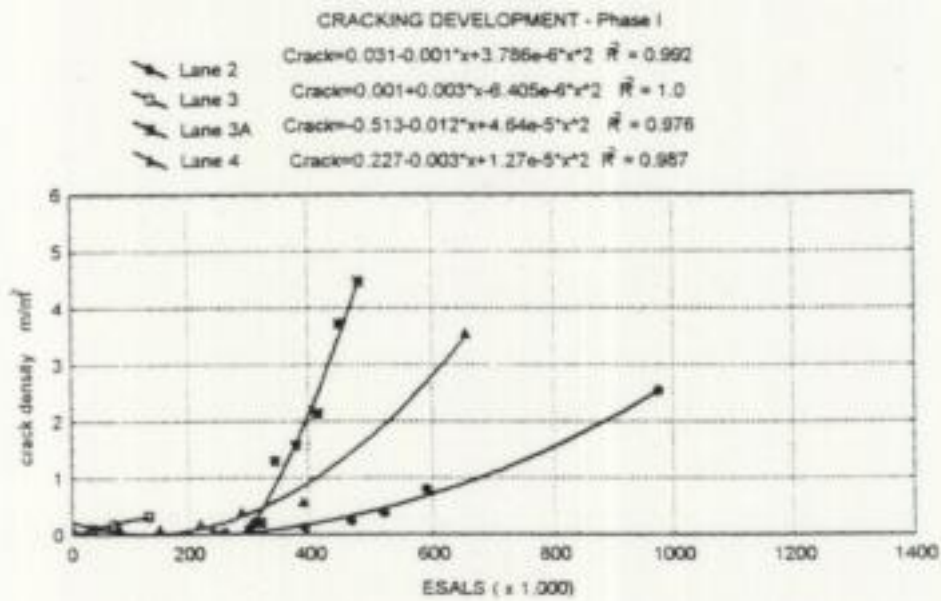


Figure 10
Cracking development - Phase I

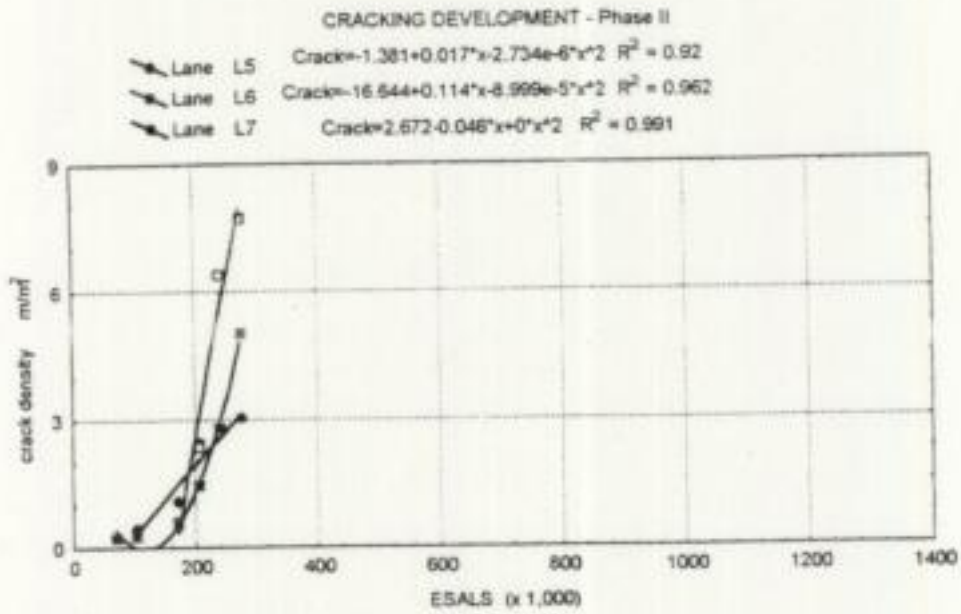


Figure 11
Cracking development - Phase II

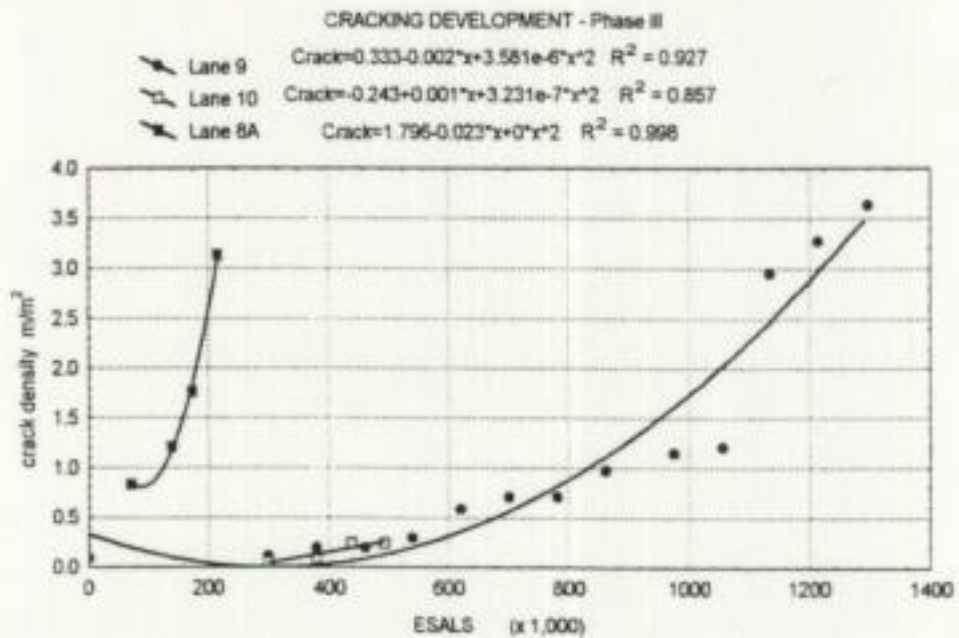


Figure 12
Cracking development - Phase III

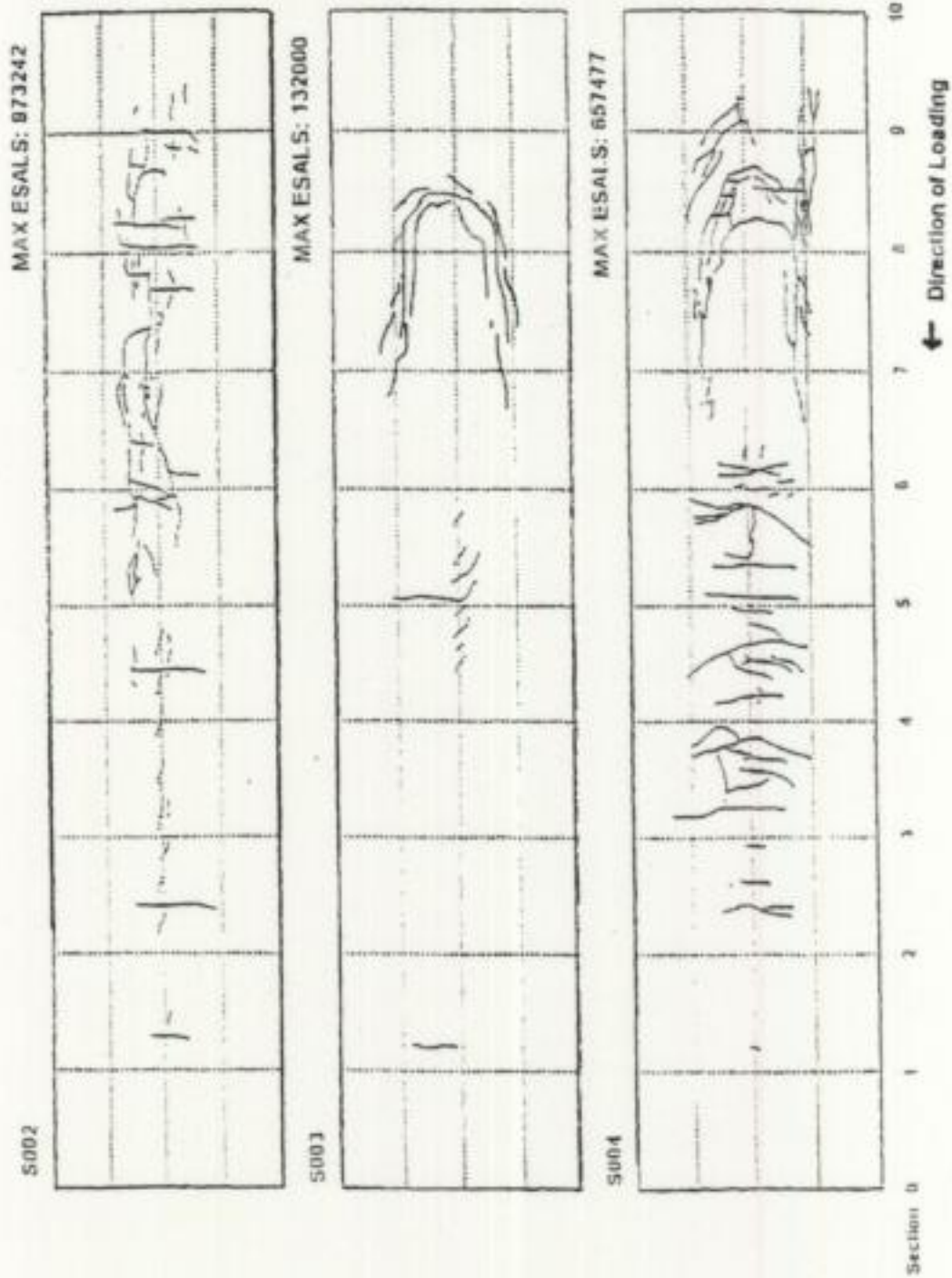


Figure 13
Crack pattern at end of loading - Phase I

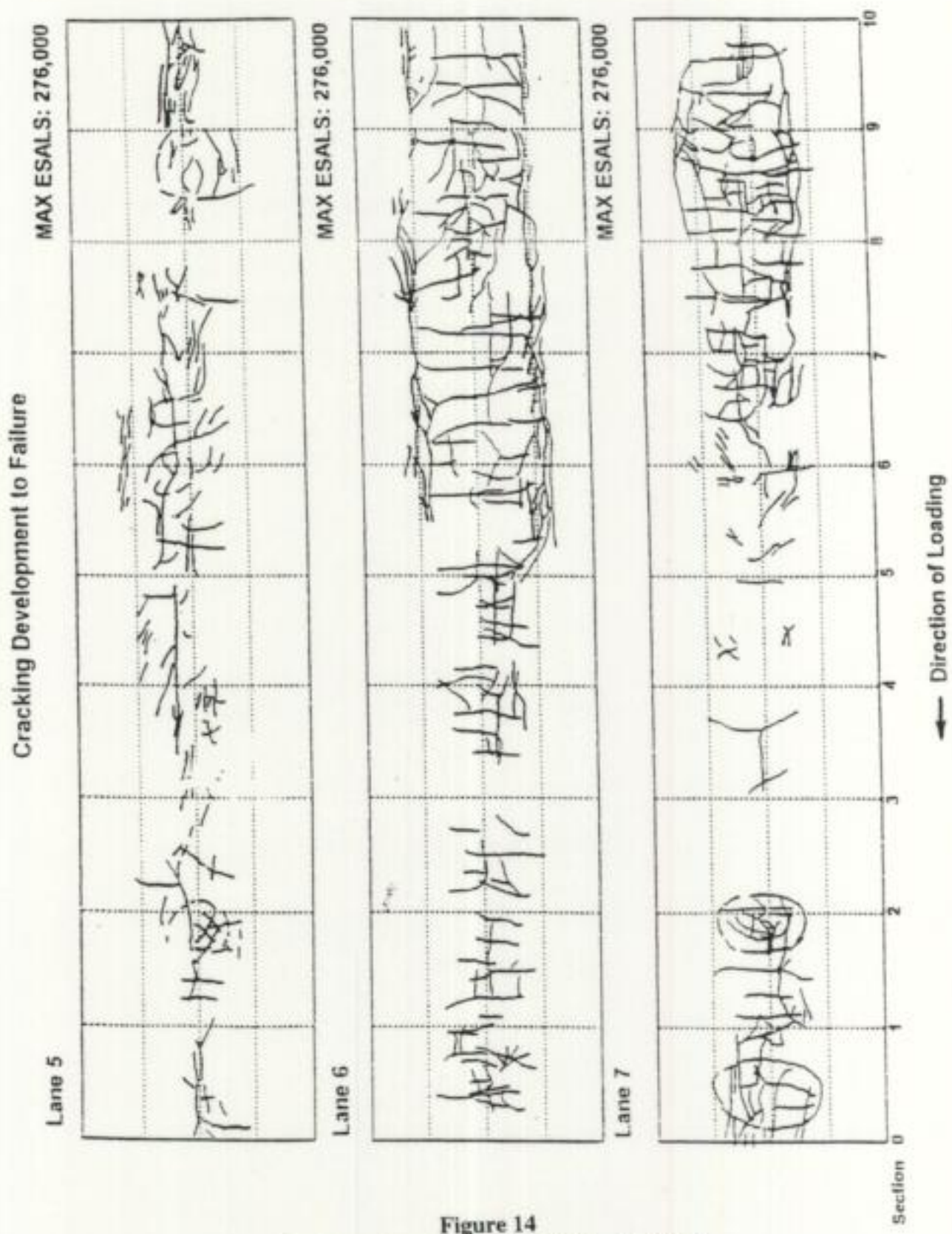


Figure 14
Crack pattern at end of loading - Phase II

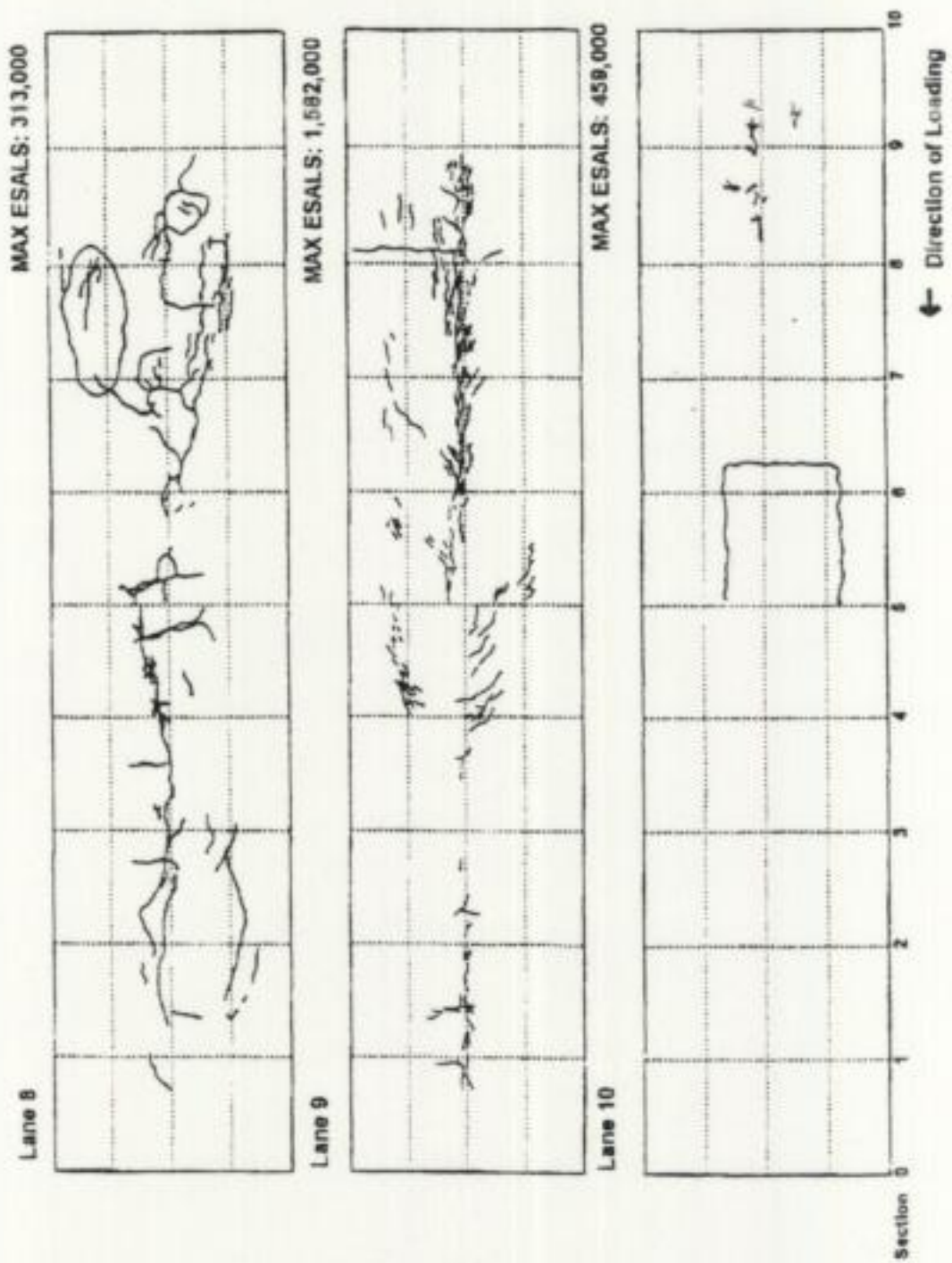


Figure 15
Crack pattern at end of loading – Phase III

Backcalculation of the resilient modulus of the pavement layers was done using the Modulus 4.0 backcalculation program [13] following the procedure described by Roberts [14]. The embankment soils and the existing subgrades were modeled as semi-infinite layers. When the A4 selected soil is the subbase material, the two soil types have similar moduli. Backcalculation cannot detect such a small difference. The modulus backcalculation process requires typical "seed" limits for the moduli of pavement materials. The values recommended by Roberts [14] and the SHRP procedure [15] were used. The backcalculated asphalt moduli values reported correspond to the standard temperature of 20°C. The temperature correction equation recommended by Ullitz [16] was used.

The backcalculated moduli for the subgrade and the asphalt concrete surface layer determined at the end of the construction of the nine lanes are presented in table 6. The coefficient of variation of the subgrade modulus for one lane was between 2.6 percent and 6.3 percent, which is within the range indicated by Freeman [12]. Over the entire site, however, subgrade moduli ranged between 35.9 and 91.1 MPa. The value at a particular station varied significantly during the testing of the lanes due to high variation in water table level.

Table 6 shows that the backcalculated moduli were not always in the expected range. In many cases, the asphalt moduli values were higher than 6.89 Gpa, which is much higher than the values recommended by the AASHTO Design Guide [17] or those from laboratory testing. Newcomb [18] mentioned that backcalculated moduli could differ from laboratory test results, the ratio of the two being between 0.8 and 4.0. It is not unusual to obtain high values and high variation in the same road section, especially in the case of thin asphalt layers. Rada and Witzak [19] reported similar variation for data assembled from 56 road sections.

The coefficient of variation of the backcalculated asphalt moduli for one lane ranged between 14 percent and 57 percent, the highest variation being for lanes 005 and 008. The average value of the indirect tensile modulus of the asphalt concrete at 20°C measured on cores was 3 GPa with a coefficient of variation of 22 percent [20]. The laboratory modulus was 4 GPa.

Table 6
FWD backcalculated moduli for the subgrade and the asphalt concrete (MPa)

Sta.	Layer	Lane								
		002	003	004	005	006	007	008	009	010
60	subgrade	49	38	45.6	60.1	66.8	64.1	64.4	58.4	79.4
	AC	4031	5142	7875	9663	5373	3517	9317	5117	7813
65	subgrade	48.3	37.3	43.5	55.2	66.5	63.0	68.0	61.6	87.0
	AC	2561	4542	7551	5658	3498	3150	1851	4583	2837
70	subgrade	48.3	35.9	42.1	54.7	62.2	62.6	57.6	58.5	87.0
	AC	3872	5777	8924	4332	4552	4646	5731	5287	3044
75	subgrade	46.2	35.2	42.8	54.0	6.6	61.8	65.3	59.7	82.8
	AC	4203	6633	8324	5785	5900	4516	4457	5936	3230
80	subgrade	46.2	35.9	42.1	56.7	64.2	63.4	57.7	57.0	83.5
	AC	4645	5767	9898	8713	3229	5844	8361	5339	4348
85	subgrade	44.2	35.9	40.0	50.9	63.1	61.6	58.2	60.3	91.1
	AC	3548	3306	9069	1994	1935	3326	3812	3915	1429
90	subgrade	44.9	37.3	39.3	53.8	64.4	64.4	65.3	57.4	78.7
	AC	463	6557	9773	2329	3633	3683	4412	6517	4272
Mean	subgrade	46.7	36.5	42.2	55.1	56.3	63.0	62.3	59.0	84.2
	AC	3927.3	5389.1	8773.4	5496.3	4017.1	4097.4	5420.1	5262.0	3853.3
C.V. (%)	subgrade	3.6	2.6	4.6	4.8	36.1	1.6	6.5	2.6	4.9
	AC	17.0	20.2	9.5	49.3	31.2	21.7	44.8	15.0	48.1

Pavement performance may be inferred directly from FWD deflection measurements, but estimating the modulus is the usual practice. The change in backcalculated moduli are shown in figures 16, 17, and 18 for lanes 005, 006, and 007, figure 19 for lane 009, and figure 20 for lane 10. Lane 005 showed a drop in the cement-stabilized base modulus after trafficking usually attributed to crack development. The same effect was not evident in lanes 006 and 007, but above 50,000 ESALs, the results were comparable. This is attributed to the higher cement content (10 percent) of lane 005 base resulting in higher initial values. Very few results were obtained from lane 008 because the FWD was out of service and there was premature pavement failure. Lane 009 results indicated that the surface asphalt and subbase cement-stabilized soil layer moduli decreased with loading and, by the time failure was declared and loading ceased, had reached stable low values. The pattern for lane 010 was similar. The moduli estimated for all cement treated layers were comparable around 100-200 Mpa given the accuracy of the backcalculation procedure and the time difference between the testing phases. The subgrade moduli were also reasonably comparable. Asphalt moduli for lanes 005, 006, 009, and 008A were reasonably close at about 5-6,000 Mpa. Lanes 007 and 010, on the other hand, showed values closer to 3,000 MPa.

Not enough data were obtained from lanes 003 and 008 due to premature failure. Lanes 008A and 003A were retested after all nine lanes were tested. The backcalculated moduli for lanes 008A and 003A are shown in figures 21 and 22. The asphalt and base moduli of lane 008A decreased with the loading and were 64 percent and 71 percent of their original values when loading was terminated due to severe cracking. However, for lane 003A, the moduli for asphalt and base did not change significantly with loading. Even when the loading was stopped because of severe

cracking, the moduli of asphalt and base were almost the same as the original values. The cement treated base of lane 008A had a higher modulus than the limestone base of lane 003A.

The in situ variability of the material stiffness is well described by the surface deflection and the backcalculated moduli. The FWD surface deflections measured the same day on all the lanes indicated a coefficient of variation for the central deflection of a lane between 3.9 percent and 9.4 percent, which is below the typical values indicated by Freeman [12]. Groenendijk [21] reported a difference in central deflection of 50 percent within 1.5 meters for a similar test on a flexible pavement.

The variation in FWD surface deflection can be attributed to the materials and also to the configuration of the FWD equipment. Because two different FWD models were used, a comparison study [20] was initiated to investigate if the equipment configuration affects the values of the surface deflection. The ratio between the backcalculated asphalt moduli from deflections measured by the two FWD devices was between 0.48 and 1.55. The average for each test section was between 0.86 and 1.15. The ratio of backcalculated moduli for the subgrade was between 0.9 and 1.25. For one lane, the average ratio was between 0.96 and 1.19. The coefficients of variation of the ratio were between two percent and four percent. As indicated by Romanoschi [20], the differences in backcalculation moduli for both the subgrade and the surface and base layers was attributed primarily to differences in equipment configurations (the falling weight, the stiffness, and the configuration of the rubber buffer system).

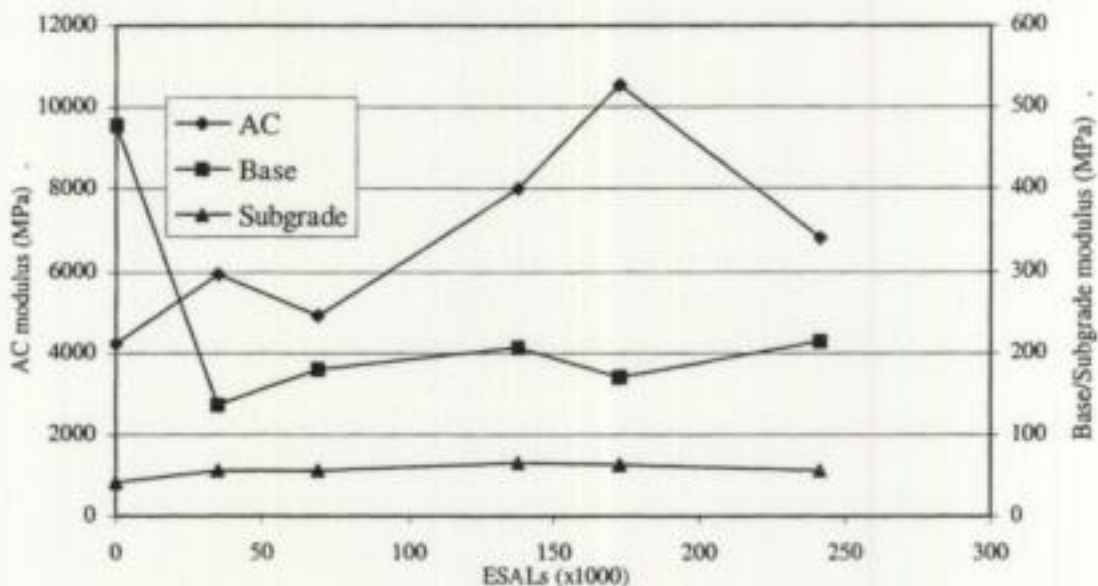


Figure 16
Backcalculated moduli - lane 005

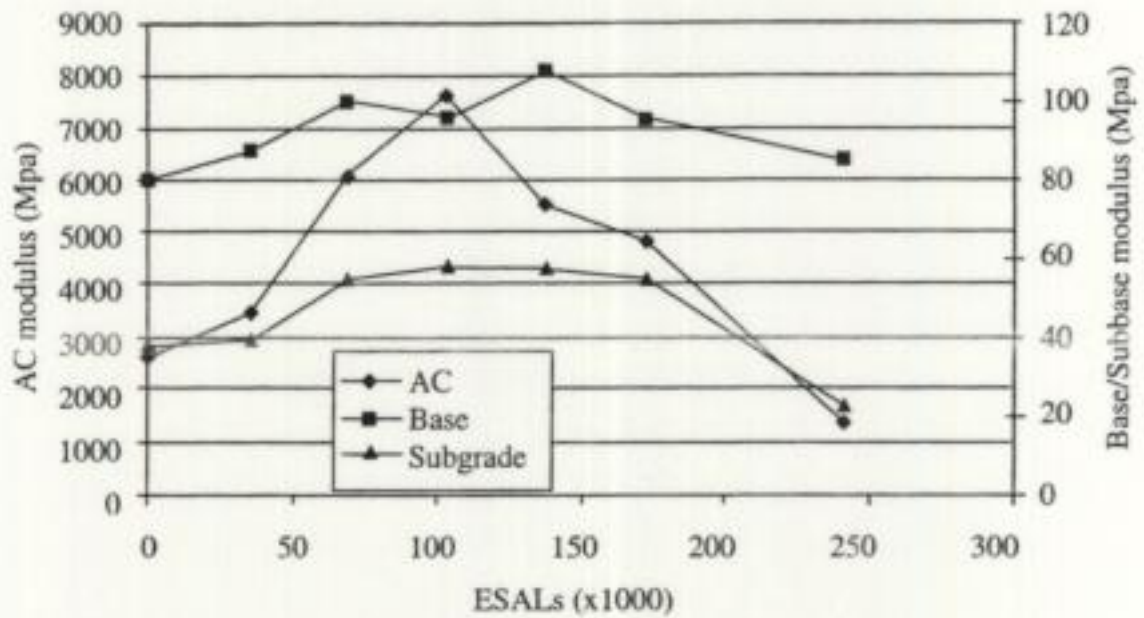


Figure 17
Backcalculated moduli - lane 006

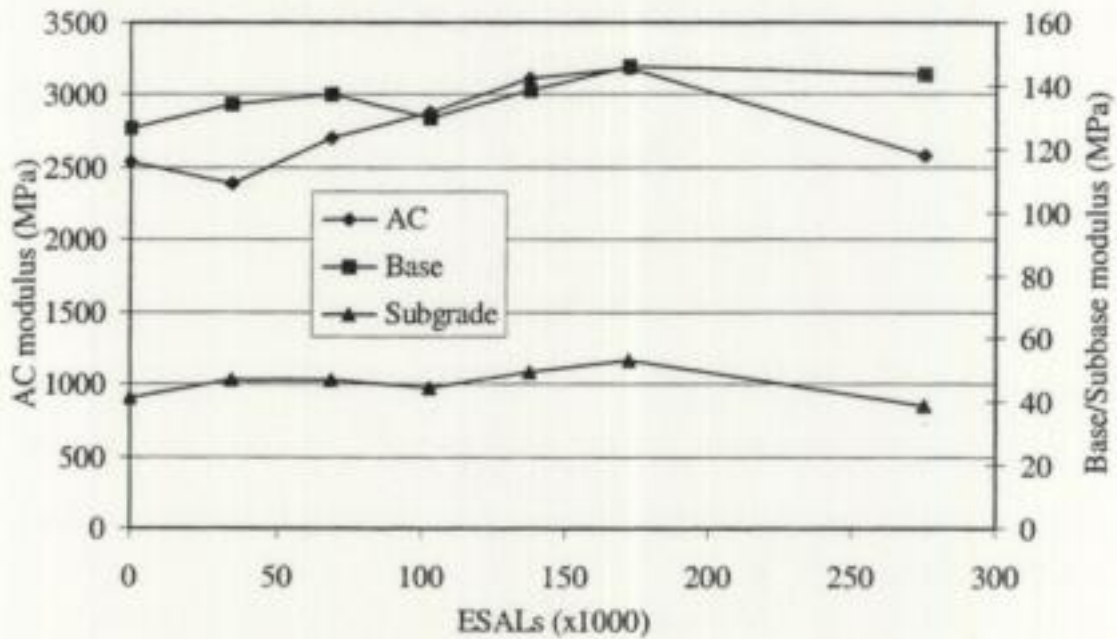


Figure 18
Backcalculated moduli - lane 007

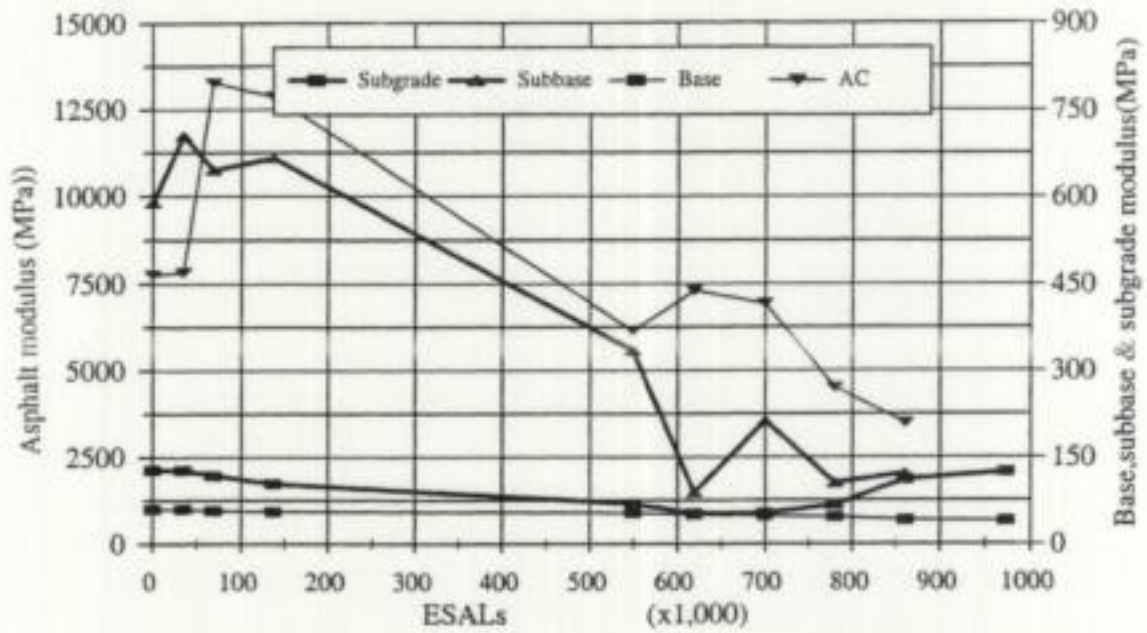


Figure 19
Backcalculated moduli - lane 009

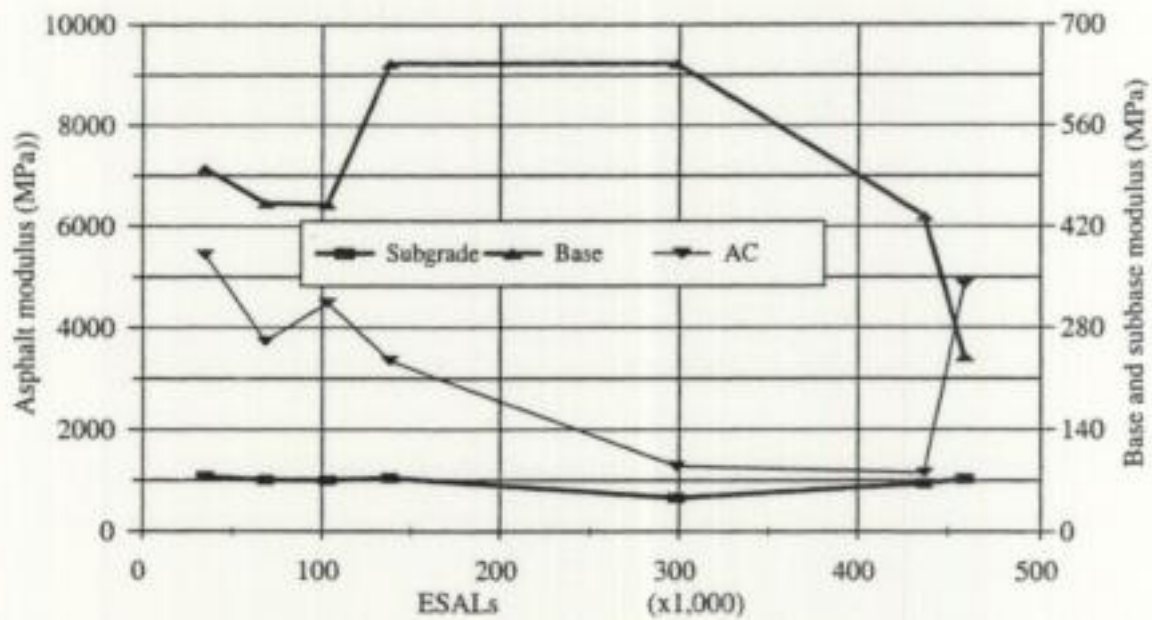


Figure 20
Backcalculated moduli - lane 010

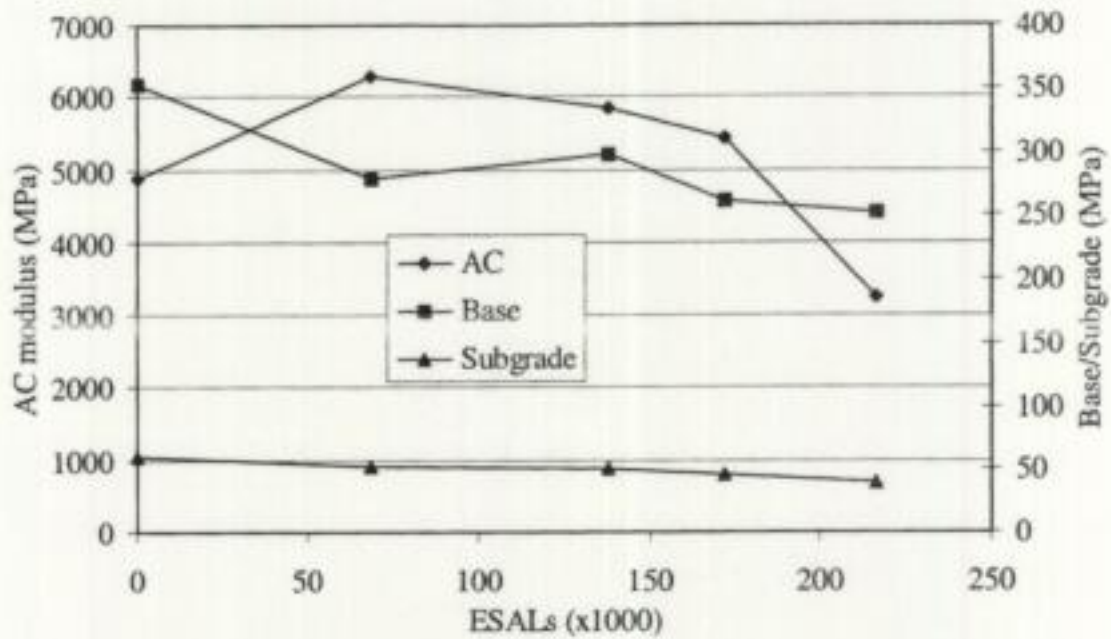


Figure 21
Backcalculated moduli - lane 008A

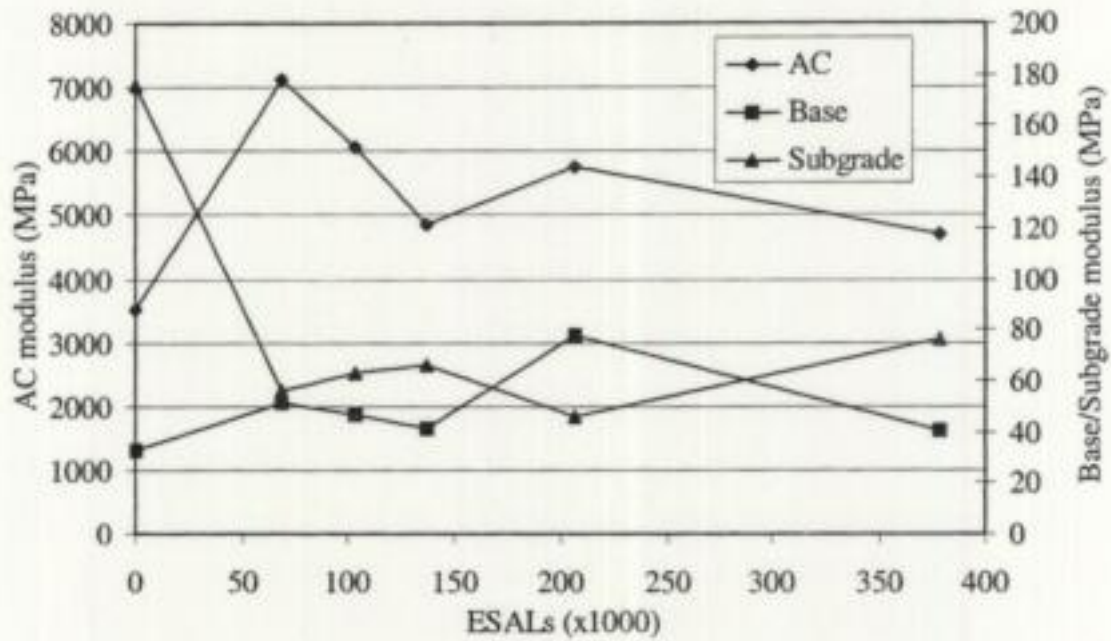


Figure 22
Backcalculated moduli - lane 003A

The FWD backcalculated modulus is an important field measurement of material properties. However, the derivation of modulus is not precise. The estimated modulus is affected by many variables, among which the layer thickness of a pavement is the most critical. Core, survey, and ground radar data show that thicknesses of the test lanes varies considerably, thus modulus data can only be interpreted broadly.

In Pavement Instrumentation

All the pavements were instrumented to measure strain at various layer interfaces and pressure at the subbase/subgrade interface. A total number of 379 strain gauges were used. Eleven pressure gauges were installed at the base/subbase interface. The strain gauges were of innovative design, using 13 mm gauge length (Micro-Measurement) and 25 mm gauge length (Kiowa) resistance gauges on a 100 mm substrate placed between two layers of bituminized tape.

Strain records were extremely difficult to interpret with the exception of reasonable strain traces obtained from lane 009. Data were affected by high noise levels (table 7). The most likely explanation is the very low strain transfer between the gauges and pavement layers, as evidenced by the excavation of gauges from the phase I test pavements [5]. Strain levels estimated from the backcalculated moduli indicate that the strains should be measurable by the equipment installed, but it is normal to have problems in interpreting strain data due to the many variables affecting the analysis.

Ambient Climate

Ambient climatic conditions were recorded by a weather station measuring air temperature, wind speed, and precipitation. The asphalt pavement temperatures were recorded by thermocouples at pavement surface, 50, 100 and 150 mm depths, and used for processing strain and deflection data. The water table level was monitored using wells. Specifications, installation procedures, and data acquisition systems along with information on materials and construction procedures are described by King [3]. The ambient temperature and rainfall mean values are given in table 5. Clearly the rainfall and water table levels affected performance of the test sections, but no definitive correlation was found.

Post-Mortem

Coring and post-mortem trench excavation showed several interesting features on lanes 005, 006, 007, and 010. Most rutting (permanent deformation) was confined to the cement stabilized soil base and not in the HMAC layer (figures 23 and 24). This was caused by the loss of material due to erosion. There was loss of bond (figure 25) in lane 003 between the two lifts of asphalt layers (Phase I) [5].

A light application of asphalt tack coat was sprayed on the top surfaces of the bases and the 50 mm binder course. On the untrafficked area, asphalt slabs were cut and lifted to evaluate the bonding conditions between asphalt layers. It was found that the bonding between asphalt and crushed stone base layers was in better condition than the bonding between asphalt and soil cement layers [22].

There was evidence of cracking at the bottom of the asphalt in all cement stabilized base lanes except lane 009. It was observed that there was a clear relationship between cracking in the

asphalt and (shrinkage) cracking in the cement-stabilized base of lane 008 as shown in figure 26.

Table 7
Strains measured and predicted from the backcalculated moduli – lane 009

Gauge	Position	Direction	Thousand ALF Passes (Thousand ESALs)													
			16 (25)	125 (218)	133 (248)	133 (248)	150 (298)	167 (340)	175 (379)	192 (432)	200 (459)	200 (459)	225 (539)	225 (539)	360 (974)	365 (990)
AT3-1	IN AC	TRANS	-238	33	25		27									
<i>FWD</i>			<i>43</i>	<i>21</i>	<i>21</i>	<i>21</i>	<i>21</i>				22	22	22	22	98 98	
AT3-3	IN AC	LONG	65		110	108	85	101	62		1066	395				
<i>FWD</i>			<i>-24</i>	<i>-20</i>	<i>-20</i>	<i>-20</i>	<i>-20</i>				<i>-21</i>	<i>-21</i>	<i>-21</i>	<i>-21</i>	<i>-50 -50</i>	
BT2-1	BOT AC	TRANS												430	95	
BT2-2	BOT AC	TRANS								-577						
<i>FWD</i>			<i>56</i>	<i>63</i>	<i>63</i>	<i>63</i>	<i>63</i>				<i>74</i>	<i>74</i>	<i>74</i>	<i>74</i>	<i>100 100</i>	
BT2-3	BOT AC	LONG								271					-39	
BT4-3	BOT AC	LONG	167	238	229	222	261	248			231	234	932	992		
BT4-4	BOT AC	LONG	197	213	281	281	215	265	191	199	263	261				
<i>FWD</i>			<i>228</i>	<i>175</i>	<i>175</i>	<i>175</i>	<i>175</i>				<i>193</i>	<i>193</i>	<i>193</i>	<i>193</i>	<i>455 455</i>	
FB1-2	BOT BASE	TRANS	-42			-49			-53		-194	-46				
FT1-2	BOT BASE	TRANS				38	36									
<i>FWD</i>			<i>8.4</i>	<i>8</i>	<i>8</i>	<i>8</i>	<i>8</i>				<i>23</i>	<i>23</i>	<i>23</i>	<i>23</i>	<i>262 262</i>	
CB3-3	BOT BASE	LONG								-65						
CB3-4	BOT BASE	LONG						38			46	47		115		
CT2-4	BOT BASE	LONG								-550						
CT3-3	BOT BASE	LONG												-31	1037	
FB1-4	BOT BASE	LONG	29													
<i>FWD</i>			<i>17</i>	<i>8</i>	<i>8</i>	<i>8</i>	<i>8</i>				<i>26</i>	<i>26</i>	<i>26</i>	<i>26</i>	<i>417 417</i>	
P3BP	TOP EMBK	Stress	0.797	0.796	0.881	0.843	0.757	0.712	0.526	0.566	0.625	0.623	0.181	0.214	0.309	0.36
<i>FWD</i>			<i>6.41</i>	<i>5.39</i>	<i>5.39</i>	<i>5.39</i>	<i>5.39</i>				<i>5.57</i>	<i>5.57</i>	<i>5.57</i>	<i>5.57</i>	<i>7.7 7.7</i>	



Figure 23
Post-mortem of lane 006

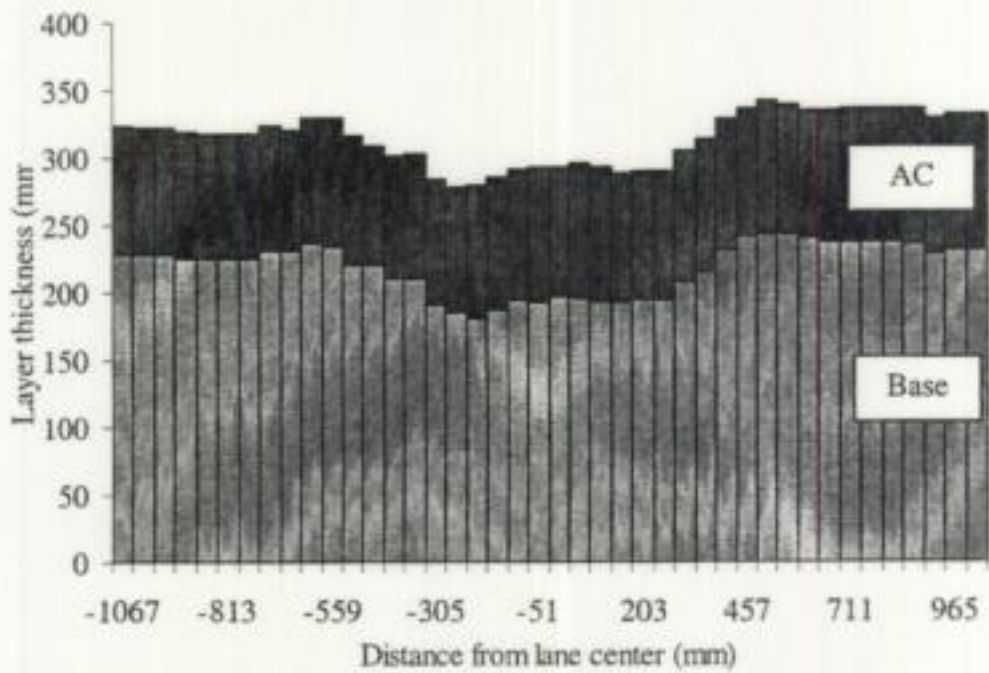


Figure 24
Base course deformation -lane 006



Figure 25

Asphalt core showing the separation of the two lifts of asphalt layer - lane 003

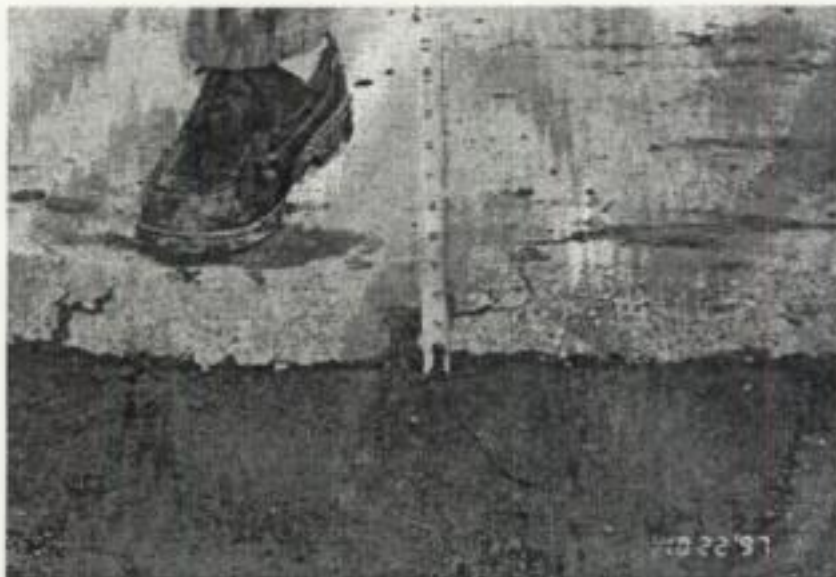


Figure 26

Crack in asphalt layer reflected from cement stabilized base - lane 008

During the ALF loading, twenty asphalt slabs, 200 x 200 mm square, were cut from the un-trafficked parts of lanes 005, 006, and 007. A known load was applied on top of the slabs and a horizontal force was applied on one side of the slab by a loading device. Where good adhesion had been created between the asphalt and the cement-stabilized soil base, the results showed that shearing failure occurred in the stabilized soil, about 20 mm below the bottom of the asphalt layer instead of at the immediate interface. This was consistent with the post-mortem observations.

Where heavy pumping and loss of fine material was observed during loading, there was clear evidence of a loss of bond between the asphalt and the cement-stabilized soil layers. The presence of free water at the interfaces and a soft layer on top of the soil cement were clearly observed upon excavation. The existence of this soft soil cement layer when free water was available may greatly increase the tensile strain at the bottom of the asphalt and, therefore, decrease the pavement fatigue life [22].

Asphalt slabs (200 mm x 200 mm) had also been cut on both trafficked and un-trafficked areas of lane 009 to investigate the bond conditions between the asphalt and crushed stone layers. There was no clear separation between the layers when the slabs were lifted up. Instead, there was crushed stone as thick as 50 mm strongly adhering to the bottom of the asphalt and forming a transition layer. This transition layer has a continuously varying modulus between asphalt and crushed stone which can significantly decrease the tensile strain in the asphalt layer, and move the highest strain down into the crushed stone layer, which has a larger capability to bear strain. Therefore, the transition layer can greatly improve the pavement fatigue life [22].

It is widely believed that load-associated cracks initiate at the bottom of asphalt layers, where tensile strain is highest, and propagate upward to the surface [23]. This statement is supported by the behavior of lanes 005-008 and 010 with cement-stabilized bases. However, all cores taken from lane 009, the "inverted" pavement, showed that cracks initiated at the surface and were less than 25 mm deep when crack density reached the failure criteria of 5 m/m². No cracks were observed at the bottom of these cores. Furthermore, post-mortem examination of this lane did not show any cracks at the bottom of the asphalt layer. Lane 002, which also had a crushed stone base, showed cracks initiating at the surface and not at the bottom of the asphalt [5]. These observations are consistent with the view that shrinkage cracking in cement-stabilized soil bases may initiate cracking. However, not all asphalt surface cracks were located above transverse shrinkage cracks in the cement-stabilized bases.

From post-mortem investigation, it is concluded that the large differences in pavement fatigue life between the cement-stabilized and the "inverted" base pavements can be attributed to the different characteristics of their interfaces. In addition, as widely recognized, a stone interlayer can delay propagation of shrinkage, environmental, and loading cracks through the asphalt layers.

Selection of Analytical Models

Use of analytical methods to estimate the stress, strain, or deflections of pavements is not a recent innovation. In the early 1940's, Burmister [24], McLeod [25], Acum and Fox [26], and Palmer [27] produced some of the basic theories applicable to analysis of flexible pavements.

Mechanistic flexible pavement design and analysis procedures are typically based on the assumption that a pavement can be modeled as a multilayer elastic or viscoelastic structure on an elastic or viscoelastic foundation. Modeling pavements in this manner allows the calculation of stress, strain, or deflection at any point within or below the pavement structure. However, researchers recognize that pavement performance is influenced by a number of factors, which are not precisely modeled by mechanistic methods. It is therefore necessary to calibrate the output from these models with observations of performance (i.e., empirical correlation). These procedures are often referred to as mechanistic-empirical procedures.

The available structural analysis methods are typically categorized into three classes:

- multilayered elastic method,
- multilayered viscoelastic method, and
- finite element method.

In multilayered elastic analysis, the pavement is modeled as a series of layers, each of which is assumed to be infinite in extent in the x and y directions homogenous, isotropic, and linear elastic in response. The layers are also defined by an elastic modulus, E, and Poisson's ratio, ν . All the layers have finite thickness except the subgrade layer, which is assumed to have infinite thickness. The surface loading is represented by circular areas with uniform contact pressures. BISAR [28], CHEV [28], and ELSYM [29] are some of the programs based on this theory. The layer interface conditions can be represented as perfectly rough or, in some cases, can vary from rough to some condition that is smoother. This feature is available in BISAR.

The multilayered viscoelastic methods are similar to the multilayered elastic analysis system. The primary difference between these two methods lies in the way that the material properties are characterized. Viscoelastic material properties vary with the time of loading and temperature at the time of loading. The series of VESYS [30] programs, developed by the FHWA, are based on this viscoelastic theory.

In the finite element method, the pavement structure is divided into a set of elements, which are connected at their joints or nodal points. The continuous variation of stresses and strains in the real system are replaced by an assumed linear or quadratic variation of displacements, causing constant stresses and strains within each element. For a given element geometry and constitutive equation describing the material behavior, the element stiffness matrix relating unknown nodal displacements and applied forces at the nodes is established using the principle of virtual work or a principle of variation. The global stiffness matrix for the entire finite element system is then developed by superimposing the individual element stiffness matrices. As a result, a set of simultaneous equations, in terms of relationships between forces and displacements, is formed. The system of linear equations is solved using a Gaussian elimination technique for displacement

at all nodal points. With the displacements of all nodal points known, strains and stresses within each element can then be computed.

The finite element method of analysis is the most versatile of these methods for calculating the pavement response for pavement materials, which exhibit non-linear elasticity. The NCHRP 1 - 26 [31] study pointed out that "the finite element solutions are theoretically the appropriate alternative" to layered elastic programs. Currently both two and three-dimensional finite element models are available. FLEXPASS [31] (flexible pavement analysis structural system) and MICHPAVE [32] are two-dimensional finite element programs, which model the pavement three-dimensionally by a two-dimensional axi-symmetric solid of revolution, while ABACUS [33] is a three-dimensional finite element program. Chen et al, [34] in his study has shown the results of the two-dimensional analyses agree with those of the three-dimensional analysis for relatively thin pavements used in highway structures. For this study, FLEXPASS is the finite element program chosen and VESYS 3A-M was chosen to represent the viscoelastic type programs.

Overview of VESYS 3A-M

The computational sequence in VESYS 3A-M [35] consists of three main steps: primary response analysis, damage modeling, and performance predictions, as shown in figure 27. First, the program calculates the primary response of the layered elastic or viscoelastic pavement section to a vertical surface stress over a finite circular area for a given set of input data.

The output of this step (stress, strain, and deflection) combined with additional input data relating to number of load repetitions and empirical damage criteria is then used to predict distress using the damage models. Finally, the output from the damage model analysis is used to calculate the performance in terms of the serviceability index and expected life.

VESYS 3A-M is one of the VESYS computer program series that first began to be available from the FHWA in 1972. Unlike others in this series that operate on mainframe computers, VESYS 3A-M is designed to run on a microcomputer. Since there are many differences in configuration and memory between mainframe and microcomputer, modifications have been made to VESYS 3A-M to permit the program to run on a microcomputer system.

For example, the probabilistic matrix formulation has been revised to allow for compatibility, and the use of finite mathematics has been revised to keep exponential values within the operating range for certain types of computers [35]. However, these modifications do not make VESYS 3A-M less powerful. Table 8 shows the VESYS attributes of all versions. This table shows that VESYS 3A-M has features that are quite powerful, which offer many advantages for use in design and analysis purposes.

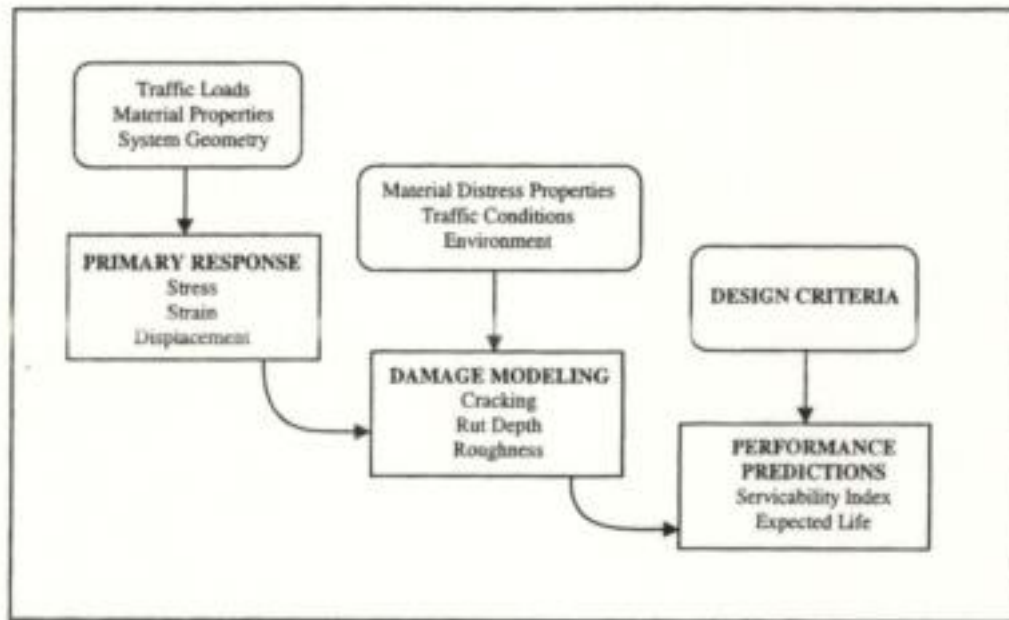


Figure 27
Modular structure of VESYS [35]

In the primary response analysis, the pavement cross section is analyzed using equations based on the theory of elasticity and a layered elastic medium subjected to vertical stationary surface loads to determine the stresses, strains, and deflections that are taken as an approximation of those due to moving traffic loads. The basic assumptions included in the analysis are: (1) the bottom layer has an infinite depth while the upper layers have finite thickness, (2) all layers are infinite in the horizontal direction, and (3) the material properties are time and temperature-dependent [35].

The input data for the primary response analysis include: (1) material properties, (2) system geometry, and (3) the design stationary load.

The input material properties for each layer include creep compliance, coefficients of variation, Poisson's ratio, and modulus. To take into account the environmental effects on the pavement, VESYS 3A-M accommodates up to 25 seasonal periods a year. Thus, the effects of seasonal moisture and temperature variations are reflected through the coefficients of variation and layer moduli for each layer for each season.

Table 8
VESYS Attributes [35]

FEATURES	VESYS VERSION										
	2M	A	G	3I	3A	4A	3B	4B	3AM	D	5
Closed form viscoelastic	x	x		x							
3 layers	x	x		x							
N layers			x	x	x	x		x	x	x	x
Viscoelastic (quasi)			x	x		x		x			
General response			x	x		x		x			
Probability	x	x	x	x	x	x	x	x	x	x	x
Minors (crack)	x	x	x	x	x	x	x	x	x	x	x
System rutting	x	x	x	x	x	x	x	x	x		x
Multiple sessions & radii	x		x	x	x	x	x	x	x	x	x
Low temperature cracking		x		x	x	x	x	x	x	x	x
Elastic (only)					x	x	x	x	x	x	x
Elastic w/ creep						x		x		x	x
Variable season length						x	x			x	
Stress dependant							x	x			
Tandem axle factor							x	x			
Tandem axles							x	x			
Tridem axle										x	x
Dynamic load										x	
Layer rutting										x	x
Microcomputer									x		

The system geometry includes thickness of each layer and number of points in the radial and vertical positions where the primary responses are to be evaluated. For example, the primary response and location of interest for fatigue cracking is the horizontal strain at the bottom of the asphalt layer directly under the load. Therefore, these locations of interest must be identified by coordinates with the center of the load at $x=0, y=0$.

The stationary load is the intensity of load to be applied to the pavement as specified in the design expressed as the load in pounds and the radius of the contact area per wheel. For example, if an 18 kip (80 kN) single-axle load with a 100 psi (0.69 Mpa) tire pressure is used in the analysis, the input must be 9,000 lbs (40 kN) for the single tire load intensity and 5.35 in (136 mm) for the radius of contact area.

Pavement damage is estimated using two models: (1) fatigue cracking and (2) rutting. These two damage models are employed in VESYS because they are the most commonly encountered traffic-induced types of damage in flexible pavements. Each model requires additional input data including traffic conditions, material properties related to the distress, and environmental data. The traffic condition data includes the number of repeated loads in axles per day for each analysis period for which damage calculations are desired. The fatigue model requires, for the hot mix asphalt layers, k_1 , k_2 , and the coefficients of variation, where k_1 is the coefficient and k_2 is the exponent in Miner's Law. Miner's law can be expressed as:

$$D = \sum_{i=1}^m \frac{n_i}{N_i} \leq 1 \quad \bullet \quad (1)$$

where:

- n_i = the number of load applications at the state (i)
- N_i = the number of cycles to failure for that particular state (i)
 $= k_1 (1/\sigma)^{k_2}$
- m = total number of cycles

The rut depth model requires permanent deformation properties α (α) and μ (μ) for each layer of the pavement. The variables α and μ are obtained from plots of data from the repeated load creep test. A detailed explanation on how to determine these coefficients is contained in the next section.

The slope variance model is used to estimate the PSI value based on the rut depth variation predictions from the rutting model. Additional input data required are the terminal serviceability level, level of reliability, standard deviation of initial PSI value, and the system performance properties.

Overview of FLEXPASS

During the NCHRP 1 - 26 project, research staff for the selection of mechanistic analysis procedures suggested an extension of the widely used ILLI-PAVE [36] finite element method. It would accommodate multiple wheel loads and at the same time employ stress-dependent modulus material characterization models. FLEXPASS is a computer program developed by Lytton and Tseng [37] of the Texas Transportation Institute with the ability to accommodate multiple wheel loads and, simultaneously, employ stress dependent material characterization models. The program is based on modifications to ILLI-PAVE, originally developed by Wilson and Duncan, and further modified by the transportation facilities group of the Department of Civil Engineering, University of Illinois at Urbana, Illinois, in 1982. The FLEXPASS program predicts the distress in terms of rutting, fatigue cracking, and slope variance. A simplified framework for FLEXPASS is given in figure 28.

The advantages of this program over layered elastic systems are [37]:

- 1) The finite element method permits pavement layers to be described using non-linear stress-strain relationships,
- 2) The slip between layers is included to account for those conditions in which the adhesion between the layers is imperfect,
- 3) The user can input vertical and horizontal tire contact stresses as nodal forces,
- 4) The pavement material properties can be varied seasonally, and
- 5) The loading configurations can vary from single or dual tires on single or tandem axles.

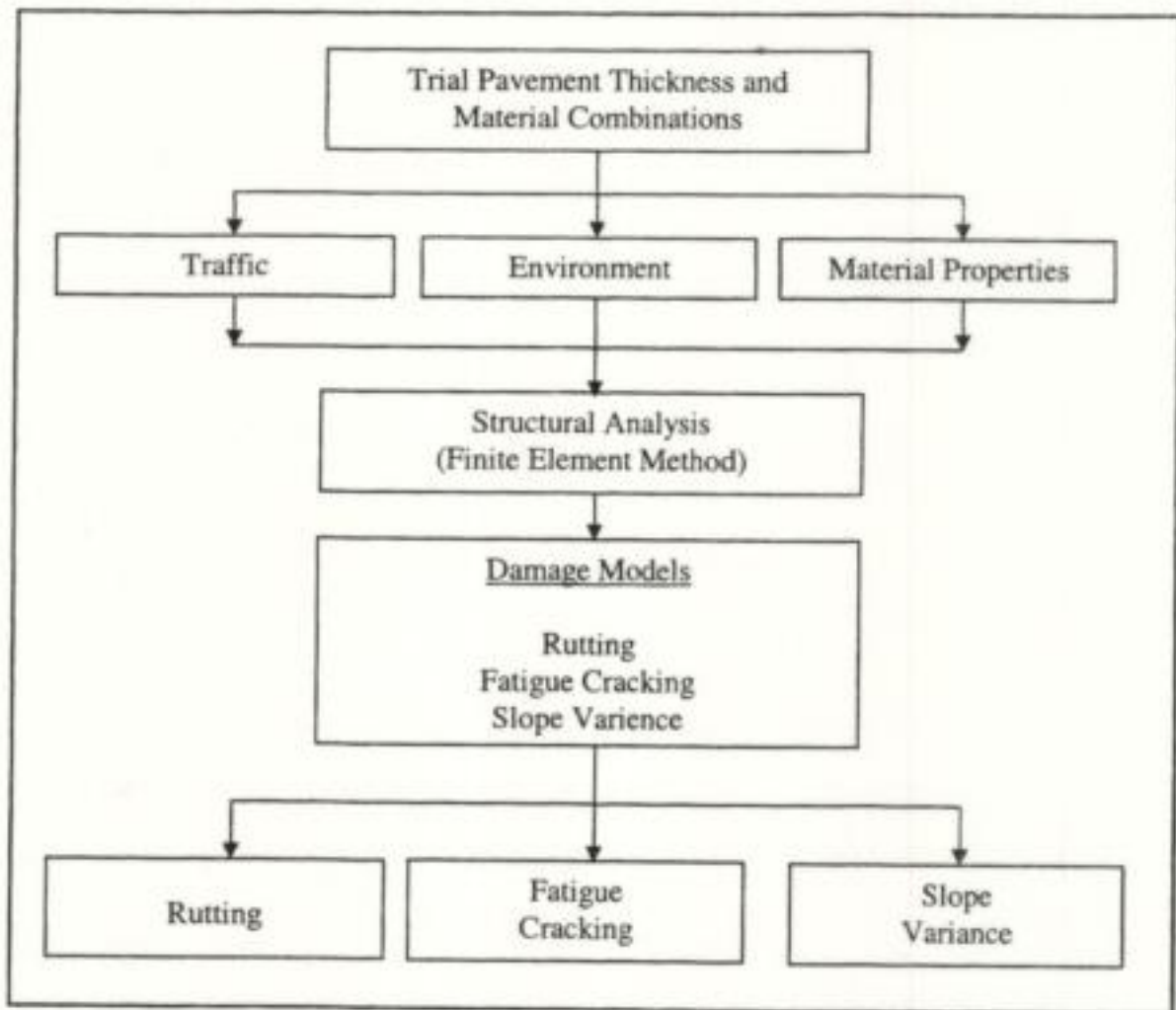


Figure 28
Simplified framework of FLEXPASS

Lytton and Tseng calibrated the rutting and fatigue models by comparing the actual measurements of 12 AASHTO road test sections to the predicted distress from FLEXPASS. They also compared the FLEXPASS predictions to the performance from the Lake Wales road test in Florida. The predicted performance from the calibrated equations matched the observed performance. Hoyt et al [38] compared the predicted performance of asphalt-rubber concrete to that of hot mix asphalt in airfield runways using this program.

The FLEXPASS program has the following limitations:

- 1) The principle stresses in the granular and subgrade layers are modified at the end of each iteration to ensure that they do not exceed the strength of the material as defined by the Mohr-Coulomb failure envelope. The validity of this method for modifying the principle stresses to satisfy the failure criterion has been questioned [39].
- 2) A rigid boundary is installed at the same depth below the subgrade. A depth to the rigid layer of 50 times the radius is generally recommended. Using a deep finite element mesh tends to produce a stiffening effect, resulting in smaller displacements at the surface [40].

Development of Data for Distress Prediction Modeling

VESYS Data

The input data required by VESYS include pavement geometry as well as load and material characteristics. The example included in this report is a prediction of distress for lane 002. Input data describing the materials were obtained from the field, laboratory tests, and from previous work by Anderson et al [41], Hadley [42], and recent data from the LTRC for fatigue. Layer moduli for each layer was backcalculated from the recent FWD testing on lane 001. The material characteristics, including resilient moduli, Poisson's ratio, and the fatigue coefficients, k_1 and k_2 , were obtained from laboratory indirect tensile testing. Permanent deformation parameters, α and μ , were obtained from references 41 and 44. The material characteristics developed by Hadley [42] for Louisiana HMA materials were typical of those used in the ALF test section. Tables 9 and 10 show the material characterization data used in this analysis.

Table 9
Estimated layer moduli, in ksi (Mpa), and fatigue coefficients, k_1 and k_2

Layer	Temperature °F (°C)				
	57.8 (14.3)	67.1 (19.5)	73.8 (23.2)	79.9 (26.6)	81.4 (27.4)
A. Moduli					
Type 8 WC	800 (5,512)	800 (5,512)	600 (4,134)	600 (4,134)	500 (3,445)
Crushed stone base	65 (448)	65 (448)	65 (448)	65 (448)	65 (448)
Select soil subbase	11 (75.8)	11 (75.8)	11 (75.8)		11 (75.8)
Subgrade	1.5 (10.3)	1.5 (10.3)	1.5 (10.3)		1.5 (10.3)
B. Fatigue coefficients for type 8 WC					
$k_1, \times E-03$	0.15	.01342	.004066	1,000	1,000
k_2	3.287	2.888	2.690	2.551	2.522

Table 10
Permanent deformation coefficients α and μ and Poisson's ratio

Layer	α	μ	Poisson's ratio
Type 8 WC	0.4706	0.0247	0.30
Crushed stone base	0.8490	0.0680	0.35
Select soil subbase	0.8900	0.0675	0.40
Subgrade	0.7350	0.0480	0.45

FLEXPASS Data

A detailed description of the input data required for FLEXPASS is contained in reference 37. FLEXPASS has multiple models available for the prediction of rutting, fatigue cracking, and roughness.

Resilient modulus values were determined and plotted by laboratory testing at 40°F (4.4°C), 77°F (25°C), and 104°F (40°C). Values of temperatures representative of when ALF loading was applied to the test lanes are shown in table 11.

Since laboratory test results were not performed on the base materials, a model from the literature was chosen to represent these materials. The model chosen to characterize the granular base material is the K- model with values of K taken from Rada and Witczak [43] as shown in table 12. Some other general material properties required by FLEXPASS for the various materials are included in table 13.

For the select subbase and subgrade material, which are fine-grained materials, the material property model relates resilient modulus to deviator stress with constants determined from laboratory tests performed by LTRC. The equation parameters are included in table 14.

Table 11
Type 8 wearing course moduli for lanes 002, 003 and 004 as determined by interpolating between laboratory test values

Lane	Resilient modulus of type 8 wearing course, ksi (MPa)						
	Pavement temperature, °F (°C)						
	58 (14)	66 (19)	72 (22)	78 (26)	84 (29)	94 (34)	114 (46)
002	722 (4978)	631 (4351)	562 (3875)	497 (3427)	452 (3116)		
003						377 (2549)	
004							278 (1917)

* weighted average pavement temperature (WAPT) at 1.2 inches depth using equations from references 37.

Table 12
Limestone base resilient modulus K-θ model parameters

Parameter	Value
Modulus failure, ksi (MPa)	650 (4482)
Coefficient k_1	14,030
Coefficient k_2	0.37

Table 13
Material characteristics for various materials used in ALF test sections

Layer Component	Density, pcf (kg/m ³)	Poisson's ratio	Liquid content (%)
Type 8 HMA	141.8 (2271)	0.30	5.3 (Asphalt content)
Lime stone base	132.8 (2127)	0.35	6.0
Lime stone stabilized select soil	112.2 (1797)	0.40	8.0
Select soil	107.5 (1722)	0.40	25.0
Heavy clay	105.4 (1688)	0.45	30.0

For the type 8 wearing course, the slope of the creep compliance curve was determined from laboratory tests conducted by LTRC at 77°F (25°C). Using equations developed by Rauhut [44] that relates k_1 and k_2 to temperature the creep compliance slope data included in table 15 was developed. Since pavement deformation tests were not performed on the base, subbase, and subgrade, the option in FLEXPASS of internally generating the permanent deformation parameters using regression equations was chosen. The regression equations are presented later in table 19.

Table 14
Select subbase and subgrade resilient modulus model parameters
determined from laboratory testing

Variable ¹	Layer	
	Subbase	Subgrade
x ₁	-35	-650
x ₂	-68	-650
x ₃	4.1	2
x ₄	11615	4896

¹Models:

$$M_R = x_4 + x_1 (\sigma_d - x_3) \quad \text{for } x_1 > (\sigma_1 - \sigma_3)$$

$$M_R = x_4 + x_2 (\sigma_d - x_3) \quad \text{for } x_1 < (\sigma_1 - \sigma_3)$$

Table 15
Slope of creep compliance plot selected for FLEXPASS analysis

Lane	Pavement temperature, °F (°C)	Slope of the log-log plot of creep compliance versus time
002	58 (14)	0.52
	66 (19)	0.54
	72 (22)	0.55
	78 (26)	0.56
	84 (29)	0.58
003	94 (34)	0.60
004	114 (46)	0.64

Repeated load indirect tensile tests were conducted on the type 8 wearing course at constant stress and 77°F (25°C). From these tests, fatigue constants were determined. In order to determine the relationship between number of loads to fatigue failure and initial strain, test results from at least two different stress levels are required. Since these data were not available, equations from Rauhut [44] were used to develop the values for k₁ and k₂ for each of the pavement temperatures used to describe the ALF loading. The values of k₁ and k₂ from both the laboratory data as well as from Rauhut's equations[44] are included in table 16.

Table 16
Fatigue constants used in FLEXPASS analysis from
LTRC laboratory testing and method suggested by reference 32

Lane	Temp. °F (°C)	k1 and k2 values determined from laboratory sample						Rauhut's method	
		Sample 1		Sample 2		Sample 3		k ₁	k ₂
		k ₁	k ₂	k ₁	k ₂	k ₁	k ₂		
002	77 (25)*	3.93E-04	2.6082	9.78E-07	3.2644	3.05E-05	2.8881	1.52E-06	3.2160
	58 (14)	1.28E-05	2.9833	3.18E-08	3.6395	9.91E-07	3.2630	1.95E-07	3.4408
	66 (19)	4.81E-05	2.8382	1.20E-07	3.4944	3.73E-06	3.1180	7.35E-07	3.2957
	72 (22)	1.45E-04	2.7171	3.61E-07	3.3734	1.13E-05	2.9969	2.22E-06	3.1746
	78 (26)	4.83E-04	2.5856	1.20E-06	3.2418	3.75E-05	2.8653	7.39E-06	3.0431
	84 (29)	1.77E-03	2.4434	4.41E-06	3.0997	1.37E-04	2.7238	2.71E-05	2.9009
003	94 (34)	1.91E-02	2.1832	4.75E-05	2.8394	1.48E-03	2.4629	2.92E-04	2.6407
004	114 (46)	4.95E+00	1.5749	1.23E-02	2.2311	3.84E-01	1.8547	7.57E-02	2.0324

Additionally the coefficients of variation for k₁ and k₂ and the correlation between k₁ and k₂ were chosen to be 0.2, 0.04, and -0.9, respectively. These are typical values recommended in the FLEXPASS manual. Other input values were selected in accordance with the FLEXPASS manual.

DISCUSSION OF RESULTS

Summary of Phase I

Lane 004 failed similarly to lane 002, but lane 003 exhibited a premature localized failure. After all nine lanes had been tested, a section of lane 003 was retested. The failure mode of the retested lane 003A was similar to that of lane 002 and 004.

The development of rutting is shown in figure 4 and the evolution of roughness in figure 7.

Cracking occurred only in areas that were subjected to ALF repeated loading. The asphalt pavement surface showed individual transverse cracks first, and, later, longitudinal cracks appeared and progressed as the transverse cracks grew longer and wider. These transverse and longitudinal cracks gradually innerconnected, forming alligator cracks with the increase in ALF loading passes. The development of cracking in the three lanes is shown in figure 10. Figure 13 shows the crack patterns of the three lanes after the test was finished.

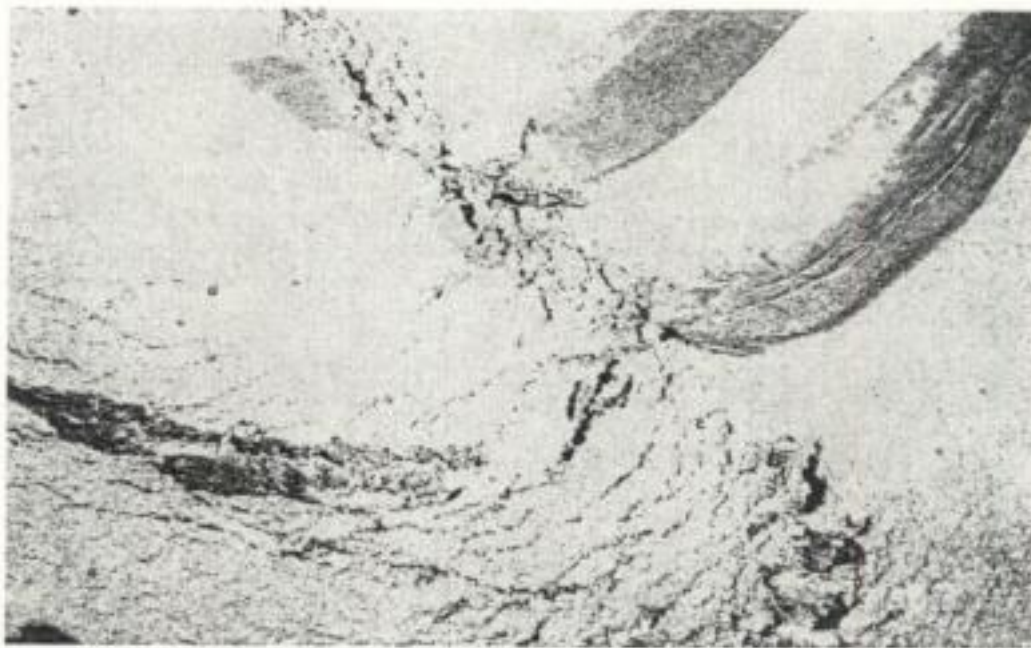


Figure 29
Pavement slippage failure - lane 003

Cracking in lane 003 took an exceptional form, in which the top asphalt layer had a large area of slippage failure. This failure occurred where the wheel loading commenced and where two in-pavement deflection transducers were installed (figure 29). A severe semi-circular wide open crack developed where it was easy to separate the top wearing course layer of asphalt from the binder course, over a longitudinal distance of two meters. Cracking in lane 004 was similar to lane 002 until partial slippage failure occurred again where the wheel first contacted the pavement.

The backcalculated moduli were not always in the expected range. Subgrade moduli estimated

from Dynaflect deflection bowls were generally higher than those obtained from FWD deflection data. The Structural Numbers (SN) measured by Dynaflect at each testing interval and the variations in the subgrade moisture content were too great to calculate changes in SNs as the pavement was loaded. Subgrade moduli values from FWD deflections were adopted for theoretical strain computations.

Strain and pressure gauges were installed to obtain information on the mechanistic behavior of the pavement structure. A total number of 36 strain gauges were used for lane 002 and 003, and 44 were used for lane 004. Pressure gauges were installed at the base/subbase interface.

Calculated strain levels indicated that the strains should be measurable by the equipment installed. Reasonable strain traces were obtained from lane 002. Traces from lanes 003 and 004 were impossible to analyze due to low strain levels. It is suspected that this resulted from very low strain transference between the gauges and the pavement layers. When the gauges were excavated, observations of poor adhesion supported this hypothesis.

Figure 30 illustrates the discrepancy between theoretical estimates of strain and measured strain for the critical bottom of asphalt location. There is great difference in these data. No acceptable results were obtained from the pressure cells mounted in the three pavements.

After completion of loading of all three lanes, trenches were cut through the asphalt layers and the crushed stone layers were excavated to the subgrade. Cone penetrometer tests were performed to estimate subgrade strengths, and nuclear density gauge readings were taken on the stone materials.

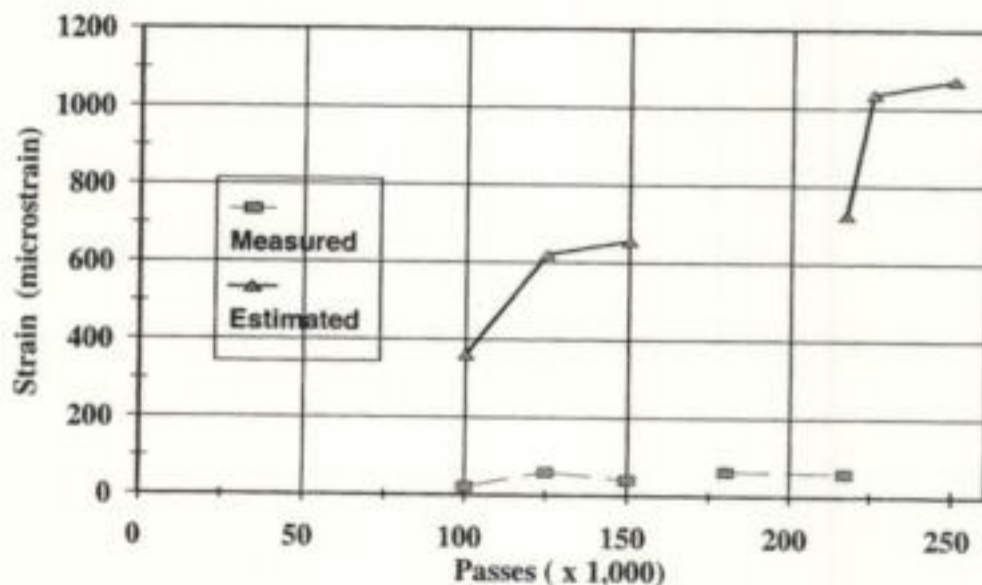


Figure 30
Discrepancy between predicted and measured strains

The presence of a soft layer and evidence of water penetration at the asphalt layer interfaces

exemplify the difficulties in interpreting the effects of the high rainfall and high ground water tables experienced.

After loading, the crushed stone grading indicated an increase in the passing No. 4 fraction from 20 to 50 percent, but there was little change in the other sizes, which suggests a breakdown of particles may have occurred under compaction and/or traffic.

The response of lane 002 to loading was typical of a flexible pavement. Failure was reached at 840,000 ESALs when rutting exceeded 25 mm and cracking exceeded 2.5 m/m². It was judged that a pavement in this condition would have been rehabilitated in DOTD practice.

The response of lane 003, however, was unexpected. The development of a large U-shaped crack at the most heavily loaded section of the test lane was found, resulting in a premature localized failure. The observed pavement life for the retested lane 003A was greater than the original lane. It should be noted that the river stage water level for the retested lane 003A (5.8 m) was much lower than that for the original lane 003 (10.4 m). Lane 004 performed and failed in a very similar manner to lane 002 but with a shorter life. Initial estimates of pavement life based on the Structural Number, as assessed by the DOTD procedure, are given in table 17 along with the actual performance from the results above.

Table 17
Estimation of layer equivalency for lanes 002 and 004

Lane	Actual ESALs (x1000)	Design** ESALs (x 1000)	a1	d1	a2	d2	a3	d3	a4	d4	Subgrade Modulus (ksi)*
002	880	863	0.44	3.5	0.14	8.5	0.06	3.5			10
004	674	648	0.44	3.5	0.14	4	0.1	6	0.06	2	10

* In first phase report, ksi was mistyped as CBR; the value used was a best estimate of subgrade condition. Note, English units are used for consistency with the AASHTO Guide. Thicknesses (d) are in inches.

** 95 % reliability.

An alternative approach, which is considered valid for comparative purposes, is to compare the life of the different pavements when a direct comparison of pavement layers and materials may be established. This is done for lanes 002 and 004 in table 17 by assuming that the initial PSI is five, the terminal PSI is 2.5, the layer thicknesses are as designed, and the layer coefficients are typical Louisiana values for the materials. The subgrade modulus is assumed as 69 Mpa (10 ksi). The reliability is 95 percent. The results indicate that where a value for the layer coefficient of the crushed stone base is 0.14, a comparable coefficient for the stabilized stone layer would be 0.10. In relative terms this means that for the same performance, the thickness of the stabilized stone required would be 30 to 40 percent greater.

The relation between PSI and ESALs estimated from the profile and cracking data for lanes 002 and 004 can be expressed for full depth crushed stone pavement by the following linear regression

model:

$$\text{Lane 002: PSI} = 5 - 0.0025 (\text{ESALs} \times 10^{-3}); R^2 = 0.91, n = 13 \quad (1)$$

$$\text{Lane 004: PSI} = 5 - 0.0049 (\text{ESALs} \times 10^{-3}); R^2 = 0.42, n = 7 \quad (2)$$

Equation (1) could be adopted as an interim means of predicting pavement performance for PMS modeling because it has a reasonable correlation coefficient and sample size (13 observations).

Summary of Phases II & III

Lanes 005, 006, and 007 failed in a similar manner after almost the same number of load repetitions. Extensive cracks formed before the rut depth reached the failure limit. Pumping of material through the cracks in the asphalt layer indicated erosion of some material and loss of support under the asphalt surface layer.

Lane 008 failed prematurely in an atypical manner. A sudden failure occurred after 130,000 ESALs with wide cracks generating potholes. Pumping was observed through the major cracks before the failure started. Trafficking was stopped after 313,000 ESAL, although apart from the localized surface failure, deformations were not extreme. However, it was decided to cease loading the lane because a major repair would have been necessary. The typical failure for structures with stiff cement stabilized bases is due to the propagation of shrinkage cracks. Lane 008 failed due to the presence of water between the asphalt surface layer and the base course. The water caused softening and erosion of the soil cement with subsequent loss of support for the wearing and binder layers.

Due to the unusual, very localized failure, lane 008 was retested at a different location. The second test, lane 008A, also failed with the formation of cracks in the asphalt layer and pumping of soil-cement through the cracks. Lane 008A had a lower pavement life than lane 008 based on cracking and rutting failure criteria, but the failure was not as localized. It should be noted that the river stage 10.4 meters for lane 008A was higher than the 7.6 meters for lane 008.

Lane 009, which had an inverted pavement structure, behaved very well and was the longest lasting pavement tested in this experiment. The failure criteria for rutting and cracking were reached after more than 1.2 millions ESALs. The failure was typical for a pavement with a crushed stone base, because rutting was primarily due to permanent deformation in the stone layer. Fatigue cracking began when the stone base did not provide enough support to the asphalt layer. Thus, it is suggested that inverted pavements are a good solution for high moisture environments and for use over a weak subgrade. The results confirm previous theories and the experimental results [45].

Lane 010 failed sooner than expected, but still in an acceptable amount of time. The failure mechanism was similar to lane 008. The distresses were pronounced but localized.

Post-mortem excavation after loading showed that most of the pavement rutting developed from the unbound crushed stone base layer for lanes 002, 003, 004, and 009. The measurement of

asphalt layer thickness, from cutting cross section trenches and cores taken from the trafficked areas, indicated only a slight reduction of asphalt concrete layer thickness. A more detailed discussion of the failure mechanisms is provided in Romanoschi [46] and Li [22].

The response of lane 009 to loading was as expected. Deflections, deformation, roughness, and cracking all increased with the number of load repetitions at an increasing rate when the wheel load was increased. The modulus backcalculated from falling weight deflectometer (FWD) data decreased with loading. Clearly the "inverted" pavement performed well. This is attributed mainly to the high modulus of the crushed stone base generated by confinement between the asphalt and the cement-stabilized subbase and creating a medium for moisture discharge and a means of absorbing cracks reflecting from the soil cement.

Initial estimates of pavement life based on the structural number, as assessed by DOTD procedure are given in table 18 together with actual observed performances. The rutting life is based on a linear regression of the mean profile data with the life in ESALs estimated at a rut depth of 25 mm. The cracking life is measured in ESALs estimated to a crack density of 2.5 m/m² by a second order polynomial regression, while serviceability life is based on a second order polynomial regression of ESALs against present serviceability (calculated from the rutting, cracking, and slope variance data).

Table 18
Pavement Life (x 1000 ESALs)

Lane Number	Design* (to PSI=2.5)	Rutting (to 25 mm)	Cracking (to 2.5m/m ²)	Serviceability** (to PSI=2.5)
002	484	628	966	825
003	233	111	-	146
003A	233	883	467	1274
004	373	359	574	488
005	1038	351	235	269
006	1038	449	198	296
007	1038	725	231	305
008	824	427	304	-
008A	824	383	196	400
009	1095	1207	1138	1348
010	844	656	-	496

* Subgrade modulus = 4,350 psi (30 Mpa) and experiment showed considerably high water table in site; Reliability = 50 %.

** Determined from quadratic regression fit of PSI against ESALs.

Comparison of Performance of Base and Subbase Materials

The performance of the base and subbase material combinations was also evaluated by comparing the development of rutting, roughness, and cracking observed during ALF loading for each test lane. Plots were prepared to graphically summarize the performance and to more easily make the comparisons among test lanes with the same or different base.

Rutting Performance Comparison

Figure 31 shows the summary of rut depth for lanes 002 through 010 versus the number of equivalent single axle loads (ESALs). The ESALs were obtained by multiplying the number of passes, which represents the number of ALF passes obtained from the field, with an axle load coefficient from Appendix D of 1993's AASHTO guidelines. To determine the conversion factor, the structural number (SN) of each section was calculated using Louisiana "a" values and the thicknesses of each layer. The calculated SN values were: 3.12, 3.03, 3.16, 3.12, 3.12, 3.12, 3.12, 2.16, and 3.22 for lanes 002 through 010, respectively. For the SN value for each lane and an axle load of 44.48 kN (10 kips), load equivalency factors (LEF) of: 1.48, 1.49, 1.48, 1.48, 1.48, 1.48, 1.48, 1.48 and 1.48 were found for lanes 002 through 010, respectively. For an axle load of 12.30 kips (54.71 kN) and the appropriate SN, LEFs of 4.01, 4.02, and 4.02 were found for lanes 008, 009, and 010. For an axle load of 14.6 kips (64.94 kN) and the appropriate SN, LEF of 6.7 was found for lanes 002 and 009. These values were obtained by the interpolation in Appendix D of the 1993 AASHTO guidelines.

One of the criteria that can be used to evaluate the performance of a flexible pavement is its ability to carry loads before reaching a critical rut depth. The slower the rut depth development, the better the pavement structure performs. Figure 31 was obtained by averaging the rut depth on stations 4, 5, 6 and 7. Since these stations are located in the middle of each test lane, the touchdown effect can be ignored and a uniform load application can be expected. As shown in figure 31, the ALF loading was terminated at different rut depths on the different test lanes. In lane 002, for example, the ALF loading continued after 721,000 ESALs, where the rut depth reached approximately 1 in (25 mm), while the loading on lanes 003, 006, 007, 008, and 010 was terminated with rut depths of less than 0.60 in (15 mm).

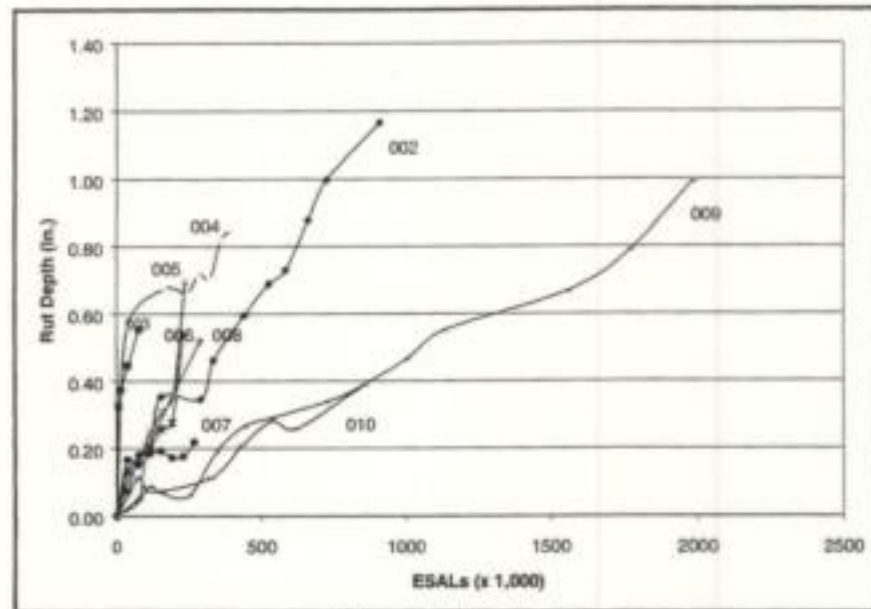


Figure 31
Average rutting development for lanes 002 through 010

Therefore, to compare the relative performance for each lane, a common rut depth of 0.75 in (19 mm) was used as the basis for the comparison. Since some lanes did not carry loads until the rut depth reached 0.75 in (19 mm), a simple regression analysis was performed to determine the relationship between rut depth and the number of ESALs for each test lane. Table 19 presents each model and the coefficient of determination (R^2).

Table 19
Regression model for rut depth versus ESALs

Lanes	Model	R^2
002	Rut = 0.0012 ESAL + 0.05	0.98
003	Rut = 0.0031 ESAL + 0.3149	0.99
004	Rut = $1E-6$ ESAL ² + $1E-4$ ESAL + 0.5689	0.90
005	Rut = $1E-5$ ESAL ² - 0.0014 ESAL + 0.1694	0.93
006	Rut = $1E-5$ ESAL ² - 0.0017 ESAL + 0.2025	0.91
007	Rut = $6E-10$ ESAL ⁴ - $4E-7$ ESAL ³ + $7E-5$ ESAL ² - 0.0054 ESAL + 0.285	0.95
008	Rut = 0.0021 ESAL - 0.0743	0.97
009	Rut = 0.0005 ESAL + 0.0126	0.98
010	Rut = 0.0004 ESAL + 0.0388	0.91

Using the above models, the approximate number of ESAL applications required to produce a rut depth of 0.75 in (19 mm) was determined. The results from the relative performance comparison are shown in figure 32. Figure 32 shows that lane 010, which was constructed using 12 in (305

mm) of four percent plant mix soil cement base without subbase material, provided the best performance in terms of rutting resistance. Lanes 009 and 002 had the next best anti-rutting characteristics, while lanes 004, 005, 006, 007, and 008 performed comparatively lower. Lane 002, which is the crushed stone control section, performed better than lanes 003, 004, 005, 006, 007, and 008.

A post-mortem evaluation showed that some permanent deformation occurred in the surface layer, but most occurred in the base layers. [47] As the pavement cracked, water penetrated and softened the very top of the soil cement base. No other pavement layer appeared to have measurable permanent deformation. Therefore, the hypothesis that the base layer contributed to the rut depth development was justified by the post-mortem evaluation.

Roughness Evaluation

The roughness of the test section was determined from the longitudinal profile as generated by the ALF profilograph. An MS Excel 97 macro, called IRI PROFILER, was written to automate the analysis. The macro was based on the algorithm proposed by Sayer and Karamihas [48, 49]. The macro first read the profile data and put it in the Excel worksheet. It then asked the user to select the profile data to be analyzed and to select the interval over which the roughness was to be calculated. There are two types of outputs from the analysis: predicted roughness of the profile in International Roughness Index (IRI) units and the ride number (RN). Figure 33 summarizes the roughness of lanes 002 through 010, respectively.

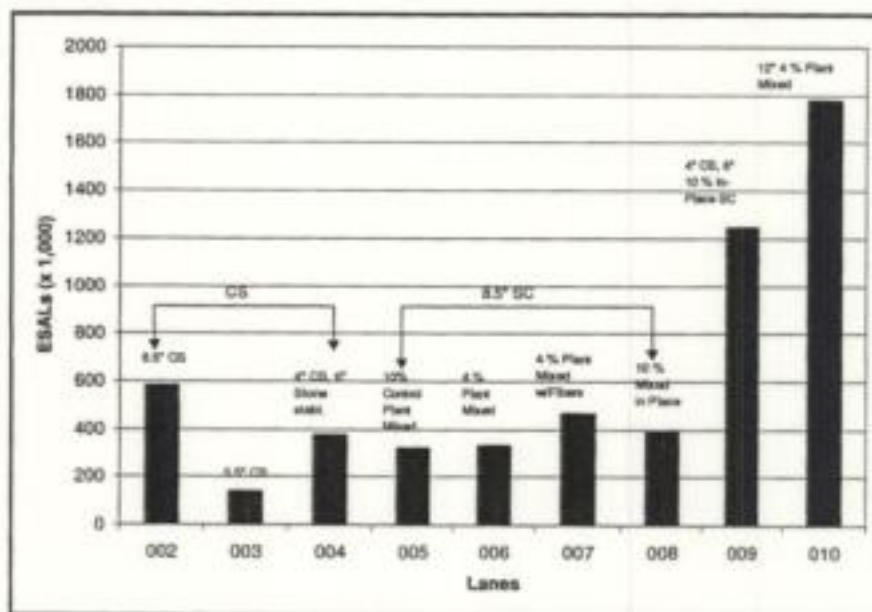


Figure 32
Performance comparison at a rut depth of 0.75 in (19 mm)

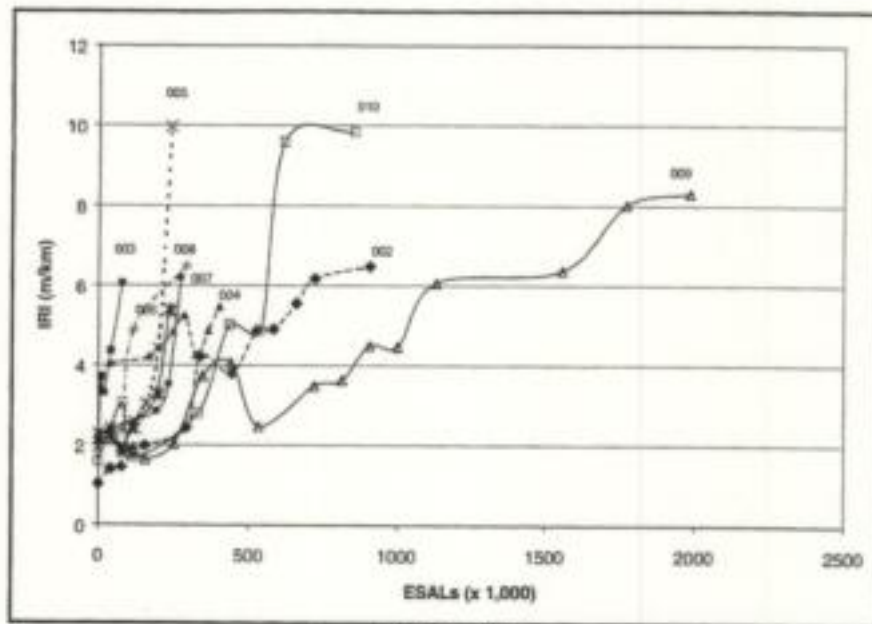


Figure 33
Summary of IRI roughness development for lanes 002 through 010

The IRI values presented in figure 33 were the average of the three lines of the profile data, the centerline profile, and those 12 in (305 mm) to the left and the right of the centerline. In addition, data from the first 60 in (152 cm) of the profile, where the touchdown of the load occurred, were excluded from the analysis to eliminate the premature distress occurring there.

Even though the FHWA has required that the roughness survey results be expressed in IRI, many engineers are not as familiar with IRI as they are with serviceability index (SI). Therefore, the above IRI results have been converted to SI using the following approximate relationship proposed by Patterson [50]:

$$SI = 5.0e^{-0.18IRI} \quad (3)$$

Using data from figure 33, the approximate SI values were calculated using equation three for each lane of the ALF sections. These values are presented in table 20. After testing all sections, the SI values were below 2.0, meaning the sections had been loaded to a point where the pavement is considered to be in an unacceptable condition.

Figure 33 shows the roughness development of each lane. There is a large variability in their behavior, making a performance comparison difficult. Therefore, to make the relative performance comparison among the lanes, an analysis was conducted similarly to that used to compare the rutting development. First, a regression analysis was performed on data from each lane to predict the relation between ESALs and IRI. Then, by setting IRI equal to 3.8 as the terminal serviceability criterion, which is equivalent to the SI value of 2.5 as suggested by Patterson [50], the number of ESALs required to produce the IRI of 3.8 was predicted from the regression equation (Table 20).

Table 20
Approximate relation between IRI, SI and RN for each lane

Lanes	Beginning of Test			End of Test		
	IRI	SI	RN	IRI	SI	RN
002	1.03	4.2	3.3	6.49	1.6	1.41
003	2.12	3.4	3.07	6.06	1.7	1.57
004	4.05*	2.4	2.16*	5.48	1.9	1.73
005	1.94	3.5	3.18	9.97	0.8	1.1
006	2.29	3.3	2.9	5.41	1.9	1.73
007	2.38*	3.3	2.93*	6.2	1.6	1.6
008	2.38*	3.3	2.93*	6.5	1.6	1.25
009	1.93*	3.5	3.04	8.32	1.1	1.02
010	1.59	3.8	3.4	9.84	0.9	0.61

*No data available at ESALs = 0

Cracking Development

Figure 34 shows the crack development for lanes 002 through 010. As can be seen, the overall evaluation showed that lanes 009 and 002 provided the best performance in resisting cracking followed by lanes 004 and 010. As for lane 010, even though it seems to have a good crack resistance, the result is not conclusive because loading was terminated at approximately 459,000 ESAL when the IRI reached 10. Lane 004 also showed good cracking resistance. This performance pattern is very similar to those obtained from the roughness and rutting evaluations.

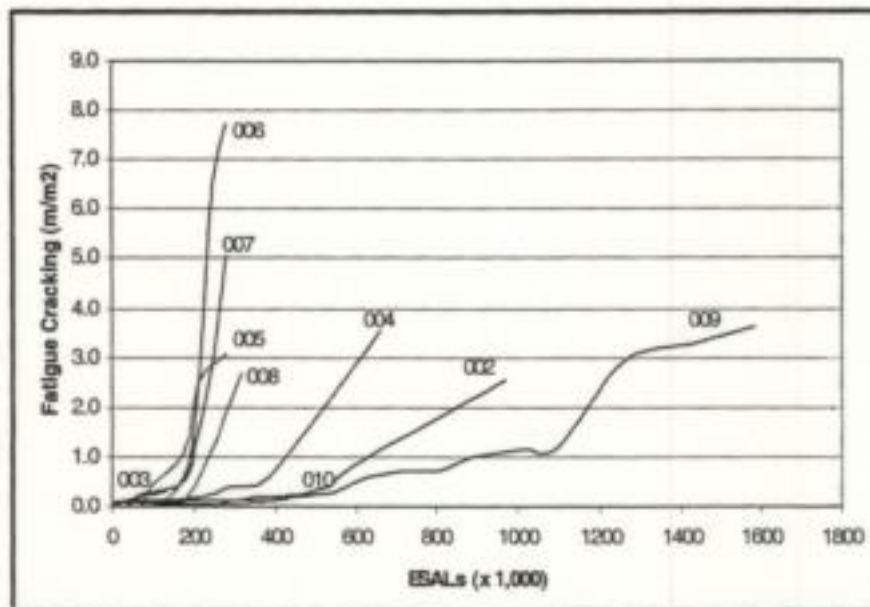


Figure 34
Crack development for lanes 002 through 010

The crack development in figure 34 also showed that crushed stone base material, lanes 002, 004, and 009, resisted cracking much better than the soil cement bases represented by lanes 005, 006, 007, and 008. It also indicated that in-place soil cement, represented by lane 008, has a slightly better performance in resisting cracking than that of plant-mixed soil cement, which occurred in lanes 005, 006, and 007. Lanes 005, 006, and 007 have the worst cracking performance. As shown in figure 34, after about 200,000 ESALs, lanes 005, 006, and 007 developed very steep crack development curves.

The data in figure 34 shows no clear difference in cracking in the soil cement of lanes 005, 006, and 007. The data also show that the best performance was achieved when using stone over a soil cement subbase as in lane 009. In other words, using soil cement as the subbase rather than as base material creates superior cracking resistance. When used as a base, the soil cement materials form shrinkage cracks that later reflect to the surface. However, the stone base intercepted those cracks and delayed their reflection to the surface. Post-mortem evaluations showed that there was evidence of cracking in the soil cement bases [47].

Reflection cracking plus softening of the soil cement immediately below the HMA may help explain why lanes 005 through 008 failed according to the roughness criteria. The rapid roughness development on these lanes may be due to premature cracking. This caused water penetration and softening of the soil cement that later contributed to the acceleration of the roughness development.

Performance Analysis

A series of questions were stated in the proposal. These questions and the responses derived from the experiment are:

What is the relative performance and strength of the 216 mm thick limestone base as compared to the other configuration of limestone bases tested in phase I of the research?

The comparison here is between lane 002 with 216 mm of limestone, lane 003 with 140 mm of limestone over a geo-grid, and lane 004 with 100 mm of limestone over 150 mm of stone stabilized soil. Figure 35 and table 18 show the results for rut and crack progression. It was evident that lane 003 suffered a premature failure when an anomalous crack developed close to the point of load initiation and where pavement instrumentation may have permitted water entry (figure 29). Whatever the cause, the local failure created a separation of the two asphalt layers. The data for lane 003 are therefore excluded from the comparison. A repeat test was conducted on lane 003. The performance this time was similar to lane 002. However, there was about a year delay between tests.

The results show that the flexible pavements (lanes 002 and 004) performed in a very similar manner; thus, the one-on-one comparison is valid. It may be estimated that the layer coefficient for the stone stabilized layer is 0.10 by backcalculation from the AASHTO formula for structural number and pavement life. These calculations assume the other layer coefficients and adopt the nominal thicknesses.

The 215 mm crushed limestone base, typical of current practice, performed in accordance with expectations and better than the other configurations tested. It is concluded that a reasonable value for the layer coefficient for stone stabilized soil base is 0.10.

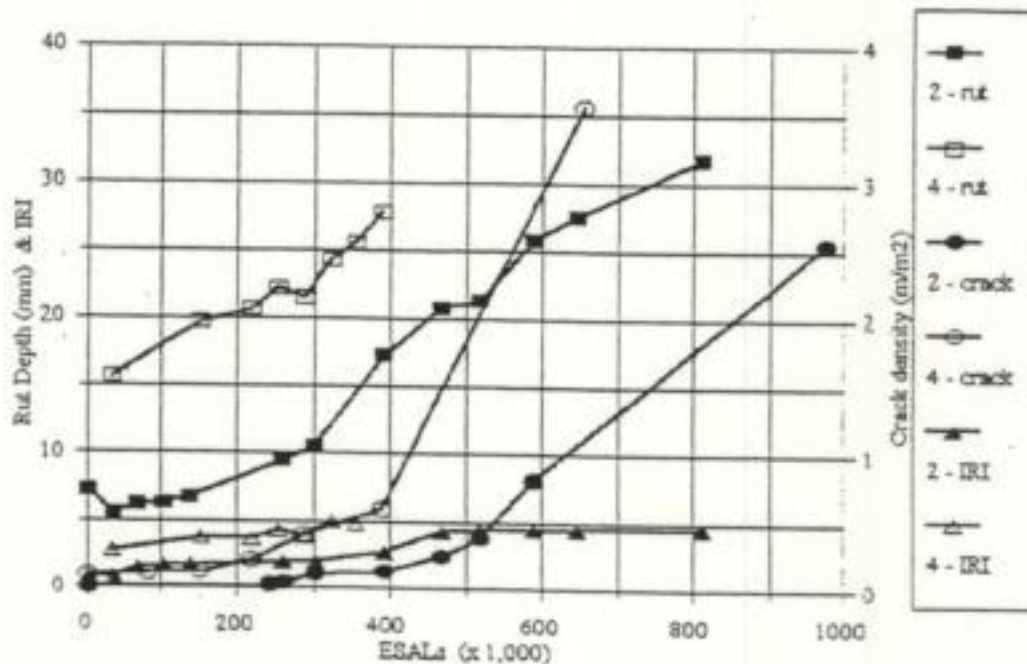


Figure 35
Performance comparison: lane 002 vs. 004

Does a high strength geo-grid placed at the bottom of a limestone base layer significantly increase the strength and long term performance of limestone bases?

Lane 003 failed prematurely at the surface and the repeat test was conducted. Lane 003A (repeat test) far outlasted expectations. This was due, in part, to very different ambient conditions. The repeat test proved the effectiveness of geo-grid materials in the pavement structure. River stages were much lower in the retest which was conducted about a year later.

Are stone stabilized subbases a feasible alternative to the other limestone configurations relative to strength, performance, and cost?

A stone stabilized subbase is a feasible alternative when assessed by accelerated loading. The stone-stabilized subbase performed as if it were a flexible pavement layer with an AASHTO layer coefficient of 0.10. This result must be regarded as tentative until further data is available from future trials. A full scale field trial is warranted to confirm this finding. However, it implies that adequate pavement could be constructed by substituting a 40 percent greater thickness of a stone-stabilized subbase for a crushed limestone base. An adequate thickness of the better-quality crushed limestone base should be retained in any design using a stone stabilized subbase to

provide high strength support to the asphalt layers.

Will pavements constructed with a reduced cement content and plant mixed soil cement base have a lower level of shrinkage cracking compared to those constructed on plant mixed soil cement base, using standard cement content design procedures?

The comparison here is between lanes 005 and 006, the "standard" 10 percent cement mix versus a four percent cement mix. Figure 36 shows very similar performance for both test lanes, therefore, a one-on-one comparison is possible. Table 18 shows that the observed lives are very similar and that surface cracking failure occurred before rutting. Evidence from the post-mortem profiles show that rutting occurred as a result of erosion and/or softening of the cement-stabilized soil base. The estimated lives suggest that lane 006 should have a longer life, in terms of rutting development, but a shorter life in terms of crack development criteria. This is consistent with early cracking development in the weaker soil cement, a matter that permits greater dynamic deflection because of a lower effective modulus and an earlier onset of fatigue cracking at the surface of the asphalt.

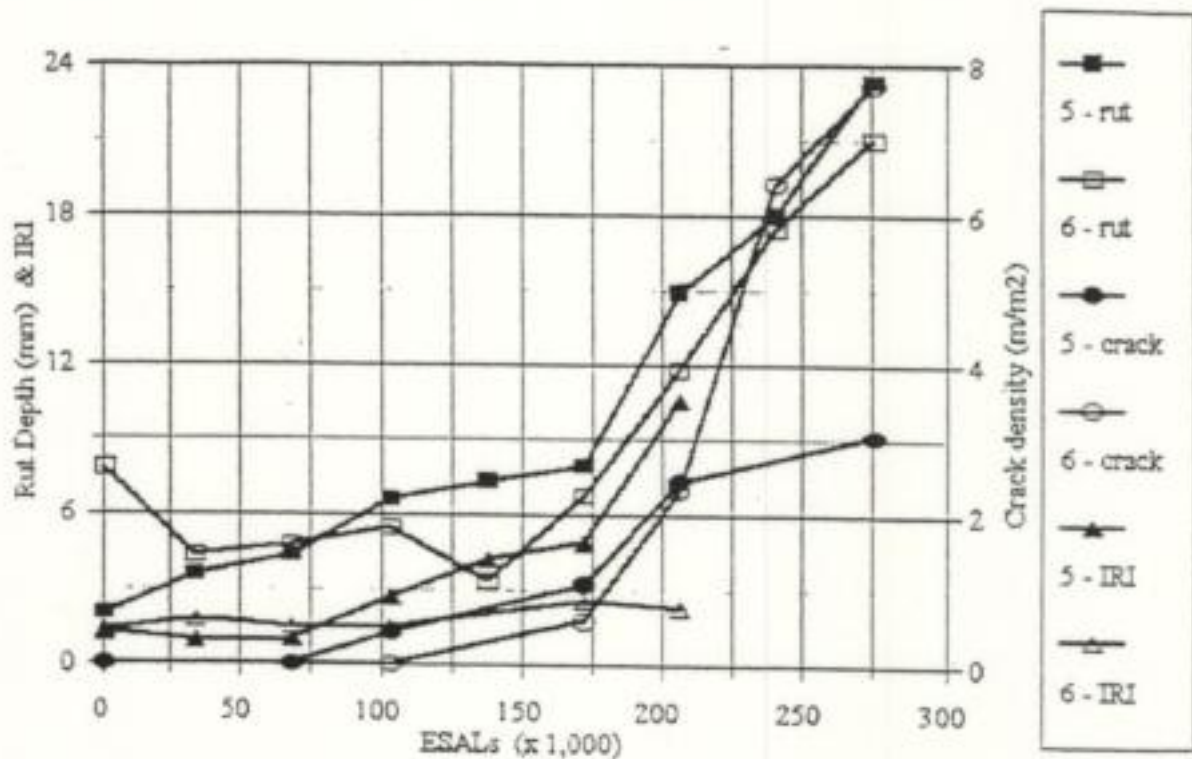


Figure 36
Performance comparison: lane 005 vs. 006

What are the relative strength and performance differences between pavements constructed on high strength soil cement bases as compared to a soil cement base with less strength, yet containing fewer cracks, when subjected to accelerated loading?

The comparison here is between lanes 006, 007 and 010, stabilized with four percent cement, and lanes 005 and 008 with 10 percent cement. Cracking and rutting development in lane 010 (305 mm thick) was slower than the other lanes (figures 37 and 38). The observed lives are shown in table 18. The interpretation based on observed values is that there is little difference between the behavior of lane 005 and lane 006 based on rutting data. The thicker layer of four percent plant mixed cement-stabilized base (lane 010) had the longest life judged by both rutting and cracking.

It is concluded that there is no practical difference detected under this accelerated loading experiment in the strength and performance of silty soil stabilized with four percent or 10 percent cement, although the laboratory unconfined compressive strength for the 10 percent cement is over two times greater than that of the four percent. However, significantly better performance is achieved by a greater thickness of the stabilized layer, and a longer term field trial should be considered.

Will the addition of fiber reinforcement significantly increase the relative strength and performance characteristics of soil cement bases designed and constructed with a reduced cement content?

The comparison here is between lanes 006 and 007 (figure 39), both with a four percent cement plant mix-stabilized base of the same thickness. Lane 007 is fiber-reinforced. Observed and estimated lives, shown in table 18, show that the estimated values for lane 007 exceeded those for lane 006. However, the extrapolated results must be viewed with caution because of the limited data.

The conservative conclusion must be that this accelerated loading trial indicated that fibers do help improve performance of pavement structures. However, additional research is recommended.

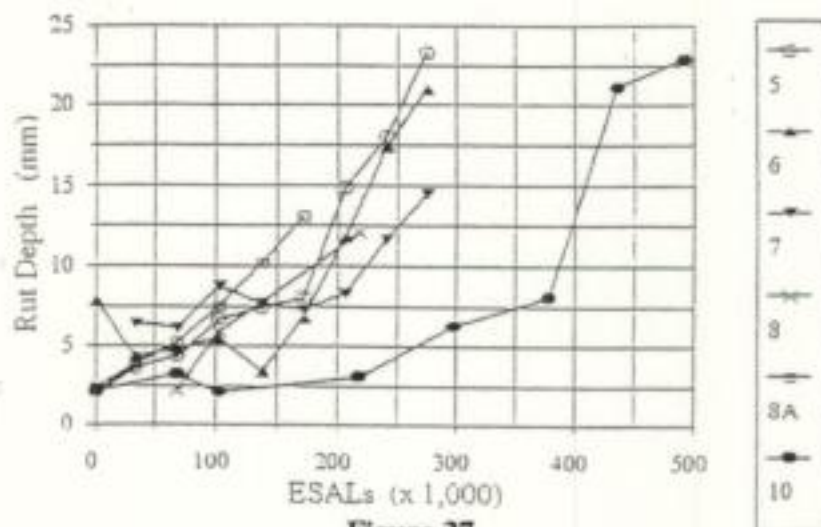


Figure 37
Crack development comparison: lane 006, 007 & 010 vs. 005, 008 & 008A

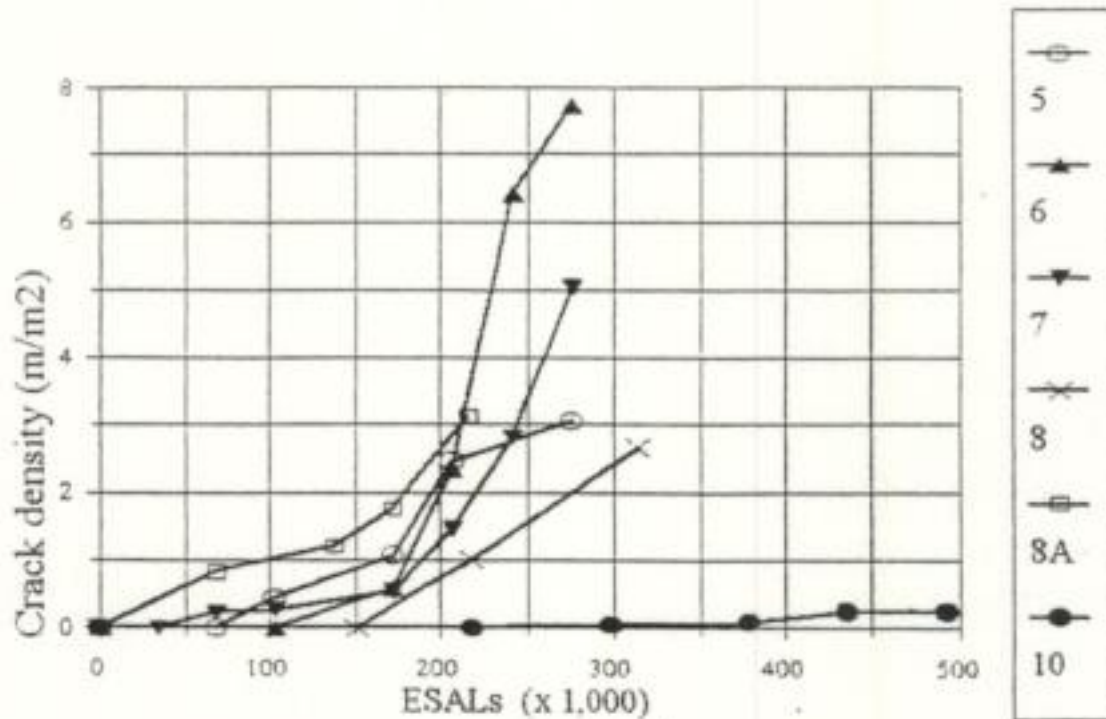


Figure 38
Rutting development comparison: lane 006, 007 & 010 vs. 005, 008 & 008A

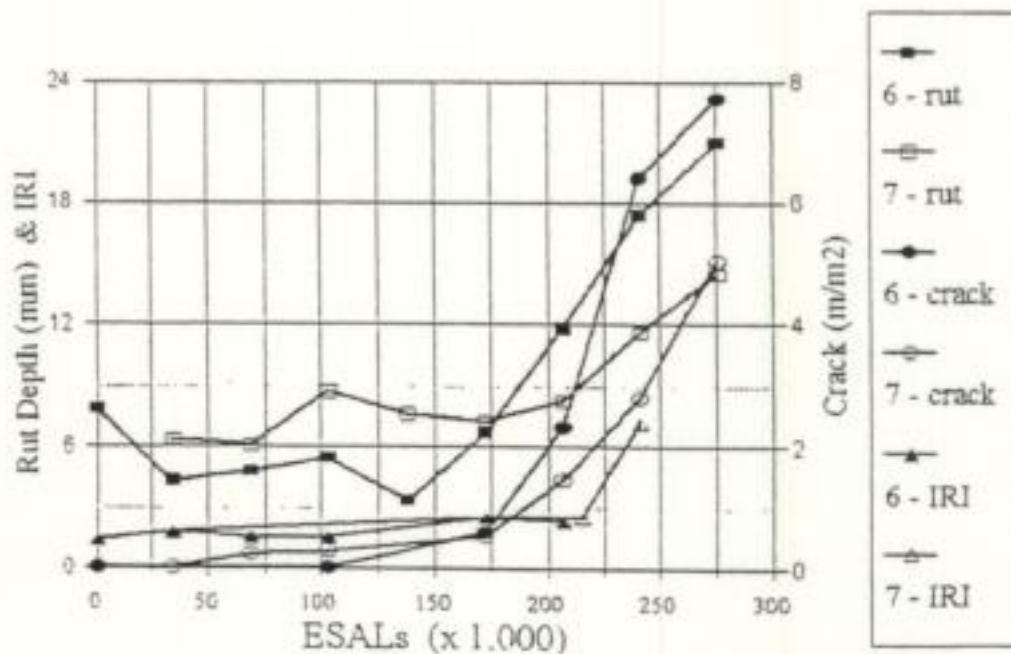


Figure 39
Performance comparison: lane 006 vs. 007

The primary questions anticipated to be answered by Phase 3 research are as follows:

Will increasing soil cement thickness resulting from a reduction in cement content overcome the potential load performance shortcomings of a lower strength base?

The comparison here is between lanes 005, 008 and 010. Lanes 005 and 008 have a 10 percent cement laid 215 mm thick, and lane 010 has a with four percent cement plant mix laid 305 mm thick (figure 40). The laboratory unconfined strength of lanes 005 and 008 (with 10 percent cement) is almost two times larger than that of lane 010 (with four percent cement). It is clear that all forms of distress developed at a slower rate in lane 010 and thus the life of that pavement was greater than that of the "thinner but stronger" pavement of lanes 005 and 008.

Does a 100 mm stone interlayer between the soil cement base and the HMAC surfacing significantly decrease reflective cracking when the pavement sections are loaded in an accelerated manner?

The comparison here is between lane 009 with the 100 mm stone layer and all other lanes. Figure 41 shows the crack progression results, indicating that the performance of the "inverted" pavement far exceeds that of all other stabilized base pavements in terms of crack progression. The rutting performance and PSI follow the same trend (figures 42 and 43). The enhanced performance is attributed, mostly, to the high strength achieved by the confined crushed stone layer, which also greatly reduced the transmission of reflective cracking and improved drainage achieved by the presence of the crushed stone layer.

It is concluded that the 100 mm stone interlayer makes a considerable contribution to the performance of the thin (150 mm) 10 percent cement-stabilized base and decreases cracking under accelerated loading. Again, a long term field trial is recommended to confirm that this advantage is retained under long term loading.

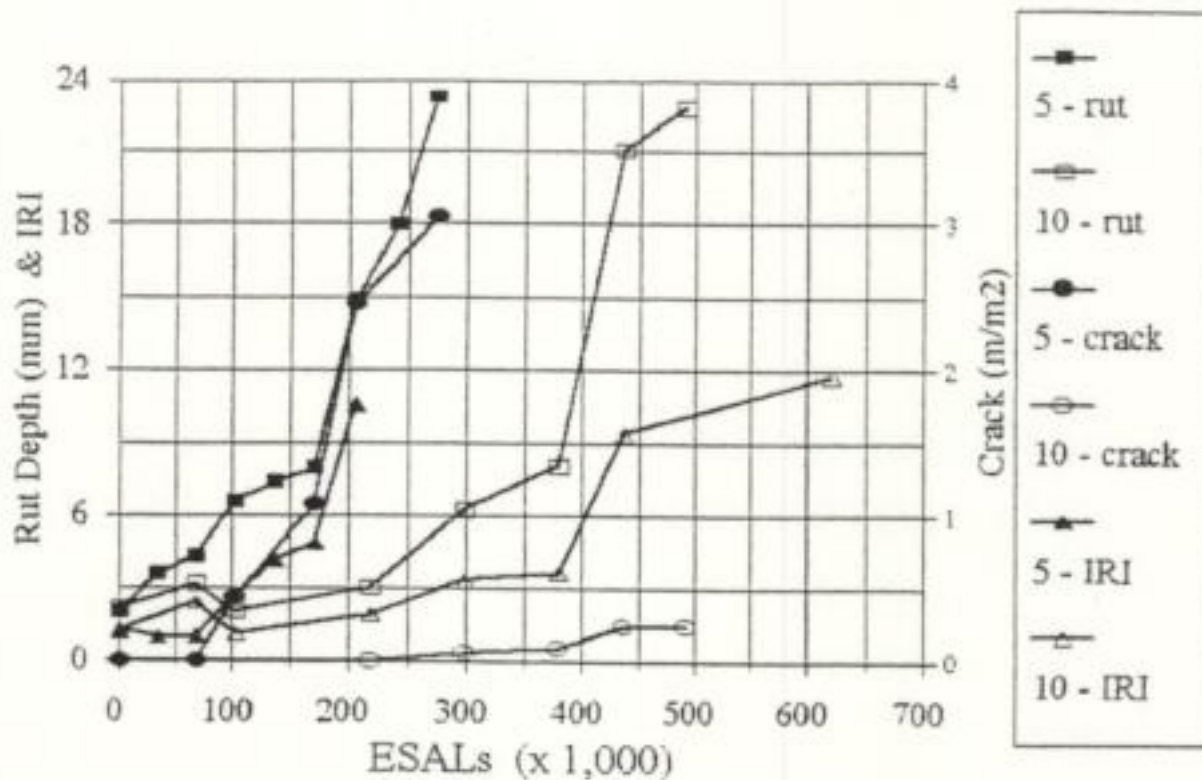


Figure 40
Performance comparison: Lane 5 vs. 10

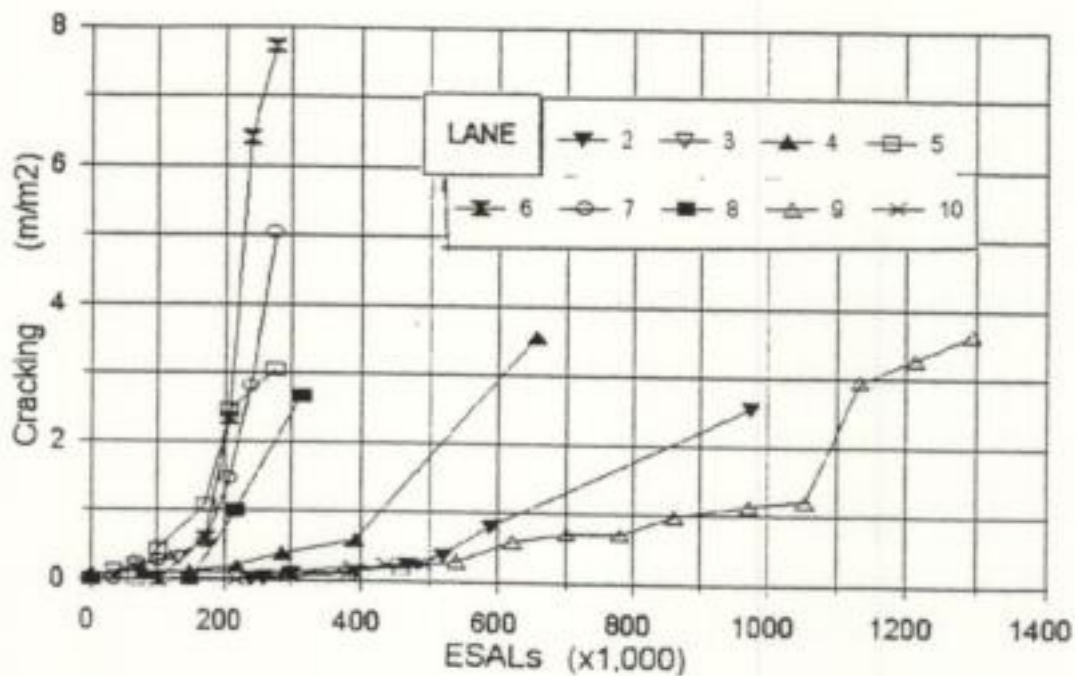


Figure 41
Cracking development - all lanes

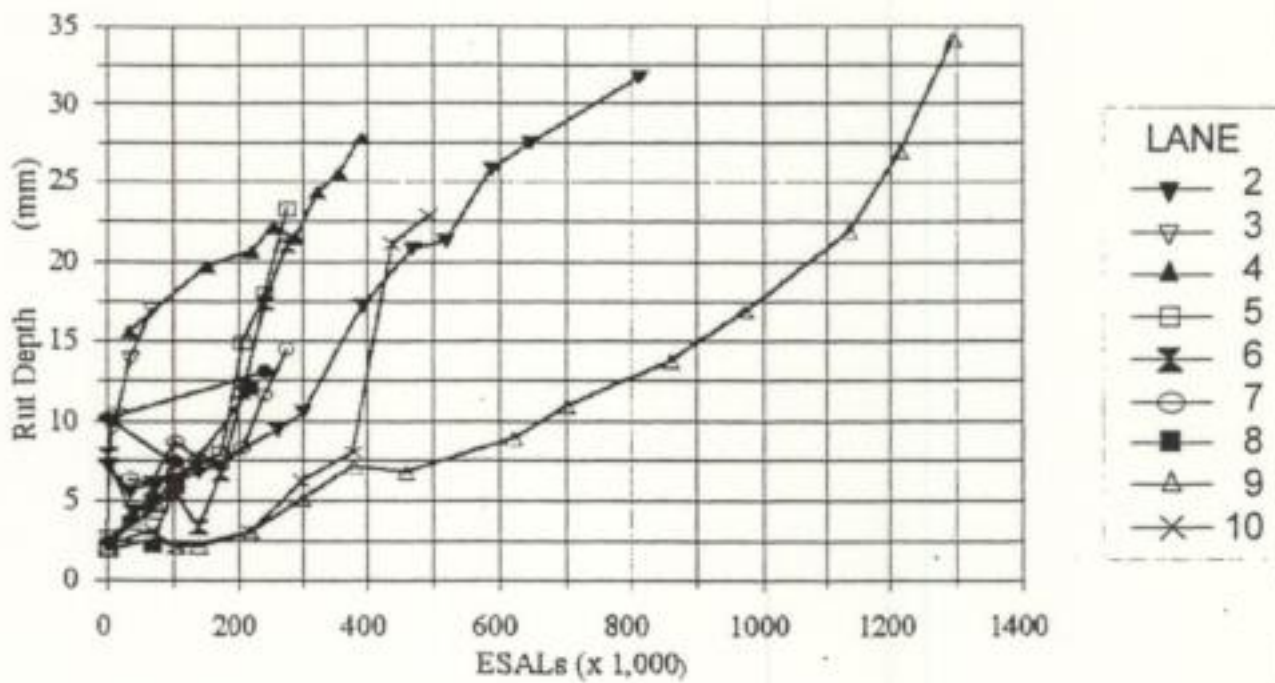


Figure 42
Rutting development - all lanes

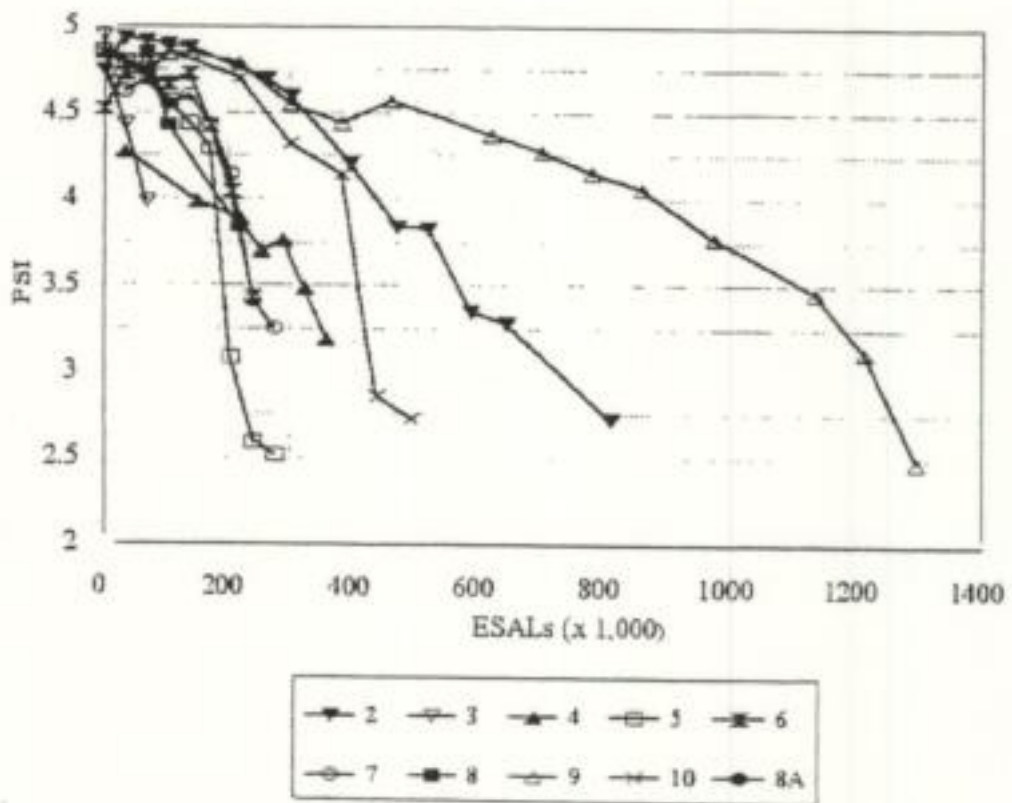


Figure 43
PSI evolution - all lanes

What are the relative strength and performance differences, when subjected to accelerated loading, between pavements built on bases constructed during this phase as compared to the bases constructed during the other phases?

An attempt to summarize the findings by comparing the various life estimates for the 9 lanes follows. Figure 29 clearly shows that lane 003 suffered a premature failure, yet the retest, lane 3A, lasted ten times longer. Not including environmental differences, the effectiveness of geo-grid fabric is shown here. Lanes 005, 006, 007 and 008, which all had cement-stabilized bases 215 mm thick but with differing cement contents including the fiber reinforcement in lane 007, gave close to the same performance for cracking and rutting. Lane 002, the full flexible stone base pavement, was the only lane to show a significant difference between the rutting and cracking behavior and the IRI. Overall, lane 009, the "inverted" pavement, gave the longest life, followed by lane 002 and lane 010.

Using the AASHTO procedure to assess these results showed that if typical values for the various layer coefficients are used with the nominal thickness data, then the pavements performed much as would be expected except for lanes 005, 006, and 007, which performed worse than would be expected as shown in table 18.

Pavement Performance Models

VESYS Output

Figures 44 and 45 contain the field data and VESYS 3A-M predicted performance. The intensity of fatigue cracking from field data was calculated as follows:

$$ICA = \frac{N}{BL} \times 1000 \quad (2)$$

where,

ICA = crack intensity, in $m^2/1,000 m^2$

N = amount of crack area, in m^2

B = band width of wheel paths, taken as 2 ft. (0.61 m), and

L = length of the pavement section = 38 ft. (12.0 m)

The crack data measured in the field was in terms of linear feet, since the typical alligator cracking patterns had not yet developed. The width of a crack was assumed to be 1 in (25.4 mm) and the crack intensity was then calculated using the ICA equation.

VESYS 3A-M outputs provide two primary sets of information: the primary responses, which include stresses, strains, and deflections that occur in the pavement, and the performance predictions, which include cracking, rutting, roughness, and PSI. The location of the stress and strain is specified in the input statements, which usually refer to any critical locations where performance is to be evaluated. For example, coordinates at the bottom of the asphalt layer need to be specified since this information is needed for fatigue cracking prediction.

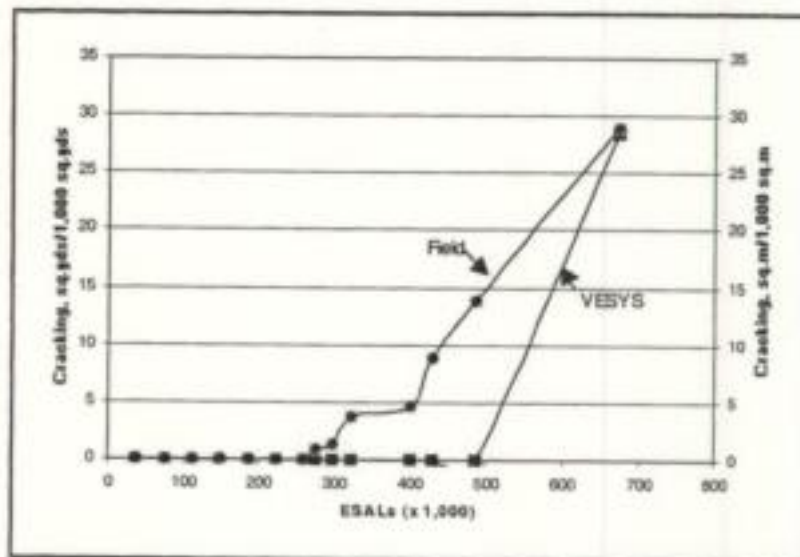


Figure 44

Predicted fatigue cracking and field data, lane 004

Figure 44 shows that at the end of loading VESYS 3A-M predicted an amount of fatigue cracking that closely matched what was observed in the field, although the pattern of crack development is slightly different. VESYS 3A-M predicts that the crack development starts after nearly 500,000 ESALs and grows at a rapid rate until it reaches $28.48 \text{ m}^2/1,000 \text{ m}^2$ at the end of loading. However, in the field, cracking started to develop earlier at about 275,000 ESALs and grew rapidly after 400,000 ESALs until cracking reached $29.02 \text{ m}^2/1,000 \text{ m}^2$ at the end of loading.

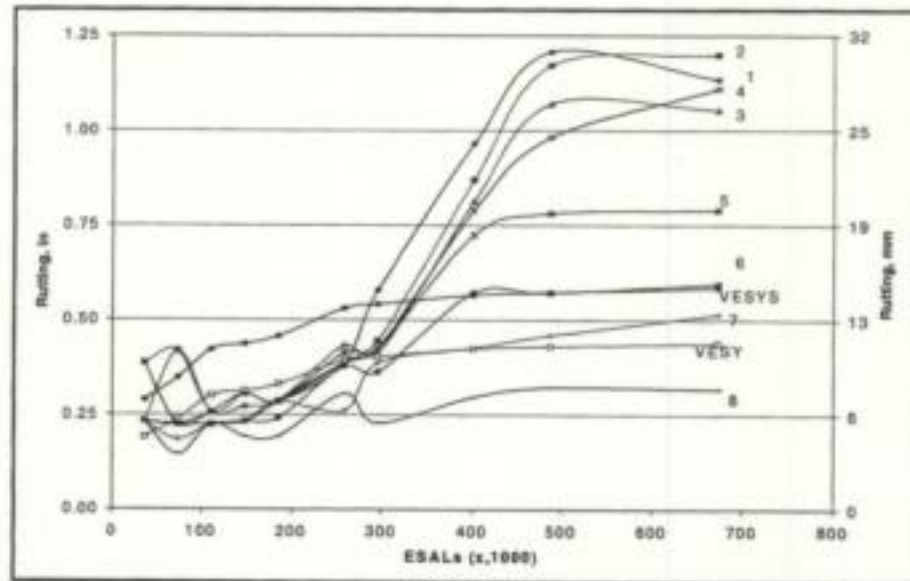


Figure 45
Predicted rutting development from VESYS (upper and lower bound)
and field data at transverse stations 1 - 8 along test lane 002

Crack development in the field progressed at a slower rate than that predicted by VESYS 3A-M. It was also observed from the survey that alligator patterns, the common manifestation of fatigue-induced cracks, did not appear. The cracks were mostly linear. One possible reason for the linear cracking is that in accelerated loading the HMA does not have time to age, so that when the HMA has hardened, the effect of loadings are not observed. Fatigue cracking in accelerated loading may not be the critical distress point and may not be used as the primary criteria for evaluating performance.

Figure 45 shows the field data and VESYS 3A-M prediction of rutting. At early loading, the VESYS 3A-M rutting prediction was higher than that observed in the field. However, after 275,000 ESALs, the observed rutting developed more rapidly at a higher load than did the VESYS 3A-M prediction. This might be due to an increase in load, from 9,800 to 14,400 pounds, after 217,000 passes. The VESYS 3A-M prediction was plotted by including its probability range of the predicted rutting plus or minus one standard error of estimate. S1 (located at the axle touchdown location) through S8 consecutively represent the transverse locations where rutting

was measured along each test lane. The higher values of rutting at S1 through S3 is understandable since the dynamic loading effect near touchdown intensifies rutting (see figure 45 curves number 1, 2, and 3). Therefore, for comparison purposes, rutting at location S4 through S7 is thought to be more representative of normal conditions and is closer to the VESYS 3A-M prediction.

The VESYS 3A-M output also showed that the predicted PSI dropped at a nearly linear rate with a steeper slope during early loading, from 3.68 at the 37,000 ESALs to 2.87 at 205,000 ESALs. Then, the PSI continued to drop to a shallower slope until it reached 2.61 at the end of loading. The failure criteria set up by LTRC started at 0.75 in (19 mm) of rutting or a PSI of 2.3. The PSI loss does not follow the typical design curve pattern, where PSI typically follows a shallow slope with the slope gradually becoming steeper as the pavement nears the end of its life. The reason for this typical pattern is not clear. However, the variation in underlying subgrade soil conditions may be a significant factor.

FLEXPASS Output

Lane 002

Figure 46 shows the crack development for lane 002. No cracking was observed in the field up to 273,000 ESALs. The field fatigue cracking increased very slightly, up to 485,000 ESALs, but then increased rapidly to 238 ft² / 1000 ft² (238 m² / 1000 m²) as the loading increased to 1,070,000 ESALs. FLEXPASS predictions for fatigue cracking were made using both Rauhut based fatigue coefficients and the LTRC laboratory determined fatigue coefficients. Figure 46 shows that predicted fatigue cracking occurred immediately upon initial loading (1.9 ft² / 1000 ft²) and increased gradually up to 485,000 ESALs. The predicted fatigue cracking then increased at an accelerated rate to 278 ft² / 1000 ft² (278 m² / 1000 m²) when Rauhut's based fatigue coefficients were used and to 327 ft² / 1000 ft² (327 m² / 1000 m²) when the laboratory determined fatigue coefficients were used. The predicted cracking is 17 percent greater than the measured field cracking when using Rauhut's based fatigue coefficients and 35 percent greater when using the laboratory-determined fatigue coefficients.

As shown in figure 47, FLEXPASS predicted that rutting would begin early in the life of the pavement. The predicted rutting begins at a rapid rate and levels off at a depth of 1.13 in (29 mm) as the loading reached 1,070,000 ESALs. The rut depth in the field also started developing early in the life of the pavement with a slight increase until the fatigue cracking began developing at about 400,000 ESALs. The rut depth in the field then increased rapidly as the cracking increased. The predicted rut depth was about 25 percent less than the measured field rut depth.

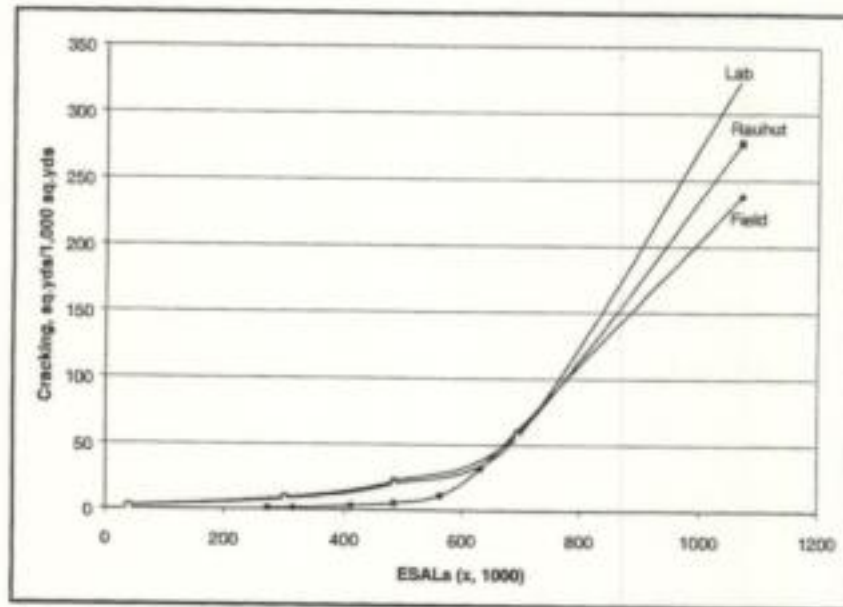


Figure 46
Fatigue crack development for lane 002

As aforementioned, the rate of development of field fatigue cracking increased after 485,000 ESALs. The rut depth prediction model in FLEXPASS does not account for this increase in rutting due to cracking, which is probably a contributing factor causing differences between the field and predicted rutting. FLEXPASS predicted a rut depth of 0.75 in (19 mm). Rut failure was expected to occur at 325,000 ESALs. Observation in the field recorded failure at 420,000 ESALs.

A plot of field and predicted PSI with the cumulative ESALs is shown in figure 48. PSI of the field was calculated using the AASHTO road test equation [51] with the measured field fatigue, rut depth, and slope variance. Slope variance is the primary contributing term to PSI in this equation to PSI.

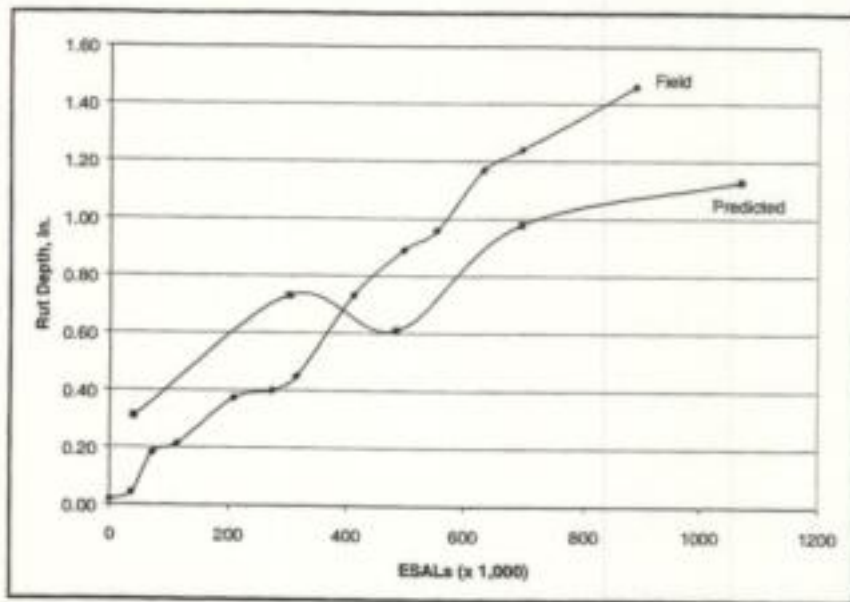


Figure 47
Rut development for lane 002

The initial slope variance measured in the field decreased the field PSI by 1.3. Hence, an adjustment was made in calculating PSI so the initial serviceability index of all the three sections was 4.5. FLEXPASS predicted the PSI would reach 2.3 at 300,000 ESALs while in the field, a PSI of 2.3 was reached at 500,000 ESALs.

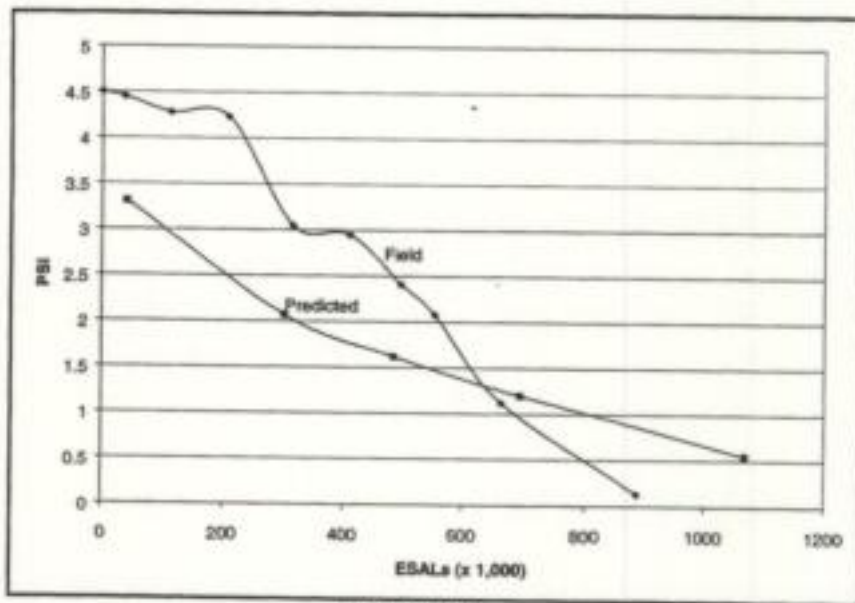


Figure 48
Present serviceability index development for lane 002

Lane 003

Loading for lane 003 was stopped after only 96,000 ALF passes because slippage cracking developed in the three feet following the loading wheel touchdown point. The balance of the lane experienced only a slight cracking. Slippage cracks are crescent-shaped cracks that point in the direction of the load and typically occur when the tack coat between the wearing course and binder course is too thin to produce a full bond between the layers. The reason for the very early failure of the first three feet could be due to the combined effect of the dynamic loading of ALF near the touchdown point and the slippage between the layers due to an inadequate tack coat. Hence, a part of the analysis for lane 003 was performed with slip occurring between the wearing courses.

Lane 003 without slip condition

As mentioned previously, analysis was made for lane 003 with both the slip and "no slip" condition. To accomplish this analysis, lane 003 was divided into two sections. The first three feet of the section was designated as the slip section, and the remainder of the lane was analyzed as lane 003 without slip. Figure 49 shows the fatigue crack development with no slip. For the no slip condition, FLEXPASS predicted a fatigue cracking of $4.2 \text{ ft}^2/1000 \text{ ft}^2$ and $4.5 \text{ ft}^2/1000 \text{ ft}^2$ using the laboratory determined results and Rauhut's based fatigue coefficients, respectively, at the end of loading. The actual, measured field fatigue cracking was $9.5 \text{ ft}^2/1000 \text{ ft}^2$. Figure 50 shows the predicted and measured rut depth with cumulative ESALs applied.

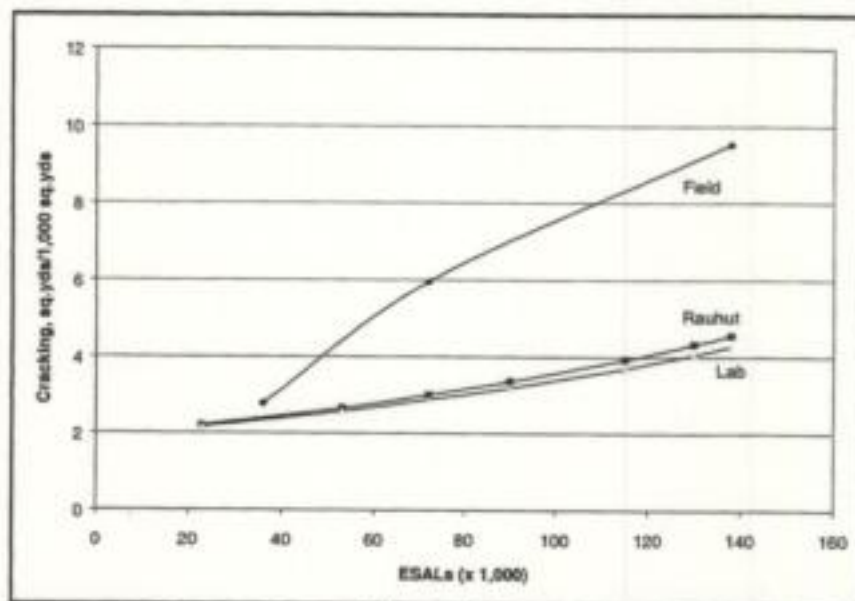


Figure 49

Fatigue crack development for the portion of lane 003 with no slip

The predicted rut depth was 24 percent less than the field measured rut depth. The failure criteria of 0.75 in (19 mm) set by LTRC was reached for lane 003 at 90,000 ESALs although FLEXPASS predicted that a rut depth of 0.57 in (14.5 mm) would occur at this loading. Figure 51 shows a plot of predicted and field PSI with cumulative ESALs applied. FLEXPASS predicted a PSI of 2.08 at the end of 138,000 ESALs. The final field data was recorded when the loading reached 72,000 ESALs at which point the predicted PSI was 2.58 and the field PSI was 2.80.

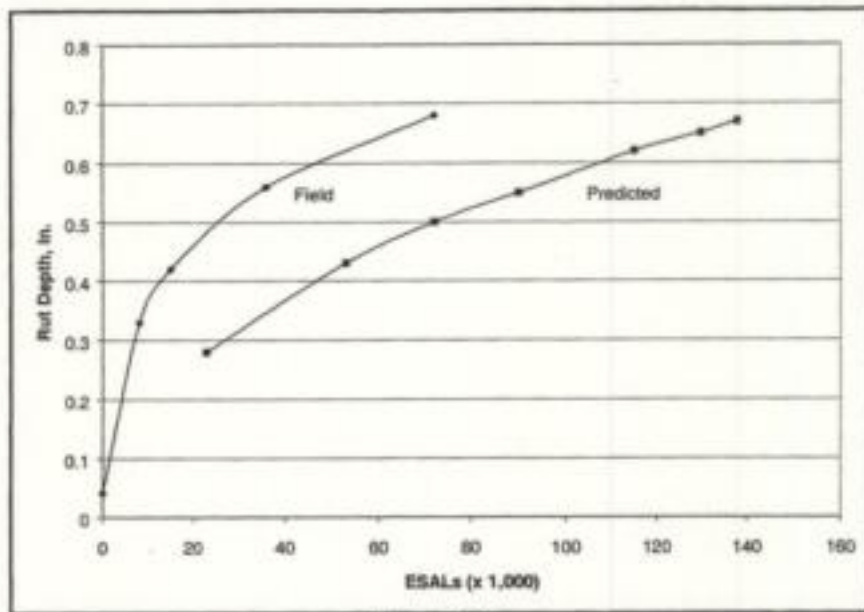


Figure 50

Rut depth development for the portion of lane 003 with no slip

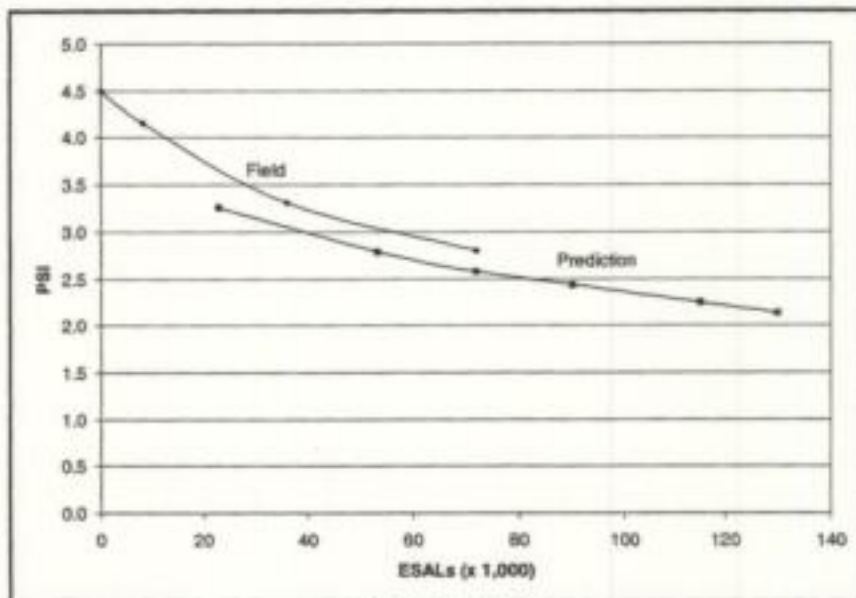


Figure 51

PSI development for the portion of lane 003 with no slip

Lane 003 with slip condition

Slippage cracking was observed in the first three feet where the ALF load wheel touched down on lane 003. Since FLEXPASS is capable of modeling slippage, an analysis of the first three feet of lane 003 was performed. Figures 52 through 54 show the plots of predicted and field performance measures with cumulative ESALs applied for the first 3 feet of lane 003. As the loading reached 138,000 ESALs, the whole section developed slippage cracking.

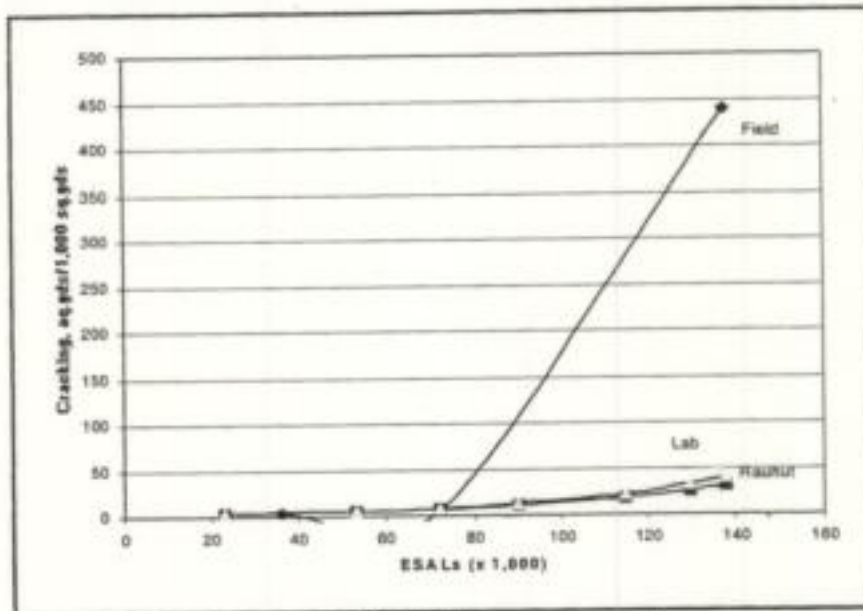


Figure 52
Fatigue crack development for the portion of lane 003 with slip

The predicted cracking, calculated by loading using laboratory determined fatigue coefficients and Rauhut's determined coefficients, was 39 sq ft /1000 sq ft and 31 sq ft/ 1000 sq ft, respectively, as shown in figure 52. It was determined from the post-failure analysis that slippage occurred between the type 8 wearing and binder courses. Since fatigue cracking models describe a phenomenon different from slippage cracking, it is not surprising that there is poor agreement between observed and predicted cracking.

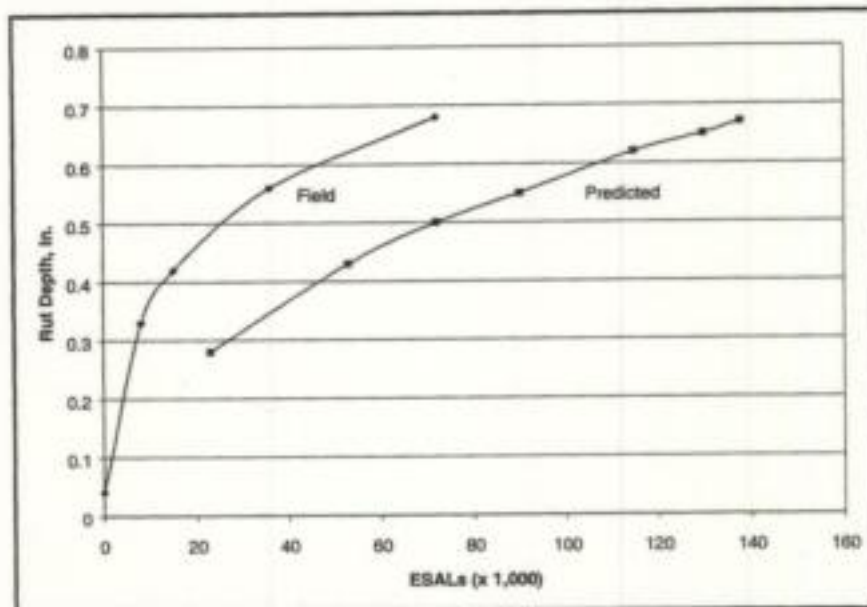


Figure 53
Rut depth development for the portion of lane 003 with slip

FLEXPASS predicted a rut depth of 0.67 in (17 mm) when the loading reached 138,000 ESALs as shown in figure 53. The last rut depth measured in the field was 0.68 in (22 mm) at 72,000 ESALs. The predicted rut depth is observed to be 40 percent less than the field rut depth. Reasons for the difference between the predicted and observed rut depth could be related to either dynamic loading in the touchdown area or to the movements in the wearing course materials that had broken loose (slipped) from the binder course. The effect of dynamic loading can be clearly seen from the initial rut depth, which is measured to be 0.12 in (3 mm).

The predicted PSI at 72,000 ESALs is 2.51 and the field PSI at the same loading was 2.36 as shown in figure 54. The difference in the predicted and field PSI is quite small.

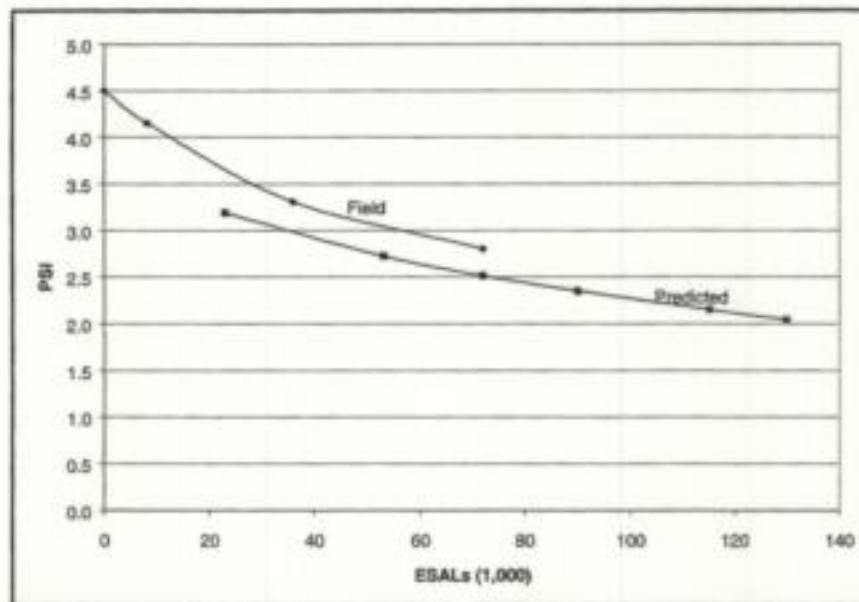


Figure 54
PSI development for the portion of lane 003 with slip

Lane 004

Field fatigue cracking started at around 85,000 ESALs and increased at a very low rate until the loading reached around 300,000 ESALs as shown in figure 55. The cracking then increased rapidly to 217 sq ft / 1000 sq ft at 713,000 ESALs. The predicted fatigue using both sets of the fatigue coefficients, was only 16 sq ft / 1000 sq ft, which is much smaller than observed field measured cracking.

One suspected reason for this difference is that the fatigue coefficients were determined from the laboratory tests at 77 °F (25°C), and, then, regression equations were used to adjust the fatigue coefficients for other temperatures. The pavement temperature during lane 004 testing was 114°F (46°C). Therefore, it is probable that better results would have been obtained if the fatigue tests were run at 104 °F (40°C) as was done for other laboratory tests.

Figure 56 shows that the field and the FLEXPASS predicted rut depths matched very well for lane 004. FLEXPASS predicted a rut depth of 1.2 in (31 mm) at 713,000 ESALs. In extrapolating the field rut depth curve, the rut depth at this loading would have been 1.23 in (31 mm). This is the best agreement for any of the sections and may be related to the high temperature that caused field rutting to develop along the parabolic path. This was typical of both FLEXPASS and VESYS predictions.

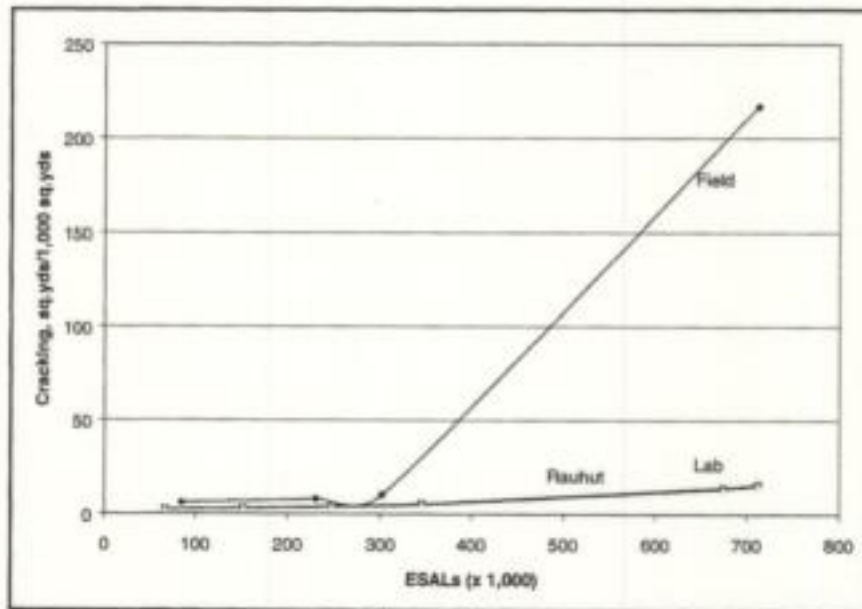


Figure 55
Fatigue crack development for lane 004

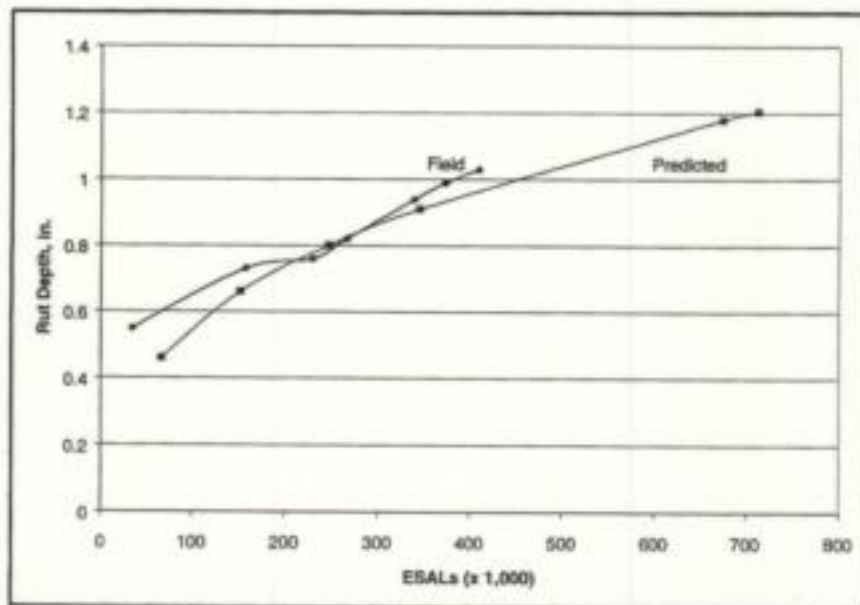


Figure 56
Rut depth development for lane 004

Figure 57 shows the predicted and field PSI with the cumulative ESALs applied. The trend of the field PSI was above that of the predicted PSI throughout the loading period. Measurement of field slope variance stopped when the PSI reached 2.3. As shown in figure 57, the shape of neither of the PSI curves takes the anticipated concave shape. The researchers anticipate that the accelerated nature of loading prevents the hot mix asphalt material from healing as occurred between load applications under field conditions. Additionally, hardening of the asphalt binder with time increased its stiffness, which also should extend the number of load applications to failure.

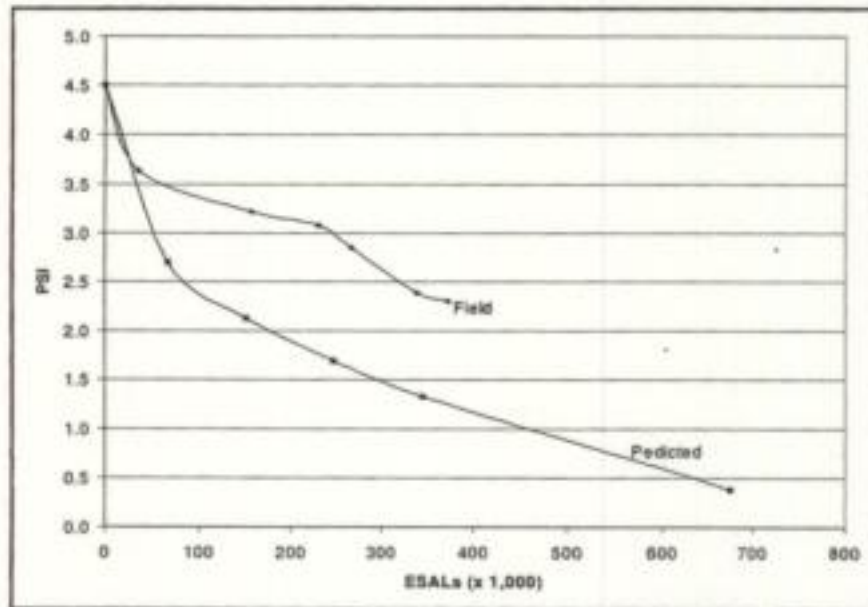


Figure 57
PSI development for lane 004

CONCLUSIONS

The 8.5 in (216 mm) crushed stone base (lane 002), the 4 in (102 mm) crushed stone base over six inches (152 mm) of ten percent mixed in-place soil cement (lane 009), and the 12 inch (300 mm) plant mixed soil cement base (lane 010) with four percent soil cement performed better than any of the other base combinations for all the performance criteria considered.

For this series of tests, the 8.5 in (216 mm) crushed stone base performed better than any of the 8.5 in (216 mm) soil cement bases in terms of rut, roughness, and crack development. This is a surprising find and is counter to the general pavement design practices in Louisiana.

The combination of 4 in (102 mm) of crushed stone base over 6 in (152 mm) of 10 percent soil cement (lane 009) outperformed all of the 8.5 in (216 mm) soil cement bases as well as the 8.5 in (216 mm) crushed stone bases. Additionally, this material configuration should have the least problem with reflection cracking from the soil cement through the asphalt concrete surface.

The four percent, 12 in (305 mm) soil cement base performed much better in both rutting and cracking than any of the other 8.5 in (216 mm) soil cement bases with either four or ten percent cement.

The soil cement bases with four percent cement performed as well as those with 10 percent cement. The mixed in-place soil cement performed as well as the plant mixed soil cement. Compare lanes 008 with 005.

Performance of lane 009, the "inverted" pavement structure, was significantly different than that of the other lanes in both failure mode and fatigue life. Cracking was the predominant failure mode for this lane. The pavement life of lane 009 is about five times longer than its counterparts, while its rut-depth was less than 25 mm.

Cracking was found to initiate at the bottom of the asphalt layer or to reflect into the asphalt layer from the soil cement base for lanes 005, 006, 007, and 010. There was no evidence showing the same thing happening in lane 009, where cracking initiated at the surface.

Post-mortem trench excavation showed several features of interest:

- There was clearly a loss of bond between the asphalt and cement stabilized layers. This was consistent with the pumping observed during loading and the presence of free water at the interfaces observed upon excavation.
- The deformation appeared to be distributed in the base layers as shown in figures 23 and 24.
- There was evidence of cracking at the base of the asphalt in lanes 008 and 010. It was observed that there was a clear relationship between cracking in the asphalt and (shrinkage) cracking in the cement-stabilized base of lane 008 as shown in figure 26. The same phenomenon was not found in lane 010 with the lower percent cement stabilization.

The life of lane 002 was in reasonable agreement with that predicted by DOTD procedures as

estimated using the AASHTO design procedure. Using the same design approach, the performance of lane 004 can be back-analyzed to suggest a layer coefficient for the stone-stabilized soil of 0.10, which is of credible value but based on limited evidence. Estimating the PSI from the roughness, cracking, and rutting results gave a reasonable relationship for lanes 002 and 004, which could be applied in pavement management systems models.

Performance of lane 003, was unexpected and resulted in a localized failure during the first test. Post-mortem examination suggests that the wearing course of the asphalt separated from the binder course, leading to slippage and cracking where the ALF wheel load was first applied to the pavement surface. At this point, the dynamic vertical load is at maximum, and there is a real possibility of surface shear loading as the wheel speed changes to balance with the bogie speed at first contact. The observed pavement life of the retested lane, 003A, was much longer than that of the original lane test results. It should be noted that the river stage of the retested lane 003 (5.8 m) conducted about a year later was much lower than that of the original lane (10.4 m).

Performance of lane 008 was unexpected and resulted in a localized failure. Examination suggested that the asphalt courses separated from the base course due to water penetration and consequent softening of the soil cement. The retest, lane 008A, failed with the formation of cracks in the asphalt layer and the pumping of soil-cement through the cracks. Based on cracking and rutting failure criteria, it had a lower pavement life than lane 008. This lower pavement life can be attributed to the fact that the river stage, 10.4 m for lane 008A, was higher than 7.6 m for lane 008.

Both VESYS 3A-M and FLEXPASS can be used to model and predict the performance of the pavements consisting of HMA wearing course over a crushed stone base. While the difference between observed and predicted performance varied with test lanes, both programs were able to adequately predict the rutting and PSI of the test lanes. Neither program did a very good job of predicting cracking for lane 003, where premature slippage between the binder and the base may have occurred.

RECOMMENDATIONS

1. Crushed stone bases should definitely be considered for use in Louisiana, especially in those areas where the subgrade is relatively soft with predicted moduli of around 35 MPa (5 ksi).
2. Combinations of crushed stone over soil cement appear to be an excellent material combination to carry traffic loads while resisting rutting. They should retard the occurrence of reflection cracking.
3. Soil cement bases using about half or less cement than the standard amount (4 percent for this silty soil) and those mixed in-place should be constructed. Performance should be observed and compared to standard mixed in-place soil cement bases. Plant-mix soil mixtures gave similar performance. The in-place mixing of cement for soil stabilization or treatment should continue.
4. Both VESYS 3A-M and FLEXPASS should continue to be used.
5. DOTD should conduct long-term field trials of stone-stabilized pavement subbase construction, assuming an AASHTO layer coefficient of 0.10 for design.
6. DOTD should conduct long-term field trial of "inverted" pavement assuming an AASHTO layer coefficient of 0.16 for the design of cement stabilized soil subbase construction.
7. Further investigation is necessary to establish geo-grid or fiber reinforcement techniques.
8. The life of the thicker but lower cement-content stabilized base course pavement was longer than those pavements constructed with thinner layers stabilized with higher cement content.

REFERENCES

1. Kim, O.K., and Bell, C.A., *Measurement and Analysis of Truck Tire Pressures in Oregon*, Transportation Research Record 1207, Transportation Research Board, Washington, D.C. 1988, pp 100-110.
2. Cumbaa, S.L., et al., *Construction and Comparison of Louisiana's Conventional and Alternative Base Courses Under Accelerated Loading*, FHWA Research Study, 1993-1996.
3. Metcalf J. B., *The Application of Full Scale Accelerated Pavement Testing*, TRB Synthesis 235, NCHRP Transportation Research Board, Washington DC, pp 110, 1997.
4. King W., *Construction and Comparison of Louisiana's Conventional and Alternative Base Course under Accelerated Loading (Interim Report)*, Louisiana Transportation Research Center, Report No FHWA/LA-97/301, 1997.
5. Metcalf J. B., Rasouljian M., Romanoschi S. and Li Yongqi, *The Louisiana Accelerated Loading Facility*, Report 2, Experiment 1, Phase 1, 1997.
6. Statton, J.E., and Kadar, P., *The Performance of Pavement Rehabilitations Under Accelerated Loading - The Callington ALF Trial*, Proceedings, 15th ARRB Conference Part 2, Australia, 1992, pp.328-345.
7. Bonaquist, R., Surdahl, R., and Mogawer, W., *Effect of Tire Pressure on Flexible Pavement Response and Performance*, Transportation Research Record 1227, Transportation Research Board, Washington, D.C., 1989, pp 97-106.
8. Johnson-Clark, J.R., Sharp, K.G., Walter, P.D., *The Performance of Pavements with Geotextile Reinforced Seals: The Brewarrina, N.S.W. ALF Trial*, Research Report 241, Australian Road Research Board Ltd., Vermont, Victoria, Australia, February 1993.
9. Sebaaly, P., Tabatabaee, N., Bonaquist, R., and Anderson, D., *Evaluating Structural Damage of Flexible Pavements Using Cracking and Falling Weight Deflectometer Data*, Transportation Research Record 1227, Transportation Research Board, Washington, D.C. 1989, pp 115-127.
10. Kadar, P., *The Performance of Overlay Treatment and Modified Binders Under Accelerated Full Scale Loading- The Callington ALF Trial*, 27 November 1990, Australian Road Research Board Ltd., Vermont, Victoria, Australia.
11. Sharp, K.G., *The Efficiency and Effectiveness of the Australian Accelerated Loading Facility (ALF) Program*, Road and Transport Research, Vol.1, No. 2, June 1992, pp. 104-107.
12. Freeman R.B. and W. P. Grogan, *Statistical Analysis and Variability of Pavement Materials*, Technical Report GL-97-12, U.S. Army Corps of Engineers, Waterways Experimental Station, Vicksburg, Mississippi, 1997.

13. Scullion T. and C. Michalak, *MODULUS 4.0, Users Manual*, Report FHWA/TX-88/1123-4, Texas Transportation Institute, Texas A&M University, College Station, Texas, January 1991.
14. Roberts F.L. and J.B. Wedgeworth, *Analysis and Evaluation of Methods for Backcalculations of M_R values*, L.T.R.C. Report Nr. 263, Vol.1, LTRC, Baton Rouge, Louisiana, August 1992.
15. SHRP Publication, *Manual for FWD Testing in the Long-Term Pavement Performance Program, SHRP Protocol P-661*, Strategic Highway Research Program, National Research Council, Washington, D.C., 1993.
16. Ullitz P., *Pavement Analysis*, Elsevier, New York, 1987.
17. Groenenedijk, J., C.H. Vogelzang, A. Miradi, A.A.A. Molenaar, L.J.M. Dohmen, *Results of the LINTRACK performance tests on a full-depth asphalt pavement*, TRB 76th Annual Meeting, Washington, D.C., January 12-16, 1997.
18. A.A.S.H.T.O., *AASHTO Guide for Design Of Pavement Structures*, American Association of State Highway and Transportation Officials, Washington, D.C., 1993.
19. Newcomb D.E., *Comparison of field and laboratory estimated resilient moduli of pavement materials*, *Proceedings of the Association of Asphalt Paving Technologists*, Vol.56, 1987, pp.91-110.
20. Rada G.R., Witczak M.W. and S.D.Rabinow, *Comparison of AASHTO structural evaluation techniques using nondestructive deflection testing*, Transportation Research Record 1207, TRB, National Research Council, Washington, D.C., 1988.
21. Romanoschi S.A., *The Correlation Between the Structural Number and the Falling Weight Deflections for Louisiana Roads*, Master's Thesis, Louisiana State University, Baton Rouge, 1996.
22. Li Y., Metcalf J.B., Romanoschi S.A. and M. Rasoulian, *Performance and Failure Modes of Asphalt Pavements with Soil-Cement Bases under Full-Scale Accelerated loading*, 1999 TRB Annual Meeting, Transportation Research Record #1673, TRB, Washington, D.C.
23. Lytton R. L., J. Uzan, R. Roque, D. Hiltunen and Stoffels, *Development and Validation of Performance Prediction Models and Specifications for Asphalt Binders and Paving Mixes*, SHRP-A-357, National Research Council, Washington, D.C., 1993.
24. Burmister, D.M., *The Theory of Stresses and Displacements in Layered Systems and Applications to the Design of Airport Runways*. Proceedings, Highway Research Board, Vol 23, 1943.

25. McLeod, Norman, W., *Some Basic Problems in Flexible Pavement Design*, Proceedings, Highway Research Board, 1953.
26. Acum, W.E.A. and Fox, L., *Computation of Load Stresses in a Three-Layer Elastic System*, Geotechnique, Vol 2, No.4, Dec., 1951.
27. Palmer, L.A., *The Evaluation of Wheel Load Bearing Capacities of Flexible Types of Pavements*, Proceedings, Highway Research Board, 1946.
28. De Jong, D.L., M.G.H. Peatz, and A.R. Korswagen, *Computer Program BISAR. Layered Systems Under Normal and Tangential Loads*, Konin Klijke Shell Laboratorium, Amsterdam, External Report AMSR.0006.73, 1973.
29. Ahlborn, G., *Elastic Layered System with Normal Loads*, The institution of Transportation and Traffic Engineering, University of California at Berkeley, 1972.
30. Kenis, W.J., *Predictive Design Procedures, VESYS User's Manual*, Research Report No. FHWA-RD-77-154, Final Report, Federal Highway Administration, January 1978.
31. Fernando, E.G., Tseng K.H., Lytton R.L., *Flexible Pavement Analysis Structural System (FLEXPASS Release 2.0) User's Guide*, Texas Transportation Institute, Texas A&M University, October 1989.
32. Harichandran, R.S., Baladi, G.Y., and Yeh.M.S., *MICH-PAVE User's Manual*, Report FHWA-MI-RD-89-03, Michigan Department of Transportation, Lansing, 1989.
33. *ABACUS, Finite Element Computer Program. Version 5.2*, Hibbit, Karlsson, Sorenson, Inc., Pawtucket, N.Y., 1992.
34. Chen, D.H., M. Zaman., J. Laguros., and A. Soltani, *Assessment of Computer Programs for Analysis of Flexible Pavement Structure*, Transportation Research Record 1482, Transportation Research Board, Washington, D.C. 1995, pp 123 -133.
35. Kenis, W.J., *VESYS 3A-M User's Manual*, FHWA, Office of Research, Development, and Technology, Washington, D.C., Undated.
36. *ILLIPAVE-A Finite Element Program for the Analysis of Pavements*, Construction Engineering Laboratory and Facilities Group, Department of Civil Engineering, University of Illinois at Urbana, May 1982.
37. Tseng, K.H., *A Finite Element Method for the Performance Analysis of Flexible Pavement*, Ph.D. Dissertation, Texas A.M. University, College Station, August 1988.
38. Hoyt, D., R.L. Lytton, and F.L. Roberts, *Performance Prediction and Cost-Effectiveness of Asphalt Rubber Concrete in Airport Pavements*, Transportation Research Record #1207, TRB, National Science Foundation, Washington, D.C., 1988.
39. Metcalf, J.B., *Application of Full-Scale Accelerated Pavement Testing, NCHRP Synthesis 235*, Transportation Research Board, Washington, D.C.
40. Sharp, K.G., *The Efficiency and Effectiveness of the Australian Accelerated Loading Facility (ALF) Program*, Road and Transportation Research Vol 1. No 2, June 1992, pp 104 - 106.

41. Anderson, D.I., Peterson, D.E., McBride, J.C., Shepherd, L.D., *Field Verification and Implementation of the VESYS IIM Structural Subsystem in Utah*, Research Report No. FHWA-RD-78-510, Final Report, Federal Highway Administration, February 1978.
42. Hadley, W.O., *A Mechanistic Evaluation and Analysis of the Performance of Louisiana Experimental Test Sections*, Research Report No. FHWA/LA-83/78-5, Louisiana Department of Transportation and Development, December 1983.
43. Rada, G., and M.W. Witczak, *Comprehensive Evaluation of Laboratory Resilient Moduli Results for Granular Material*, Transportation Research Record 810, Transportation Research Board, Washington, D.C. 1981, pp 23 - 32.
44. Rauhut, J.B., Jordahl, P.R., *Effects of Flexible Highways of Increased Legal Vehicle Weights Using VESYS IIM*, Research Report No., FHWA-RD-77-116, Federal Highway Administration, January 1978.
45. Tutumluer E. and R.D. Barcksdale, *Inverted flexible pavement response and performance*, Transportation Research Record 1482, TRB, National Research Council, Washington, D.C., 1995.
46. Romanoschi S.A., Metcalf J.B., Li Y. and M. Rasoulia, *Assessment of Pavement Life at First Full-Scale Accelerated Pavement Test in Louisiana*, 1999 TRB Annual Meeting, Transportation Research Record #1655, Washington, D.C.
47. Metcalf, J.B., M. Rasoulia, M., S. Romanoschie, and L. Yongqi, *The Louisiana Accelerated Loading Facility Experiment 1, Phase III. Report 2*. The Louisiana Department of Transportation and Development, Baton Rouge, 1998.
48. Sayers, M.W., *On the Calculation of International Roughness Index from Longitudinal Road Profile*, Transportation Research Record 1501, TRB, National Research Council, Washington, D.C., 1995, pp. 1 - 12.
49. Sayers, M.W., and S.M. Karamihas, *Estimation of Rideability by Analyzing Longitudinal Road Profile*, Presented at the 1996 TRB Meeting, Washington, D.C., 1996.
50. Patterson, W.O., *International Roughness Index: Relationship to Other Measures of Roughness and Riding Quality*, Transportation Research Record 1084, TRB, National Research Council, Washington, DC, 1986.
51. *The AASHO Road Test, Report 5, Pavement Study*, Highway Research Board Special Report 71E, Washington, 1962.

This public document is published at a total cost of \$1442.00. Three hundred and seventy five copies of this public document were published in this first printing at a cost of \$992.00. The total cost of all printings of this document including reprints is \$1442.00. This document was published by Louisiana State University, Graphic Services, 3555 River Road, Baton Rouge, Louisiana 70802, and Louisiana Transportation Research Center, to report and publish research findings for the Louisiana Transportation Research Center as required in R.S. 48:105. This material was duplicated in accordance with standards for printing by state agencies established pursuant to R.S. 43:31. Printing of this material was purchased in accordance with the provisions of Title 43 of the Louisiana Revised Statutes.